Changing ecology, hydrology and permafrost in circum-Arctic peatlands

Richard Edward Fewster

Submitted in accordance with the requirements for the degree of Doctor of Philosophy

The University of Leeds

School of Geography

May 2023

Publication statement

The candidate confirms that the work submitted is their own, except where work which has formed part of jointly authored publications has been included. The contribution of the candidate and the other authors to this work has been explicitly indicated below. The candidate confirms that appropriate credit has been given within the thesis where reference has been made to the work of others.

The work presented in Chapter 2 of this thesis has been published in *Nature Climate Change*, with additions for the format of the thesis:

Fewster, R.E., Morris, P.J., Ivanovic, R.F., Swindles, G.T., Peregon, A.M. and Smith, C.J. 2022. Imminent loss of climate space for permafrost peatlands in Europe and Western Siberia. *Nature Climate Change*. **12**(4), pp.373-379.

In this study, R.E.F. designed the research, performed all meta-analyses, data collection, reanalysis and downscaling of climate model outputs, statistical modelling, and statistical analyses, and wrote the manuscript, under supervision from P.J.M., R.F.I. and G.T.S.. A.M.P. contributed the landform classification data for Western Siberia. C.J.S. provided critical analysis of future climate projections from CMIP6 models. All authors edited the final manuscript.

The work in Chapter 3 of this thesis has been published in *Quaternary Science Reviews*, with additions for the format of the thesis:

Fewster, R.E., Morris, P.J., Swindles, G.T., Ivanovic, R.F., Treat, C.C, and Jones, M.C. 2023. Holocene vegetation dynamics of circum-Arctic permafrost peatlands. *Quaternary Science Reviews*. **307**(108055).

In this study, R.E.F. designed the research, conducted all research methods including all meta-analyses, dataset construction, data analysis, age-depth

modelling, and statistical analyses, and wrote the final manuscript, under supervision from P.J.M., R.F.I. and G.T.S.. C.C.T. and M.C.J. contributed research data and provided expert advice on code development, data analysis and the interpretation of the results. All authors edited the final manuscript.

The work in Chapter 4 of this thesis has been submitted for publication to *Water Resources Research*, with additions for the format of the thesis:

Fewster, R.E., Morris, P.J., Swindles, G.T., Baird, A.J., Turner, T.E., and Ivanovic, R.F. (in review). Controls on saturated hydraulic conductivity in a degrading permafrost peatland complex. *Water Resources Research*. Submitted; in review.

In this study, R.E.F. designed the research, conducted all fieldwork, sample collection, laboratory analyses, data analysis, statistical modelling, and wrote the manuscript, under supervision from P.J.M., G.T.S., and R.F.I.. P.J.M. also contributed code and training data for model evaluation. A.J.B. and T.E.T. designed components of the laboratory method. All authors edited the final manuscript.

Rationale for submitting the thesis in an alternative format

This thesis addresses three specific research gaps regarding the past, present and future development of permafrost peatlands. The thesis introduction outlines each research objective, establishes their context to the relevant peer-reviewed literature, and summarises the research methods employed. Three subsequent research chapters are then presented, with each containing an abstract, introduction, methods section, results summary and discussion. Each of these research chapters are therefore considered independent research outputs and have either been published or submitted for publication in peer-reviewed journals. Each research chapter has been reformatted for the purposes of this thesis, although some components of the thesis inevitably overlap between chapters. Any supplementary material is presented at the end

of the relevant research chapter, while supplementary datasets and the supplemental age-depth models for Chapter 3 are available alongside the online version of this thesis. The concluding chapter of this thesis binds this research into a cohesive body of work, providing a summary of the key findings, an agenda for future research, and conclusions.

This thesis is structured with an overall introduction and review of the relevant literature (Chapter 1), three core research chapters that fulfil the identified research objectives (Chapters 2–4), a discussion of the key findings, future research agenda and conclusions (Chapter 5).

Acknowledgements

Undertaking a PhD is challenging, unpredictable, but incredibly rewarding, and I am eternally grateful for the brilliant supervision team that has supported me on my journey from an undergraduate at the University of Leeds. Firstly, Paul, thank you for recognising my potential, for inspiring me to become an academic, and for guiding me throughout my postgraduate research, even when I struggled to see the path ahead. We've come a long way together. Graeme, your wide-ranging expertise and continued encouragement have been greatly appreciated, as have your famous fieldwork sayings: "nil desperandum" and "where there's a will, there's a way". Ruza, thank you for your expertise in climate modelling, for asking the questions others are thinking, and for always lending a listening ear during my PhD.

I extend my thanks to my co-authors: Anna Peregon, Chris Smith, Claire Treat, Miriam Jones, Andy Baird and Ed Turner. Your expert advice has been invaluable. Special acknowledgements go to David Ashley, Holly Armitage, Josh Greenwood, Antony Windross, and Stephen Burgess for providing technical and logistical support for my laboratory analyses, combined with a great deal of patience.

A special mention too for my colleagues and friends in the research groups: River Basins: Processes and Management, Climate-Ice group, Peat Club and Leeds Quaternary.

I thank the NERC Panorama DTP for funding my PhD research and fieldwork in summer 2022. Thanks to the Abisko Scientific Research Station and its staff for providing accommodation and Isaac Smith for logistical support during my fieldwork, and to the County Administrative Board of Norrbotten for granting permission to sample in the beautiful Rautas fjällurskog nature reserve.

Lastly, to Anna, Mum, Dad, and Cath, thank you for your endless love and support, for always being there for me, particularly during the pandemic, for believing in me, and for invariably providing some much needed perspective. This thesis is for you.

Abstract

Projected 21st-century climate change could cause widespread permafrost peatland degradation with implications for global radiative forcing. In this thesis, I address three research gaps regarding the climatic controls, ecological trajectories, and hydraulic properties of permafrost peatlands. To simulate the changing future climate space of permafrost peatlands in Europe and Western Siberia, I fitted climate envelope models to their modern distribution and drove these models with CMIP6 climate projections. My bioclimatic modelling indicates that permafrost peatlands persist close to their climatic threshold in Fennoscandia, where suitable climates are projected to disappear by 2040. By the 2090s, large parts of Western Siberia are projected to become climatically unsuitable for peatland permafrost, with simulated climate space losses under moderate- to no-mitigation scenarios potentially affecting a peatland area storing 37.0–39.5 Gt of peat carbon. Once climates become unsuitable, the fate of peatland carbon is likely to be strongly determined by changes to peatland vegetation and hydrology. To investigate Holocene vegetation dynamics of circum-Arctic peatlands, specifically peatland shrubification, I synthesised 76 previously-published plant macrofossil records and analysed normalised time series of these data at hemispheric and regional scales. My meta-analysis indicates that woody vegetation and *Sphagnum* mosses have increased in abundance in circum-Arctic peatlands since ~8,000 years BP, while peatland shrubification has been spatially heterogenous in recent centuries, owing to variability in peatland surface drying. To measure the horizontal saturated hydraulic conductivity (K_h) of peat in degrading Swedish palsas, a property that influences lateral drainage, I analysed 82 near-surface samples in the laboratory. By fitting a linear mixed-effects model, I demonstrated that simple measurements of peat properties can skilfully predict K_h in degrading palsas. Unexpectedly, I found no significant difference in K_h between desiccating palsas with permafrost and collapsed palsas without permafrost. Together, these findings could improve large-scale model representations of permafrost peatland dynamics.

Table of Contents

List of Figures

List of Tables

List of Abbreviations

AICc	Corrected Akaike Information Criterion
AUC	Area under the receiver operating characteristic curve
BP	Before present
CMIP	Coupled Model Intercomparison Project
CRU TS	Climatic Research Unit (CRU) Time-series (TS)
DBD	Dry bulk density
DGVM	Dynamic global vegetation model
ECS	Equilibrium climate sensitivity
ESM	Earth system model
FBT	Fen-bog transition
GDD_5	Growing degree days (above 5°C)
GVIF	Generalised variance-inflation factor
H	Hydraulic head
K_h	Horizontal saturated hydraulic conductivity
KOI	Kerner Oceanity Index
K_{sat}	Saturated hydraulic conductivity
K_v	Vertical saturated hydraulic conductivity
LMM	Linear mixed-effects model
MAT	Mean annual temperature (°C)
MNRA	Mean normalised relative abundance
NMDS	Non-metric multidimensional scaling
PFT	Plant functional type
PVC	Polyvinyl chloride
r^2	Standard coefficient of determination
RCP	Representative Concentration Pathway
r_s	Spearman's Rank correlation coefficient
SOC	Soil organic carbon
SSP	Shared Socioeconomic Pathway
TCR	Transient climate response
TRANGE	Seasonal temperature range
UOM	Unidentified organic matter
ρ_c	Lin's concordance correlation coefficient

Chapter 1
Introduction

1.1. Circum-Arctic peatlands under changing climate

1.1.1. Peatlands and permafrost

Northern peatlands form one of the world's largest terrestrial carbon stores, covering an estimated 3.7 ± 0.5 million km^2 and containing 500 ± 100 Gt of soil organic carbon (SOC) (Hugelius et al., 2020a; Yu et al., 2021). Peat accumulates where cold or wet conditions restrict decomposition, preventing plant detritus from fully decomposing (Clymo, 1984; Lourenco et al., 2022). An estimated 1.7 ± 0.5 million km^2 of northern peatlands lies within the circum-Arctic permafrost zone, containing 185 ± 70 Gt peat SOC (Hugelius et al., 2020a). The presence of permafrost, to varying extents and depths, beneath many circum-Arctic peatlands renders these perennially frozen ecosystems highly vulnerable to 21st-century climate change, which could rapidly transform their morphology, ecology and hydrology (Olefeldt et al., 2021).

Permafrost is defined as ground that remains consistently below 0°C for two or more years (Muller, 1945). Permafrost aggrades where cold, dry climates prevent deep winter frosts from fully thawing during summer, when maximum monthly temperatures are reached (Seppälä, 1986; Luoto et al., 2004). The distribution of circum-Arctic permafrost has been subdivided into zones of areal coverage, namely the continuous (90–100 % coverage), discontinuous (50–90 %), sporadic (10–50 %), and isolated (< 10 %) permafrost zones (Brown et al., 2002). At coarse spatial scales, the extent of permafrost broadly aligns with the latitudinal or altitudinal positions of suitable temperature thresholds (Brown, 1960). At its southern limit, permafrost is restricted to ground overlain with thick organic soils, such as peats, which insulate ground temperatures more effectively against surrounding air temperatures than

mineral soils (Smith and Riseborough, 2002; Zoltai, 1995). Peatland permafrost is most widely distributed across Alaska (Fewster et al., 2020), Canada (Zoltai et al., 2000), northern Fennoscandia (Luoto et al., 2004), north-western Russia (Zhang et al., 2018; Piilo et al., 2023), and Siberia (Peregon et al., 2008; Kirpotin et al., 2011), although more isolated permafrost peatlands have also been observed in Svalbard (Sim et al., 2021a) and Greenland (Wetterich et al., 2019).

1.1.2. Types of circum-Arctic peatlands

A range of peatland types exist across the circum-Arctic, including fens, bogs, palsas, peat plateaus and polygon mires (Zoltai and Tarnocai, 1975; National Wetlands Working Group, 1998; Minke et al., 2007; Treat et al., 2016). During the Holocene (i.e., the past ~11,700 years BP), circum-Arctic peatlands predominately initiated as fens—saturated wetlands that are dominated by herbaceous vegetation (e.g., *Carex* spp. and *Eriophorum* spp.) and exhibit comparatively high rates of peat decomposition and methane (CH_4) release (Väliranta et al., 2017; Treat et al., 2021b). Over time, fens have widely transitioned into raised bogs—ombrotrophic peatlands characterised by *Sphagnum* sect. *Acutifolia* and acidic surface waters that are considered more effective net carbon sinks than fens (Turunen et al., 2002; Loisel and Bunsen, 2020; Magnan et al., 2022). This fen-bog transition (FBT) is often triggered once surface peats are disconnected from the influence of the local water table, either by shifting climate or by surface elevation following the aggradation of underlying permafrost, autogenic accumulation of peat, or vertical growth of *Sphagnum* (Hughes and Barber, 2003; Treat and Jones, 2018; Loisel and Bunsen, 2020).

Permafrost has aggraded in circum-Arctic peatlands since ~9,000 years BP (Treat et al., 2021b), creating distinct landforms that characterise the local permafrost dynamics (Zoltai and Tarnocai, 1975). Palsas are perennial, peat-covered frost mounds up to 10 m high (Seppälä, 1994) often colonised by ericaceous dwarf shrubs (e.g., *Salix sp*. and *Betula nana*), *Rubus*

chamaemorus, *Sphagnum fuscum*, or lichens (Railton and Sparling, 1973; Zuidhoff and Kolstrup, 2005; Kuhry, 2008) (Figure 1.1). Palsas develop in cold, dry climates where thin snow covers facilitate deep winter freezing, creating segregated ice lenses that are only partially thawed during summer and progressively expand to elevate the peat surface (Seppälä, 1986, 2011). Peat plateaus are morphologically similar to palsas, but are lower lying (often raised ≤ 1 m high), more aerially expansive (up to several km^2), and are commonly treed in North America (e.g., with *Picea mariana*) (Zoltai and Tarnocai, 1975; Zoltai, 1993; Kuhry, 2008). Because of the morphological similarities of palsas and peat plateaus, this thesis does not hereafter distinguish between these permafrost landforms, unless specified. Palsas/peat plateaus are distributed broadly across the discontinuous and sporadic permafrost zones of North America (Fewster et al., 2020), Fennoscandia (Luoto et al., 2004), and western Siberia (Peregon et al., 2008).

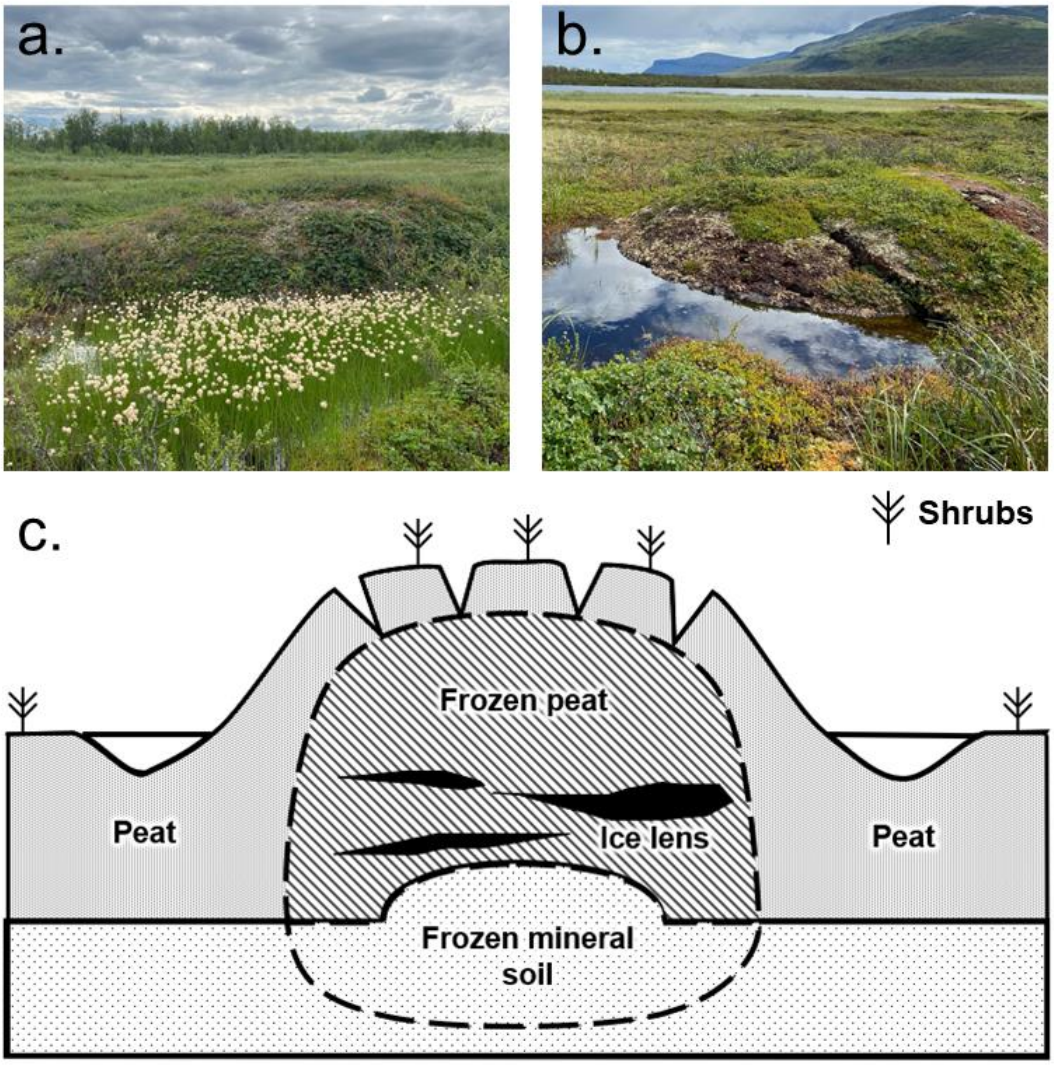

Figure 1.1. Degrading palsas in northern Sweden at (a) Rensjön palsa mire, near Kiruna; and (b) Stordalen Mire, near Abisko (own images). Cross-section of a mature palsa (adapted from Seppälä (1986)).

Under colder climates further north, ice-wedge polygons have developed following centuries of intense freeze-thaw processes and thermal cracking of peat surfaces, which enables meltwater to accumulate in summer and subsequently refreeze and expand during winter (Minke et al., 2007; Olefeldt et al., 2021). Low-centred polygons form where ice wedge formation uplifts sediments, forming marginal ridges that retain water-saturated conditions in intervening depressions (Figure 1.2) (Minayeva et al., 2016). High-centred polygons form where consistent peat accumulation elevates the polygon into

a central dome (Figure 1.2) (Zoltai and Tarnocai, 1975). In polygon mires, low-centred depressions are often colonised by *Carex* spp. and non-*Sphagnum* mosses (de Klerk et al., 2011), trenches are dominated by *Sphagnum* spp. (Zoltai and Tarnocai, 1975), while raised centres and ridges can exhibit ericaceous dwarf shrubs and lichens (Minayeva et al., 2016). Polygon mires dominate northern Siberia and the arctic coastal plains of North America (Minke et al., 2007; Minayeva et al., 2016) (Figure S2.4).

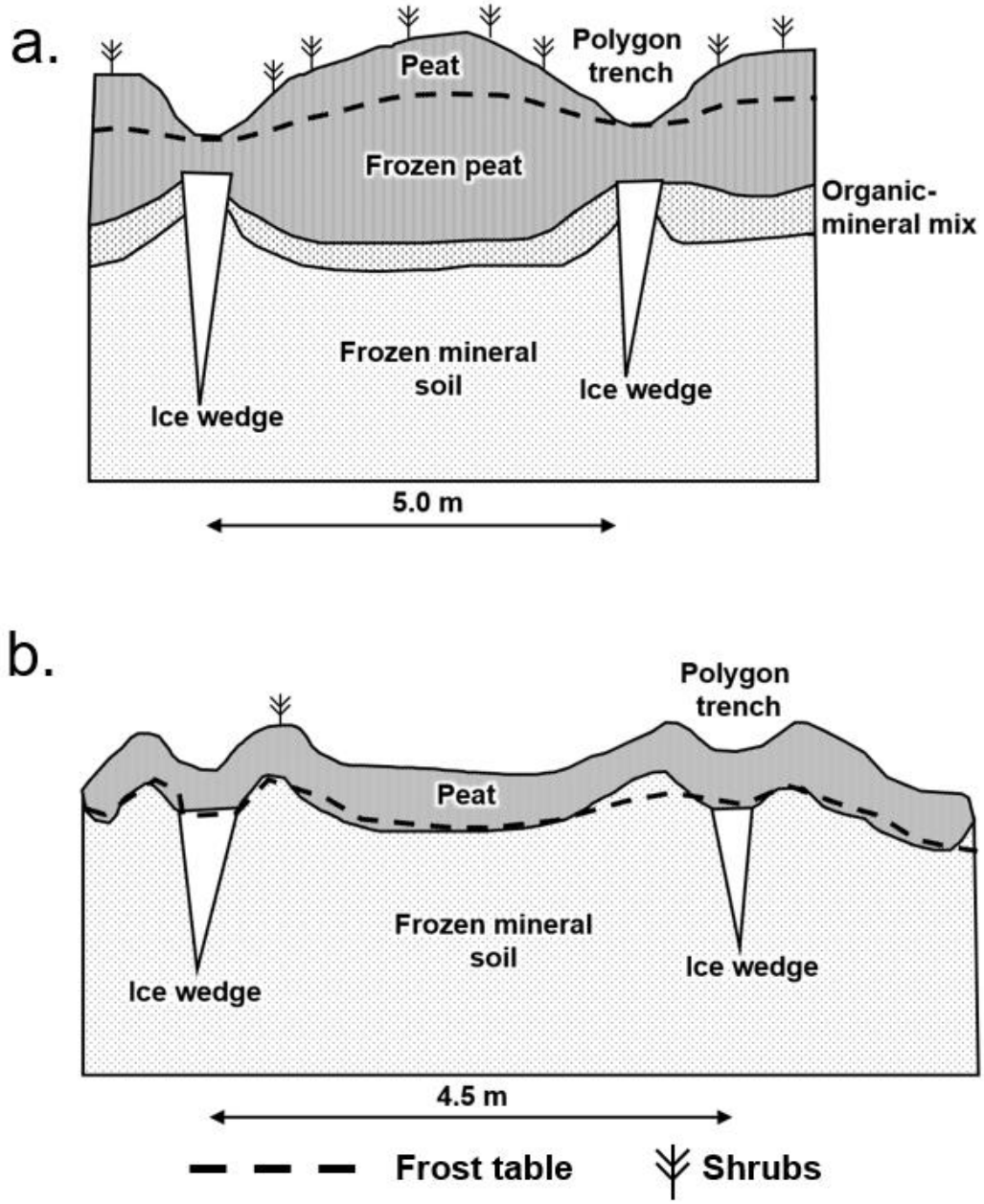

Figure 1.2. Cross sections of typical polygon mire forms, showing (a) a high-centred polygon and (b) a low-centred polygon (adapted from (Minayeva et al., 2016)).

1.1.3. Drivers of ecohydrological change in circum-Arctic peatlands

1.1.3.1. Climate

At coarse spatial scales, the distribution of circum-Arctic peatlands is strongly controlled by climate, because peatlands require cool, moist climates to form and do not exist under extremely arid climates, such as polar deserts (Gajewski et al., 2001). Prolonged reductions to precipitation can lower water tables in fens and drive hydroseral succession, by enabling peat surfaces to be increasingly colonised by dry-favouring *Sphagnum* (Hughes, 2000; Elliott et al., 2012). Alternatively, palaeoecological records from eastern Canada indicate that persistently raised water tables during Holocene wet periods have reversed FBTs, although this process requires long timescales (Van Bellen et al., 2013; Robitaille et al., 2021). The southernmost extent of peatland permafrost is closely aligned with mean annual temperature (MAT) thresholds, and the depth of seasonal thaw is primarily determined by summer temperatures (Vitt et al., 1994; Sannel et al., 2016). Precipitation also exerts an important influence, because the high thermal conductivities of water-saturated peats make them conducive to deep winter freezing, while surface waterbodies formed by intense summer rainfall can increase permafrost thaw (Jorgenson et al., 2010; Seppälä, 2011). Snowfall is widely considered to exert a critical control on the formation and persistence of permafrost in palsas/peat plateaus, because thick snow covers insulate ground temperatures, which limits the depth of winter frost penetration (Jorgenson et al., 2010; Seppälä, 1986, 1994, 2011). Snow depths are highly spatially variable across individual peatlands, with reduced snow covers found on exposed *Sphagnum* hummocks (Camill and Clark, 1998) and palsas (Seppälä, 2011), or beneath dense tree stands (Zoltai, 1995).

In response to recent climate change, circum-Arctic peatlands have evidenced abrupt thawing of permafrost (e.g., Camill, 2005; Payette et al., 2004; Olvmo et al., 2020), peatland vegetation shifts (e.g., Sim et al., 2019; Magnan et al., 2022; Varner et al., 2022) and changes to their hydrological functioning (Quinton et al., 2019; Disher et al., 2021). Such observations demonstrate the

potential for peatlands to exhibit non-linear, threshold responses to changing climate (Belyea, 2009; Swindles et al., 2015). For example, Swindles et al. (2015) conceptualised a five-phase model for palsa degradation in Fennoscandia, suggesting that increased drying under continuous climate warming causes surface cracking, which can trigger runaway permafrost degradation resulting in surface collapse and inundation. Alternatively, permafrost thaw can sometimes also increase peatland drainage, for example, in polygon mires where ice-wedge thaw removes impermeable barriers to groundwater flow (Olefeldt et al., 2021). Boreal peatlands undergoing surface drying, either because of reduced precipitation or increased evapotranspiration, have recently evidenced accelerated ecological succession into *Sphagnum*-dominated peatlands, for example, in northern Alberta (Magnan et al., 2018) and eastern Canada (Magnan et al., 2022).

1.1.3.2. Internal mechanisms

At local scales, peatland vegetation composition, hydrology, and permafrost extent are also determined by a myriad of alternative, internal mechanisms. For example, peatland permafrost can persist for some time under unsuitable climates where *Sphagnum* peats are present, because their low dry bulk densities insulate permafrost against summer thaw, while their high thermal conductivities when saturated increase the depth of winter freezing (Camill and Clark, 1998; O'Donnell et al., 2009). These properties have enabled relict permafrost to persist for several decades under unsuitable climates at its most southerly limit in central Canada (Halsey et al., 1995) and Fennoscandia (Olvmo et al., 2020), although the duration of this temporal lag in permafrost thaw remains unquantified. Peat layers need to be sufficiently thick to restrict summer thaw (Luoto and Seppälä, 2002; Jorgenson et al., 2010), although polygon mires exhibit thin peat covers due to climatic restrictions on plant productivity and thus peat accumulation (Zoltai and Tarnocai, 1975). While *Sphagnum* peats are characteristic of FBTs, *Sphagnum* establishment can also follow permafrost aggradation, because frost-heaved, elevated surfaces in saturated sedge fens become dry and nutrient-poor (Treat et al., 2016;

Kjellman et al., 2018; Sannel et al., 2018; Olefeldt et al., 2021). Continued permafrost aggradation may facilitate the growth of lichens, shrubs, and trees (Treat et al., 2016; Wolter et al., 2016), although established *Sphagnum* communities can also engineer acidic, nutrient-poor, anoxic environments that restrict vascular plant growth (van Breemen, 1995).

1.1.4. The future of circum-Arctic peat carbon: sink or source?

Ongoing and future changes to peatland permafrost, vegetation, and hydrology have important implications for the circum-Arctic peatland SOC store, but it remains unclear whether these potentially fragile ecosystems will represent an overall carbon sink or source by 2100, due to continuing disagreements between field observations and model simulations (Schädel et al., 2018; Miner et al., 2022). In permafrost peatlands, thaw-driven wetting and vegetation shifts to more readily decomposed sedges can increase release of methane (CH_4), a potent greenhouse gas (Masson-Delmotte et al., 2021), although such changes can simultaneously supress carbon dioxide (CO_2) release (Holmes et al., 2022). Observations indicate that palsa/peat plateau thaw can increase the export of dissolved organic carbon (Olefeldt and Roulet, 2014; Burd et al., 2020), while increased wildfire occurrence in drying sites can exacerbate the release of deep peat carbon (Turetsky et al., 2015). However, recent observations of increased plant productivity (Crichton et al., 2022; Hough et al., 2022), rapid terrestrialisation of thermokarst pools (Payette et al., 2004), and *Sphagnum* expansion under recent warming (Magnan et al., 2022; Piilo et al., 2023), indicate that greenhouse gas emissions from degrading permafrost peatlands may be partly offset by increased carbon sequestration in the coming decades. Uncertainty regarding the relative, future strengths of these opposing carbon-cycle feedbacks mean model projections currently range from scenarios where the circum-Arctic permafrost region becomes a substantial net carbon source by 2100 (Zhao and Zhuang, 2023) to those where a net carbon sink will persist (Gallego-Sala et al., 2018; Chaudhary et al., 2020, 2022).

The overarching aim of this thesis is to improve scientific understanding of the response of peatland permafrost, vegetation, and hydraulic structures to changing climate. In sections 1.2, 1.3 and 1.4 (below), I identify three important knowledge gaps regarding the climate space of permafrost peatlands, and climate-induced changes in permafrost peatland vegetation and peat hydraulic properties, which presently limit scientific estimations of the radiative forcing potential of circum-Arctic peatlands. These three knowledge gaps form the research objectives of this thesis.

1.2. Changing future climate space of permafrost peatlands

1.2.1. Distribution of permafrost peatlands and peat carbon

Coarse-scale peatland mapping products indicate that permafrost peatlands are most spatially expansive in Alaska, Canada, Fennoscandia and Siberia (Hugelius et al., 2020a), but maps that distinguish permafrost peatland landforms, for example palsas/peat plateaus and ice-wedge polygons, have been developed primarily at regional scales (Luoto et al., 2004; Peregon et al., 2008; Fewster et al., 2020). The modern spatial extent of palsas/peat plateaus is most confidently constrained in Fennoscandia, where several studies have collated observations from geomorphological surveys, aerial imagery and field excursions (Luoto et al., 2004; Parviainen and Luoto, 2007; Aalto et al., 2017; Borge et al., 2017). Remote sensing studies have identified a latitudinal gradient of permafrost peatland landforms in Western Siberia, with palsas/peat plateaus occupying the boreal zone and polygon mires located in northernmost Arctic regions (Peregon et al., 2008; Terentieva et al., 2016). Fewster et al. (2020) mapped the distribution of palsas/peat plateaus in North America from published observations, although the limited availability of observational data caused some underestimation of their true distribution in Labrador (Wang et al., 2023). Similar meta-analysis techniques have recently been employed to map the circum-Arctic distribution of ice-wedge polygons, which exist in both peatland and mineral soil settings (Karjalainen et al., 2020). Since the

publication of Chapter 2 of this thesis (Fewster et al., 2022), Könönen et al. (2022) have compiled observations of palsas/peat plateaus from across the circum-Arctic, producing a mapped distribution that closely aligns with my own circum-Arctic estimate (presented later in this thesis, in Figure S2.4). Mapped estimates for the SOC stock of circum-Arctic peatlands were recently revised by Hugelius et al., (2020), who also estimated the fraction of peatland permafrost using a broad relationship with MAT. The widespread availability of published observations of permafrost peatland landforms and new datasets describing the distribution of peat SOC presents an opportunity to further investigate the modern and future climate spaces of permafrost peatlands at broad spatial scales.

1.2.2. Modern climate space of permafrost peatlands

Although several Earth system models (ESMs) now incorporate permafrost components, the latest-generation of ESMs still fail to distinguish between different permafrost forms, for example ice lenses or ice wedges (Burke et al., 2020), and peatlands remain poorly represented (Chadburn et al., 2022). To establish the climatic controls on permafrost peatlands, climate envelope models have been used to statistically relate modern climate to maps of landform distribution in Fennoscandia (Luoto et al., 2004; Fronzek et al., 2006; Parviainen and Luoto, 2007; Aalto et al., 2014, 2017) and North America (Fewster et al., 2020). For Fennoscandia, a variety of modelling techniques, spatial scales, and predictor combinations have been used to quantify the modern climate space of palsas/peat plateaus, but models consistently agree that cold, dry climates are most suitable (Luoto et al., 2004; Parviainen and Luoto, 2007; Aalto et al., 2017). Parviainen and Luoto (2007) reported that palsas/peat plateaus exist alongside a MAT range of -4.42–0.42°C and total annual precipitation of 403–868 mm yr^{-1}, while several studies have indicated an important role for seasonal climate metrics, such as thawing degree days (Luoto et al., 2004; Fronzek et al., 2006; Aalto et al., 2014). A model developed by Fewster et al. (2020) predicted that the more spatially expansive distribution of palsas/peat plateaus in North America are supported by a broader range of

suitable MATs (-11.32–0.19°C). Climate envelope models do not currently exist for other types of permafrost peatland, such as polygon mires (Figure 1.2). Limited meteorological measurements taken near polygon mires suggest that these landforms are supported by colder climates than palsas/peat plateaus (Teltewskoi et al., 2016; Wolter et al., 2016), and may therefore exhibit rapid responses to climate warming (Karjalainen et al., 2020). Furthermore, at the time of writing Chapter 2, no previous study had modelled the climate space of permafrost peatland landforms in Western Siberia, which prevented regional comparisons of their modern climatic controls and SOC stocks.

1.2.3. Changing future climate space of permafrost peatlands

Climate envelope models have simulated the past (Fewster et al., 2020) and future distribution of suitable climates for palsas/peat plateaus in specific geographic regions (Fronzek et al., 2006; Aalto et al., 2014, 2017; Könönen et al., 2022), and indicate the potential for substantial redistribution of peatland permafrost under warming climates. Using future climate projections from the second phase of the Coupled Model Intercomparison Project (CMIP), Fronzek et al. (2006) demonstrated that a 1°C temperature rise could halve the present palsa distribution in Fennoscandia and that suitable climates could disappear from the entire region by 2070–2099 under moderate to high anthropogenic emissions. Using more recent CMIP5 climate projections, Aalto et al. (2017) simulated substantial losses of suitable climate space for palsas/peat plateaus by 2040–2069 even under low warming across a smaller subregion of Fennoscandia. Since Chapter 2 was published (Fewster et al., 2022), Könönen et al. (2022) have attempted to simulate the future redistribution of suitable climates for palsas/peat plateaus across the circum-Arctic, again using CMIP5 projections, and found that moderate- to high-anthropogenic emissions could threaten 89–98 % of their suitable environmental space by 2061–2080. This finding aligns with simulations by Karjalainen et al. (2021), which showed that under a CMIP5 high emission scenario the circum-Arctic environmental space of ice-wedge polygons could more than halve by 2061–2080, although this

modelling was not specific to peatlands. At the time of writing Chapter 2 no previous study had established the climatic controls of polygon mires, modelled the modern climate spaces of permafrost peatland landforms in Western Siberia, or projected the future redistribution of suitable climates using the latest generation of global climate models, CMIP6 (Eyring et al., 2016).

CMIP6 ESMs incorporate improved climate physics that commonly project higher levels of 21st century warming than earlier CMIP generations (Zelinka et al., 2020). Additionally, CMIP6 model projections have been driven by a new suite of future emission pathways, the Shared Socioeconomic Pathway (SSP) scenarios, which are based on revised assessments of 21st century societal development and recent anthropogenic emissions (O'Neill et al., 2016) (Table 1.1). These models project that future warming is likely to occur most quickly at high northern latitudes due to polar amplification feedbacks (Davy and Outten, 2020), while Arctic precipitation is projected to both increase in volume and be more frequently unfrozen (McCrystall et al., 2021). The unprecedented rate and magnitude of 21st-century warming projected by CMIP6 ESMs suggests that previous bioclimatic modelling may have underestimated the timing and extent of near-future changes to the climate space of permafrost peatlands, which has important implications for their radiative forcing potential. Projections from climate envelope models of permafrost peatlands have also rarely been compared to maps of SOC, meaning the peatland SOC stock at risk from future, climate-induced permafrost degradation remains uncertain.

Thesis objective 1

Simulate the changing climate spaces of permafrost peatlands in Europe and Western Siberia under a range of 21st-century climate scenarios, and estimate the associated risk for present-day peatland SOC stocks (Chapter 2).

Table 1.1. Description of the four primary Shared Socioeconomic Pathway (SSP) scenarios used to drive the CMIP6 future climate projections in Chapter 2 and comparisons to CMIP5 representative concentration pathways (RCPs). Adapted from O'Neill et al. (2016, 2017).

Scenario	Description	2100 forcing (W m^{-2})	Equivalent CMIP5 iteration
SSP1-2.6	*Sustainability – Taking the green road*: Global societies move toward a more sustainable and less resource-intensive lifestyle. Mitigation strategies are aggressively implemented with few barriers to adaptation.	2.6 (low)	RCP2.6
SSP2-4.5	*Middle of the road*: Global societies, economies and technologies continue to follow recent trajectories. Sustainable development is uneven across the world, with some countries implementing stronger mitigation and adaptation strategies than others.	4.5 (medium)	RCP4.5
SSP3-7.0	*Regional rivalry – A rocky road*: Climate adaptation and mitigation is hindered by a political shift towards national and regional self-interests. Environmental issues are not an important priority for global societies. Slow economic growth restricts sustainable development.	7.0 (high)	N/A
SSP5-8.5	*Fossil-fuelled development – Taking the highway*: The economic success of industrialising nations leads to increased exploitation of plentiful natural resources. Environmental problems are solved at a local level by new technologies, with few attempts to tackle global issues. Global population reaches its peak this century.	8.5 (high)	RCP8.5

1.3. Holocene vegetation shifts in circum-Arctic peatlands

1.3.1. Peatland succession and shrubification

Once climates become unsuitable and peatland permafrost begins to degrade, the radiative forcing attributable to thawing peatlands is strongly determined by changes to the composition of peatland vegetation (Johansson et al., 2006; Holmes et al., 2022). The vegetation communities of circum-Arctic peatlands have changed through time in response to shifting climate (e.g., Magnan et al., 2018, 2022), altered hydrological conditions (e.g., Van Bellen et al., 2013; Sim et al., 2021b), and permafrost aggradation and thaw (e.g., Olefeldt et al., 2021; Treat et al., 2021b). Saturated, sedge-dominated fens exhibit increased CH_4 emissions compared to *Sphagnum*-dominated bogs and permafrost peatland landforms, such as palsas/peat plateaus, which are often considered more effective net carbon sinks (Treat et al., 2018; Holmes et al., 2022; Varner et al., 2022), although permafrost aggradation can also produce unvegetated peat surfaces that are net sources of CO_2 (Väliranta et al., 2021). Many observational studies have identified a poleward expansion of trees and woody shrubs across the Arctic tundra in recent decades due to climate warming (Elmendorf et al., 2012; Myers-Smith et al., 2015, 2020; Myers-Smith and Hik, 2018; Heijmans et al., 2022), a process termed shrubification (Mekonnen et al., 2021). These findings indicate a potential trajectory where trees and shrubs become increasingly dominant at high latitudes under future climate warming, increasing the carbon sink potential of Arctic environments, but the shrubification of peatlands remains understudied at large spatial scales. Tree and shrub growth can increase aboveground biomass in peatlands and woody detritus is slow to fully decompose (Camill et al., 2001). Conversely, trees and shrubs increase fuel availability for wildfire, which can exacerbate peat permafrost degradation through deep heating (Gibson et al., 2018) and combustion of dry peat layers (Turetsky et al., 2011, 2015). Thaw of peatland permafrost following burning can rapidly reverse hydroseral succession even under stable climates, and repeated cycles of wildfire-initiated succession are evident in Canadian peat records (Zoltai, 1993).

Previous research into circum-Arctic peatland shrubification has primarily been experimental (Holmgren et al., 2015; Limpens et al., 2021), although a recent remote sensing analysis has identified woody encroachment in a fen in the Hudson Bay Lowlands (Robinson et al., 2021). Field experiments by Limpens et al. (2021) in subarctic peatlands have shown that tree seedlings survive most effectively on the sides of hummocks and beneath shrubs, where sheltered microclimates persist, and found the presence of permafrost restricted seedling establishment. Field observations of polygon mires have similarly found woody shrubs to be most prevalent atop raised peat surfaces, for example ridges and high-centred polygons (Wolter et al., 2016), suggesting that local hydrological dynamics may exert an important control. Indeed, experiments in permafrost-free, boreal peatland settings have found that shrub and tree establishment is most successful on hummocks and following temperature increases and drought, which deepen water tables, extend growing seasons, and limit growth of competing mosses (Heijmans et al., 2013; Limpens et al., 2014b; Holmgren et al., 2015). A process-based, dynamic global vegetation model (DGVM) recently projected future shrub expansion in circum-Arctic peatlands under 21st-century climate change (Chaudhary et al., 2022), while evidence of recent, widespread peatland drying (Zhang et al., 2022) may provide suitable peat surfaces for woody encroachment. However, the spatiotemporal dynamics of recent and long-term peatland shrubification remain understudied at broad spatial scales.

1.3.2. Palaeoecology of circum-Arctic peatlands

Core-based analyses of plant macrofossils present archives for the past *in situ* composition of peatland vegetation and may be recorded for each peat layer as the dominant peat-forming vegetation, numerical counts (e.g. for seeds and fruits), or directly-comparable, relative abundances (%) of individual species or plant functional types (PFTs) (Mauquoy et al., 2010). Plant macrofossils are often sampled contiguously and dated using radioisotopes, for example radiocarbon (^{14}C) or lead-210 (^{210}Pb). Probabilistic age-depth models are then fitted to analyse vegetation change through time (e.g., Blaauw and Christen,

2011; Aquino-López et al., 2018). Despite palaeoecological analyses being time-intensive to undertake, plant macrofossils have been studied in circum-Arctic peatlands for > 25 years, meaning large numbers of published records are now available.

Compilations of plant macrofossil records have previously shown spatially-consistent trends in peatland vegetation change during the Holocene at regional (Magnan et al., 2022; Piilo et al., 2023) and hemispheric spatial scales (Treat et al., 2016, 2021b; Treat and Jones, 2018). Treat et al. (2016) classified changes in the wetland type and primary vegetation of 280 circum-Arctic peatlands based on the dominant macrofossil component (> 30 %) or lithological description of individual peat layers. This analysis showed that past permafrost aggradation in boreal and tundra sites has led to peatland vegetation communities resembling modern permafrost-free bogs and fens, respectively. Later studies that reanalysed this dataset by Treat et al. (2016) have shown that Holocene permafrost aggradation was most prevalent in circum-Arctic peatlands during neoglaciation and the Little Ice Age (Treat and Jones, 2018), and that late-Holocene FBTs and permafrost aggradation caused a ~20 % decline in CH_4 emissions. However, because this dataset only contained information for the dominant vegetation of each peat layer (Treat et al., 2016), changes to the relative composition of PFTs through time have not previously been assessed. At regional scales, compositional plant macrofossil data for the last ~200 years has been synthesised from 17 peatlands in Quebec by Magnan et al. (2022). This study identified a northwards progression of *Sphagnum* sect. *Acutifolia* under late 20th-century climate warming, but found no evidence for concurrent peatland shrubification. Piilo et al. (2023) have recently analysed plant macrofossil compositions for 16 sites in Fennoscandia and European Russia and similarly recorded consistent transitions to dry, *Sphagnum*-dominated microhabitats during recent centuries.

Despite the recent publication of several plant macrofossil catalogues, previous studies have not examined the circum-Arctic extent of Holocene peatland shrubification, which limits our understanding for how permafrost peatland vegetation may change under changing climate. Furthermore, several recent palaeoecological reconstructions have recorded late 20th-

century shrub expansion in high latitude peatlands, for example in northern Alaska (Gałka et al., 2018) and High Arctic Canada (Sim et al., 2019), but these studies are not included in existing catalogues. Given the breadth of published palaeoecological data available for circum-Arctic peatlands, the spatiotemporal dynamics of Holocene peatland shrubification should now be investigated further.

Thesis objective 2

Determine the recent and long-term spatiotemporal dynamics of peatland vegetation succession, including shrubification, across the circum-Arctic (Chapter 3).

1.4. Hydraulic properties of permafrost peatlands

1.4.1. Controls on peat hydraulic properties

Besides the succession of peatland vegetation, an important component for understanding the effect of permafrost peatland degradation on radiative forcing regards changes to peatland hydrology. In addition to strongly determining plant community composition, peat surface wetness influences near-surface peat decomposition, the relative magnitudes of plant productivity and ecosystem respiration, and CH_4 fluxes (Holden, 2006; Limpens et al., 2008; Voigt et al., 2019). A rise in the peatland water table, for example, following palsa/peat plateau thaw, increases the thickness of the anoxic zone in which peat decomposition and vascular root growth are inhibited (Clymo, 1984; van Breemen, 1995) and where restricted oxidation promotes CH_4 release (Heikkinen et al., 2002; Holmes et al., 2022). Peatland wetness is controlled by climate, peatland topography, and permafrost dynamics (Swindles et al., 2019; Zhang et al., 2022), but also peat hydraulic properties, which influence peatland groundwater flows and drainage (Ingram, 1982; Quinton et al., 2008). A pressing research gap in peatland hydrological research concerns the water retention capacity of permafrost peatlands,

specifically palsa mires, and their response to climate-induced permafrost degradation.

A hydraulic property that has been studied for several decades in peatlands is saturated hydraulic conductivity (K_{sat}), a measure of peat permeability with dimensions of L T^{-1}. Under any given hydraulic gradient, peats with low K_{sat} drain slowly, resulting in shallow water tables and increased moisture retention. Horizontal saturated hydraulic conductivity (K_h) strongly determines near-surface groundwater flows in Arctic peatlands, due to the widespread presence of impermeable permafrost (Quinton et al., 2008), while vertical saturated hydraulic conductivity (K_v) is useful for studying infiltration and atmospheric exchanges of moisture (Rycroft et al., 1975). A range of methods exist for measuring peat K_{sat} in the field (e.g., using piezometers) and in the laboratory (e.g., using permeameters or the modified cube method) (Morris et al., 2022).

Peat K_{sat} generally reduces with increasing depth, compaction (for example, dry bulk density), and degree of humification (e.g., measured using the von Post scale) (Päivänen, 1973; Morris et al., 2022). Feedbacks between K_{sat} and peat properties are closely interrelated; recently-deceased plant litter has stronger material structures and larger open pores than deeper, older peats, which have undergone prolonged decomposition and compaction. Permafrost peats are subjected to distinct climatic and ecohydrological processes that may cause differences in peat K_{sat} from boreal and temperate sites, but measurements from permafrost peatlands are spatially limited. Cold, dry climates mean permafrost peatlands experience annual freeze-thaw cycles, which have been found to generally reduce peat K_{sat} (Liu et al., 2022). Wildfires can also reduce K_{sat} in peat plateaus, through peat shrinkage and pore infilling with ash (Ackley et al., 2021). Observations of peat profile collapse following palsa/peat plateau thaw (e.g., Swindles et al., 2015) and differences in peat properties between permafrost and permafrost-free peatlands (Smith et al., 2012; Treat et al., 2016) suggest that permafrost degradation may cause important changes to peat hydraulic structures, but the impact of thaw on peat K_{sat} remains understudied.

Large-scale pedotransfer functions have recently been developed to predict peat K_{sat} based on large catalogues of published data from boreal and temperate regions (e.g., Lennartz and Liu, 2019; Liu and Lennartz, 2019; O'Connor et al., 2020; Morris et al., 2022). The most skilful of these models predict peat K_{sat} using continuous measurements of peat properties (e.g., depth, dry bulk density and degree of peat humification) and categorical descriptors (e.g., trophic type, microform and climate) (Morris et al., 2022); and evidence similar predictive power to site-specific models (e.g., Morris et al., 2019). Pedotransfer functions have the potential to improve hydrological characterisations of peatlands in ESM land surface schemes (Chadburn et al., 2022) and greatly reduce the time required for field and laboratory analyses of peat K_{sat}. However, existing large-scale models have been trained almost-exclusively on boreal and temperate peatlands, meaning their applicability in permafrost regions remains to be evaluated.

1.4.2. Peat hydraulic conductivity in permafrost regions

For permafrost peatlands, K_{sat} has been primarily measured in peat plateaus at the long-term research station at Scotty Creek, NWT, Canada (Quinton et al., 2008, 2019; Quinton and Baltzer, 2013; Nagare et al., 2013; Gharedaghloo et al., 2018; Ackley et al., 2021) and organic-rich soils (including peats) on the Alaskan North Slope (O'Connor et al., 2019, 2020). At Scotty Creek, Quinton et al. (2008) measured peat K_h using laboratory and field techniques, and made direct comparisons to tracer test measurements from organic tundra soils at Granger Creek, Yukon (Quinton et al., 2004) and Siksik Creek, NWT (Quinton et al., 2000). This between-site comparison identified similar depth profiles for near-surface permafrost peats: an upper zone (≤ 0.1 m depth) of homogeneously high K_h (1.2×10^{-4} to 1.2×10^{-2} m s^{-1}); a transitionary zone (0.1–0.2 m depth) where K_h rapidly declined with depth; and a deeper zone (≥ 0.2 m) of consistently low K_h (5.8×10^{-6} to 5.8×10^{-5} m s^{-1}) (Quinton et al., 2008, 2019). Quinton and Baltzer (2013) incorporated these measurements into simulations of peat plateau runoff at Scotty Creek, demonstrating that thaw can reduce groundwater flows by decreasing hydraulic gradients and lowering

the unfrozen, saturated zone into deep, low K_{sat} peats. Later studies have recorded similar vertical profiles of K_{sat} in peat plateaus at Scotty Creek (Nagare et al., 2013; Gharedaghloo et al., 2018; Ackley et al., 2021) and elsewhere in North America, for example, near Churchill, Manitoba (Morison et al., 2017). Alternatively, dry bulk density has been identified as a universally strong predictor of K_{sat} in organic soils on the Alaskan North Slope (O'Connor et al., 2020).

Peat hydraulic properties have been rarely measured in permafrost peatlands outside of North America (Gupta et al., 2021). For palsa mires in Fennoscandia, the only previous measurements of peat K_{sat} have been made by Wetzel et al. (2003) near Kautokeino, Norway. This study analysed nine, near-surface samples, which evidenced high peat bulk densities (up to 0.3 g cm^{-3}) and reductions to K_v with depth (3.0×10^{-6} to 2.9×10^{-4} m s^{-1}). However, no measurements currently exist for K_h in European permafrost peatlands. It therefore remains unclear whether peat properties exert similar controls on peat K_h in Fennoscandian palsa mires as in boreal and temperate peatlands, and whether existing, large-scale pedotransfer models of peat K_{sat} (e.g., Morris et al., 2022) are applicable to permafrost peatlands. Furthermore, palsa mires often contain mosaics of desiccating, albeit intact, palsas and collapsed, permafrost-free areas, which provides an opportunity to study the effect of permafrost degradation on peat hydraulic properties for the first time.

Thesis objective 3

Establish the controls on saturated hydraulic conductivity in a degrading permafrost peatland complex in northern Europe, and evaluate the predictive performance of an existing model trained on boreal and temperate peatlands (Chapter 4).

1.5. Research strategy

1.5.1. Bioclimatic modelling of permafrost peatlands (Chapter 2)

To simulate the modern and future distribution of suitable climates for palsas/peat plateaus and polygon mires in Europe and Western Siberia (thesis objective 1), I will develop climate envelope models fitted specifically to the modern distribution of each landform. To accomplish this, Chapter 2 will firstly define the distribution of extant permafrost peatland landforms across the circum-Arctic by constructing a spatial catalogue of published observations from a structured literature search. I will then use one-vs-all logistic regression modelling to establish the modern climate spaces of palsas/peat plateaus and polygon mires in Europe and Western Siberia, by statistically relating the landform distributions to modern climate. Future climate projections from 12 CMIP6 ESMs will then drive my climate envelope models to simulate the changing climate space of permafrost peatlands for each decade from the 2020s to the 2090s. These CMIP6 simulations of 21st century climate will cover four Shared Socioeconomic Pathway (SSP) scenarios: SSP1-2.6 (strong climate change mitigation), SSP2-4.5 (moderate mitigation), SSP3-7.0 (no mitigation baseline) and SSP5-8.5 (no mitigation, worst case) (Table 1.1). I will constrain my bioclimatic simulations to loci that are environmentally plausible using published maps of peatland distribution. Finally, I will compare the modern and future climate spaces of each landform to a map of peat SOC (Hugelius et al., 2020a), to estimate the risk associated with the loss of suitable climates.

1.5.2. Meta-analysis of palaeoecological records (Chapter 3)

To investigate the Holocene vegetation dynamics of circum-Arctic peatlands (thesis objective 2), I require directly-comparable palaeoecological records of past vegetation composition. To achieve this, Chapter 3 will firstly employ a meta-analysis approach to construct a catalogue of plant macrofossil relative abundance data from previously-published records from the circum-Arctic permafrost region. To ensure that the age estimation of each sample is

consistent, I will fit new age-depth models for each core using the latest IntCal20 radiocarbon calibration curve (Reimer et al., 2020) and available chronological controls, including uncalibrated radiocarbon (^{14}C) dates and lead-210 (^{210}Pb) dating. To analyse changing compositions of peatland vegetation through time, the plant macrofossil data will be grouped into four plant functional types (PFTs): woody vegetation, herbaceous taxa, *Sphagnum*, and non-*Sphagnum* mosses. I will also normalise the data in each core to magnify the direction of change in PFT abundance. To investigate spatiotemporal variation in Holocene peatland vegetation shifts, I will aggregate these palaeoecological data between sites and by geographic regions and zones of modern permafrost coverage (Brown et al., 2002). Temporal trends of peatland vegetation change will then be identified from time series of aggregated and normalised data. Lastly, I will undertake a multivariate statistical analysis to identify associations between PFTs.

1.5.3. Measuring saturated hydraulic conductivity in degrading palsas (Chapter 4)

To establish the controls on peat K_h in degrading palsas (thesis objective 3), I will firstly sample near-surface peat cores from desiccating and collapsed palsas near Rensjön, Arctic Sweden. To characterise the site, I will survey surface vegetation and active-layer thickness. In the laboratory, I will measure at continuous depth intervals within each core: peat K_h using a permeameter method; dry bulk density (g cm^{-3}); and the degree of humification (von Post score). To identify significant controls on peat K_h, I will fit a linear mixed-effects model (LMM) from continuous predictors of peat properties (depth, dry bulk density, von Post score), a categorical factor describing the stage of palsa degradation, and a random effect describing core identity. This modelling will also determine whether peat K_h differs significantly between desiccating and collapsed palsas. Lastly, I will statistically evaluate the performance of an existing pedotransfer model by Morris et al. (2022), which has been fitted to primarily temperate and boreal sites, for predicting peat K_h in degrading palsas.

1.6. Thesis structure

This thesis is broadly structured around three core research chapters (Chapters 2, 3, and 4), written in the format of journal articles to address each research objective (outlined in sections 1.2, 1.3, and 1.4, above). Each research chapter contains a focussed review of the relevant literature, a description of the methods, and an independent discussion of the results. Where appropriate, supplementary materials are presented at the end of each chapter, while supplementary data for each chapter and the supplemental age-depth models for Chapter 3 have been uploaded online alongside this thesis. Chapter 5 provides a summary of the research completed, additional context and discussion of the main findings, and an agenda for future research. As such, this thesis is structured as follows:

1. Thesis introduction
2. Imminent loss of climate space for permafrost peatlands in Europe and Western Siberia
3. Holocene vegetation dynamics of circum-Arctic permafrost peatlands
4. Controls on saturated hydraulic conductivity in a degrading permafrost peatland complex
5. Extended discussion, priorities for future research, and conclusions.

Chapter 2
Imminent loss of climate space for permafrost peatlands in Europe and Western Siberia

2.1. Abstract

Human-induced climate warming by 2100 is expected to thaw large expanses of northern permafrost peatlands. However, the spatio-temporal dynamics of permafrost peatland thaw remain uncertain due to complex permafrost-climate interactions, the insulating properties of peat soils, and variation in model projections of future climate. Here we show that permafrost peatlands in Europe and Western Siberia will soon surpass a climatic tipping point under scenarios of moderate-to-high warming (SSP2-4.5, SSP3-7.0, and SSP5-8.5). The total peatland area affected under these scenarios contains 37.0–39.5 Gt carbon (equivalent to twice the amount of carbon stored in European forests). Our bioclimatic models indicate that all of Fennoscandia will become climatically unsuitable for peatland permafrost by 2040. Strong action to reduce emissions (SSP1-2.6) by the 2090s could retain suitable climates for permafrost peatlands storing 13.9 Gt carbon in northernmost Western Siberia, indicating that socioeconomic policies will determine the rate and extent of permafrost peatland thaw.

2.2. Main

2.2.1. Introduction

Permafrost peatlands represent ~45 % (185 Gt) of the soil organic carbon (SOC) stored in northern peatlands (Hugelius et al., 2020a) and are particularly threatened by rapid 21st century climate change across the Arctic (Davy and Outten, 2020). Thawing of peatland permafrost enhances CO_2 emissions

(Voigt et al., 2019), while waterlogging from surface collapse can increase CH_4 emissions (Swindles et al., 2015). Peatland permafrost responds differently to changing climates than mineral-soil permafrost, due to the insulating properties of organic soils (Du et al., 2022), but peatlands remain poorly represented in Earth system models (Hugelius et al., 2020a). Some dynamic global vegetation models (DGVMs) have approximated permafrost distribution in peatlands using simulated soil temperatures (Chaudhary et al., 2020; Müller and Joos, 2021), but do not distinguish different permafrost forms (e.g. ice lenses or ice wedges) or their differing relationships with climate. Modelling of permafrost-temperature relationships has predicted that a warming of 2°C above preindustrial climates would thaw 700,000 km^2 of peatland permafrost along its southern limit, which would shift northern peatlands from a net carbon sink to a net carbon source (Hugelius et al., 2020a). However, the timing of such changes is highly uncertain. Furthermore, snow cover and summer rainfall are known to play important roles in determining the distribution of peatland permafrost (Seppälä, 2011; Karjalainen et al., 2020), meaning future changes to precipitation regimes must also be considered. The latest generation of global climate models (CMIP6) project substantially warmer climates by 2100 than previous generations (e.g. CMIP5) (Fan et al., 2020; Tebaldi et al., 2021), raising the pressing question of how these new projections may impact estimates of 21st century permafrost peatland thaw.

Peatland permafrost distributions can be mapped from the presence of characteristic landforms. Peat-covered frost mounds, termed palsas or peat plateaus depending on their spatial extent (Zoltai and Tarnocai, 1971), are formed through the frost heaving of segregated ice lenses and predominantly exist in regions of discontinuous permafrost (Seppälä, 2011). Further north, where permafrost is continuous, ice-wedge polygons form where extreme winter temperatures cause thermal cracking of peatland surfaces (Minke et al., 2007; O'Neill et al., 2019). Modern permafrost peatland distributions are well-constrained in Fennoscandia (Luoto et al., 2004; Fronzek et al., 2006) and Western Siberia (Peregon et al., 2008; Terentieva et al., 2016), but observations from North America are more sporadic (Zoltai et al., 2000; Fewster et al., 2020) and are absent across much of central and eastern

Siberia. We may expect these distinct ice forms, and their carbon stocks, to exhibit different responses to climate, yet large-scale, forward-looking simulations have never compared them.

Bioclimatic models fitted specifically to palsa/peat plateau distributions in Fennoscandia (Luoto et al., 2004; Fronzek et al., 2006; Parviainen and Luoto, 2007; Aalto et al., 2017) and North America (Fewster et al., 2020) suggest that these landforms occupy narrow climate envelopes of cold, dry conditions. Such models have suggested that a 1°C temperature increase could halve the present palsa extent in Fennoscandia, and that medium to high anthropogenic emissions could render the entire region climatically unsuitable for palsas by 2070–2099 (Fronzek et al., 2006). Future modelling of ice-wedge polygons, including those from non-peat soils, suggest that these ice forms are supported by intensely cold environments with < 300 mm yr^{-1} rainfall: an envelope that could halve by 2061–2080 under very high emissions (Karjalainen et al., 2020).

Anthropogenic climate change is expected to cause widespread thawing of permafrost peatlands (Fronzek et al., 2006; Chaudhary et al., 2020; Hugelius et al., 2020a). The increased warming projected by CMIP6 models suggests that previous studies may have underestimated the extent of near-future permafrost peatland degradation. Climate envelope models are powerful tools for understanding permafrost peatland responses to changing climate (Fronzek et al., 2006; Aalto et al., 2017; Fewster et al., 2020; Karjalainen et al., 2020), but such models have not yet been fitted to palsas, peat plateaus and polygon mires in Western Siberia. Here, we determine the changing climate envelopes of permafrost peatlands in Europe and Western Siberia during the 21st century, and estimate the associated risk for peat carbon stocks. To achieve this, we compiled a new dataset of permafrost peatland landforms and developed bioclimatic models which were driven by CMIP6 climate projections. We then compared our simulations to a peat carbon map (Hugelius et al., 2020a), to identify peatlands at risk under future climate change.

We used one-vs-all logistic regression modelling to establish the modern baseline (1961–1990) climate envelopes that support palsas/peat plateaus

and polygon mires in Europe and Western Siberia. We drove these bioclimate models using future climate projections from the Coupled Model Intercomparison Project phase 6 (CMIP6) (Eyring et al., 2016) for each decade from the 2020s to the 2090s, to estimate likely spatiotemporal changes in permafrost peatland climate envelopes. We combined our bioclimate projections with a map of peatland SOC (Hugelius et al., 2020a), as a measure of the risk associated with shrinking climate envelopes. CMIP6 represents the latest generation of general circulation and Earth system models, many of which provide higher estimates of climate sensitivity than previous CMIP generations (Fan et al., 2020; Tebaldi et al., 2021). We selected an ensemble of 12 independent CMIP6 models (i.e., without shared components or a common origin) (Brunner et al., 2020) (see methods). Our CMIP6 ensemble has an equilibrium climate sensitivity range of 1.9–4.8°C (median of 3.0°C) (Table S2.2). To produce 21st century climate projections, CMIP6 models were driven by Shared Socioeconomic Pathways (SSPs), a range of scenarios that span potential future societal developments and anthropogenic emissions (O'Neill et al., 2016). We selected four scenarios for analysis: SSP1-2.6 (strong climate change mitigation), SSP2-4.5 (moderate mitigation), SSP3-7.0 (no mitigation baseline) and SSP5-8.5 (no mitigation, worst-case).

2.2.2. Modern climate envelopes of permafrost peatlands

Our study presents a newly compiled, binary, 0.5° × 0.5° spatially-gridded catalogue of observed permafrost peatland landforms across the northern hemisphere, with 885 grid cells containing observed palsas/peat plateaus and 510 grid cells containing observed polygon mires (supplementary datasets S2.1 and S2.2). The majority (71 %) of gridded observations were concentrated in Europe and Western Siberia, between 25°W and 95°E (Figure S2.4). By comparison, the low density of observations in Canada, Alaska, and central and eastern Siberia suggests that the true distribution of landforms in these regions is underestimated by published records. We therefore focused on regional predictions for Europe and Western Siberia, where we have greatest confidence in the modern observed distribution of permafrost peatlands (see methods for details on the study domain).

Our climate envelope models for Europe and Western Siberia (Tables S2.3 and S2.4) showed predictive accuracies of 94 % for palsas/peat plateaus, and 96 % for polygon mires (Table S2.5), indicating that climate is the primary control of permafrost peatlands at broad spatial scales (Luoto et al., 2004; Parviainen and Luoto, 2007; Fewster et al., 2020; Karjalainen et al., 2020). Our models slightly overpredict the southern extent of observed permafrost peatland landforms (Figure 2.1a,b), which suggests that our projections of future climate space likely represent an upper limit. Our results indicate that cold, dry climates are optimal for palsa/peat plateau persistence in Europe and Western Siberia (spatial medians of 30-year mean annual temperature (*MAT*) = -4.7°C; and mean annual rainfall = 283 mm yr^{-1}) (Table S2.6). Palsas in Fennoscandia were previously identified alongside an average MAT of -2.6°C–-2.4°C during 1961–1990 (Luoto et al., 2004; Parviainen and Luoto, 2007), which suggests that Fennoscandian palsas exist under warmer climates than elsewhere, for example those in Western Siberia. Polygon mires require even colder temperatures (*MAT* = -8.3°C) and < 300 mm yr^{-1} of snowfall, which agrees with previous pan-Arctic modelling (Karjalainen et al., 2020). We estimate that 1.14 million km^2 of Europe and Western Siberia, and 34.4 Gt peat C, existed within the suitable climate envelope for palsas/peat plateaus during the modern baseline period (1961–1990); whilst 591,000 km^2, and 15.3 Gt peat C, existed within the suitable climate envelope for polygon mires (Figure 2.1).

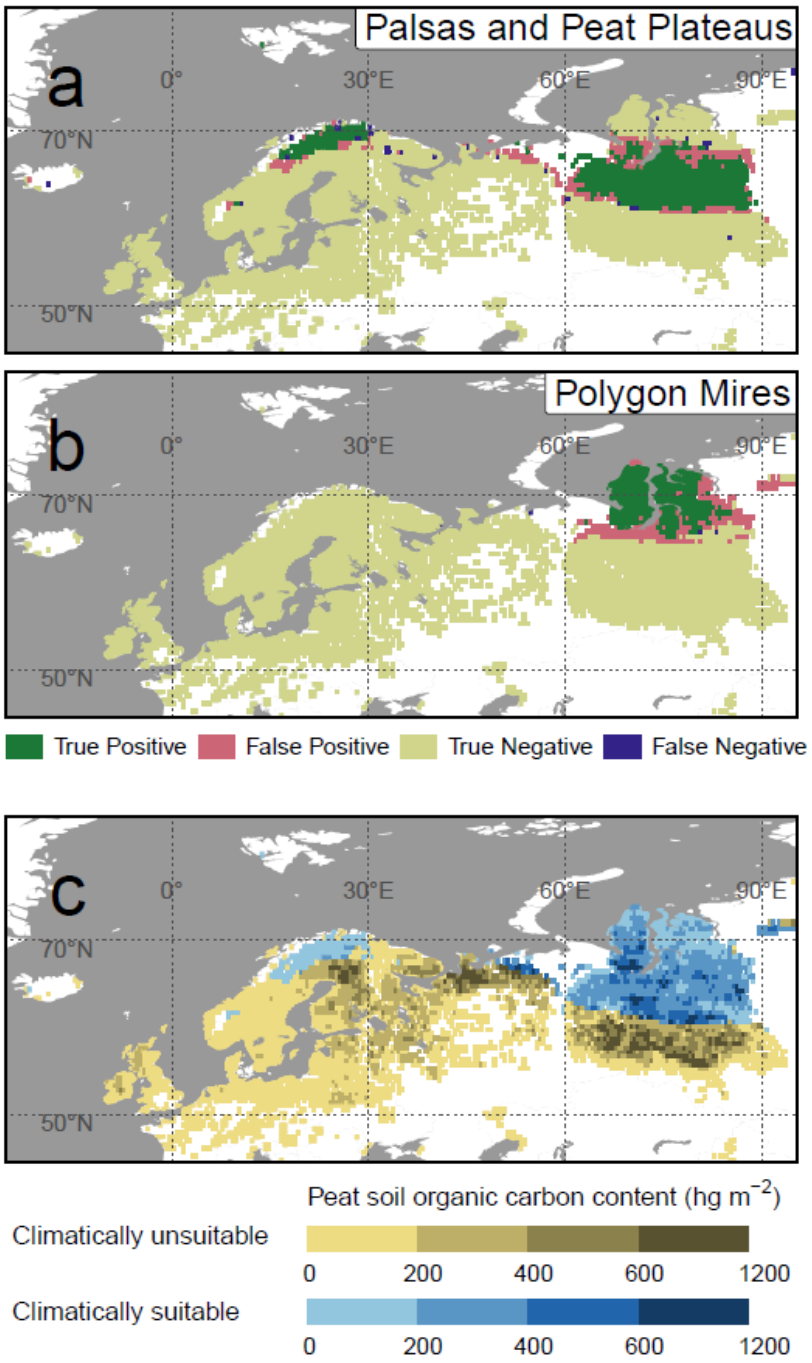

Figure 2.1. Distributions of the suitable climate space for permafrost peatlands in Europe and Western Siberia during the modern baseline period (1961–1990). Maps showing: a) the predictive performance of our palsa/peat plateau model; b) the predictive performance of our polygon mires model; and c) the distribution of gridded peat soil organic carbon content (hg m^{-2}), based on recent soil maps (Hugelius et al., 2020a, 2020b) (see methods for details) and coloured according to the predicted presence and absence of suitable climatic conditions for permafrost peatlands. For gridded peat soil organic carbon mass (Mt), see Figure S2.5. Map outlines are from Brownrigg (2022).

2.2.3. Climate space loss under the strongest mitigation scenario

SSP1-2.6 represents a low emissions pathway with strong climate mitigation policies, where global net CO_2 emissions become negative after 2075. Radiative forcing peaks and begins to decline during the late 21st century (Fan et al., 2020), reaching 2.6 W m^{-2} by 2100 (O'Neill et al., 2016). Our CMIP6 model ensemble projects an inter-model median change in *MAT* from the modern baseline period (1961–1990) of +2.8°C (interquartile range (IQR) = 1.7–3.1°C) during the 2090s under SSP1-2.6 for peatlands of Europe and Western Siberia, compared to +2.0°C (IQR = 1.7–2.5°C) globally (Table 2.1). Previous projections of peatland permafrost thaw under +0.5°C to +2.0°C equilibrium warming scenarios (Fronzek et al., 2006; Aalto et al., 2014; Hugelius et al., 2020a) therefore underestimate the levels of warming that our estimates project for the late 21st century. Where climates do become unsuitable, the insulating properties of peat soils could allow relict peatland permafrost to endure for some time, although new permafrost would no longer develop (Halsey et al., 1995; Camill and Clark, 1998).

Table 2.1. Projected regional mean annual temperatures for 2090–2099, with comparisons to the modern baseline period (1961–1990). Median projected, bias-corrected values of mean annual temperature (*MAT*) by 2090–2099; the change from the modern baseline period (1961–1990) (Δ *MAT*); and standard deviations of *MAT* across our CMIP6 model ensemble (Std. dev). *MAT* values were averaged across all grid cells that were classified to be climatically suitable for palsas/peat plateaus and polygon mires during the modern baseline period (Figure 2.2), for Fennoscandia and Russia. Our Russia region excludes the Kola Peninsula and Karelia, which are included in Fennoscandia. Antarctica is not included in CRU TS 4.04 (Harris et al., 2020), so we exclude it from our global terrestrial average. For projected changes in other relevant climate predictors, see Tables S2.7–S2.10. For details on the bias-correction of climate variables, see methods.

Scenario	*MAT* (Δ *MAT*, Std. dev) (°C)			
	Palsas/peat plateaus in Fennoscandia	Palsas/peat plateaus in Russia	Polygon mires in Russia	Global land surface, excluding Antarctica
SSP1-2.6	-0.3 (+2.6, ±1.1)	-1.6 (+3.5, ±1.3)	-4.6 (+3.7, ±1.6)	11.0 (+2.0, ±0.6)
SSP2-4.5	1.1 (+4.0, ±1.0)	-0.4 (+4.7, ±1.2)	-3.0 (+5.2, ±1.5)	12.2 (+3.3, ±0.7)
SSP3-7.0	2.7 (+5.6, ±1.3)	2.2 (+7.3, ±1.7)	0.0 (+8.2, ±1.9)	13.6 (+4.7, ±0.9)
SSP5-8.5	3.7 (+6.6, ±1.6)	4.4 (+9.5, ±2.2)	2.1 (+10.4, ±2.4)	14.6 (+5.7, ±1.3)

Under SSP1-2.6, our simulations suggest that between 1961–1990 and 2020–2029 the suitable climate envelope for palsas/peat plateaus will have contracted by 38 % or 431,000 km^2 (Figures S2.6 and S2.7). During this period, our modelling projects the envelope in Fennoscandia to have contracted by 89 % (129,000 km^2). Late 21st century cooling following a mid-century temperature peak under SSP1-2.6 will not be sufficient to re-establish suitable climatic conditions in Fennoscandia. Given the comparatively low levels of warming presented by SSP1-2.6 (Table 2.1), this suggests that permafrost peatlands in Fennoscandia are close to, or may have already

passed, a climatic tipping point. It therefore seems possible that large areas of the suitable climate space seen in the baseline period may have already been lost. Published observations indicate that palsa/peat plateau thaw has occurred throughout the late 20th century in Fennoscandia (Borge et al., 2017), with degradation accelerating at several sites from the mid-1990s (Åkerman and Johansson, 2008; Olvmo et al., 2020). Our estimates show permafrost peatlands in Fennoscandia contain substantially less SOC (1.5 Gt C) than those in Western Siberia (35.9 Gt C), but widespread thaw could also cause extensive inundation (Payette et al., 2004; Swindles et al., 2015), habitat and vegetation shifts (Treat et al., 2016; Dearborn et al., 2021), and release of dissolved organic carbon (Olefeldt and Roulet, 2012; Burd et al., 2020) and heavy metals (Klaminder et al., 2008) into aquatic systems. Ongoing ecological and hydrological changes in Fennoscandian peatlands over the coming decades will provide important early indications of likely ecosystem trajectories elsewhere across the pan-Arctic.

Our modelling projects mean losses of the palsa/peat plateau climate envelope under SSP1-2.6 of 70,000 km^2 per decade from the 2030s to the 2070s, reaching a minimum extent of 357,000 km^2 by the 2070s (Figures S2.6 and S2.7). Unlike in Fennoscandia, a partial climatic recovery in Western Siberia by the 2090s is projected to return the climatically suitable area there to 563,000 km^2, with 257,000 km^2 located further north than during 1961–1990 (Figure 2.2), covering a region currently characterised by polygon mires (Minke et al., 2007; Peregon et al., 2008). However, this median projected area is less certain than some of our other predictions because our CMIP6 12-model ensemble presents a wide range of projections for the 2090s under SSP1-2.6 (IQR = 508,000 km^2) (Figure S2.6).

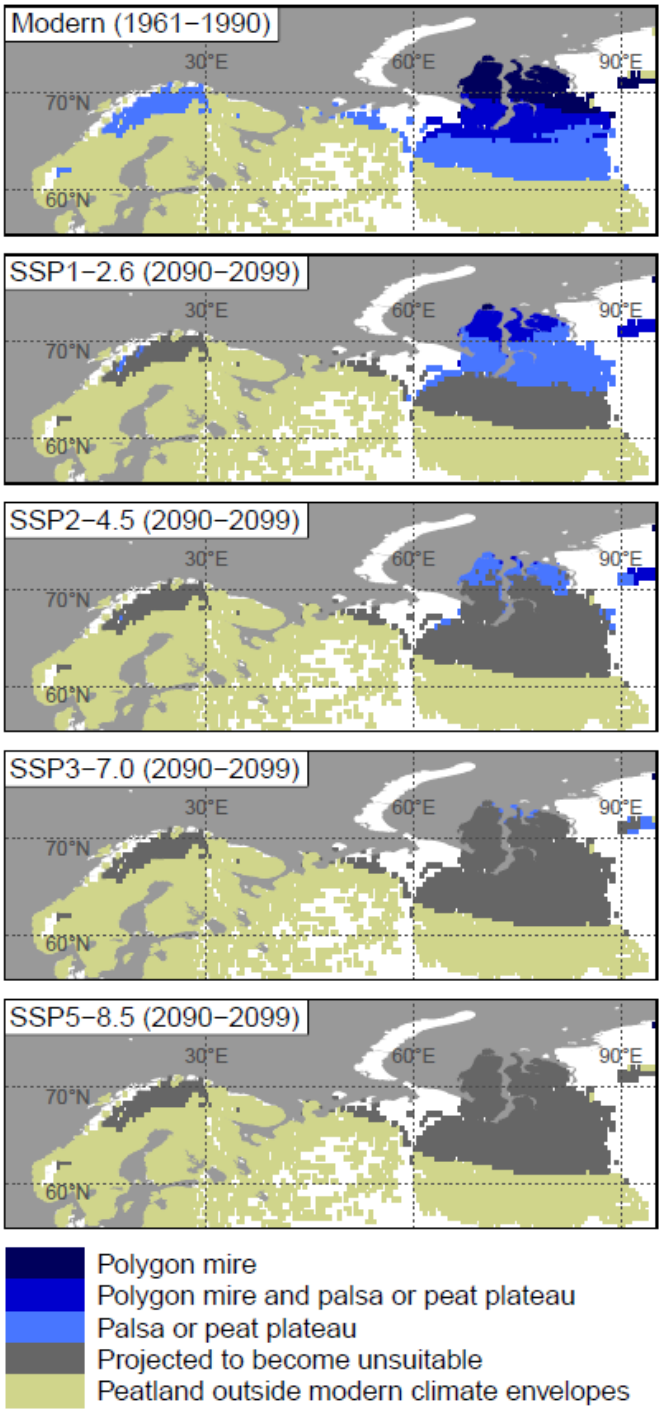

Figure 2.2. Future climate space for permafrost peatlands in Europe and Western Siberia. Projected distributions of the suitable climate envelopes for palsas/peat plateaus and polygon mires in Europe and Western Siberia during the modern baseline period (1961–1990), and during 2090–2099 under four SSP scenarios: SSP1-2.6 (strong climate change mitigation), SSP2-4.5 (moderate mitigation), SSP3-7.0 (no mitigation baseline) and SSP5-8.5 (no mitigation, worst-case). For earlier projections from 2020–2029 to 2080–2089 see Figures S2.7–S2.10. Map outlines are from Brownrigg (2022).

By the 2090s, our simulations indicate that peatlands containing 24.9 Gt SOC will no longer exist within the suitable climate envelope for palsas/peat plateaus under SSP1-2.6. An additional 7.6 Gt SOC may be affected by the temporary contraction of the climate envelope, before a partial recovery beginning in the 2080s (Figure 2.3). The resilience of permafrost peatlands to temporary periods of climatic deterioration and recovery have rarely been considered. Observations from Finland have shown palsas completely thawing in less than 10 years (Luoto and Seppälä, 2003; Seppälä, 2011), although frozen soils may persist longer where local environmental conditions offset unsuitable climates. For example, in central Canada some relict peatland permafrost has persisted since the Little Ice Age (Halsey et al., 1995; Vitt et al., 2000; Turetsky et al., 2007). Once thawed, thermokarst ponds and changing vegetation may prevent permafrost from re-aggrading for several decades, even if suitable climates return (Jorgenson et al., 2010; Magnússon et al., 2020).

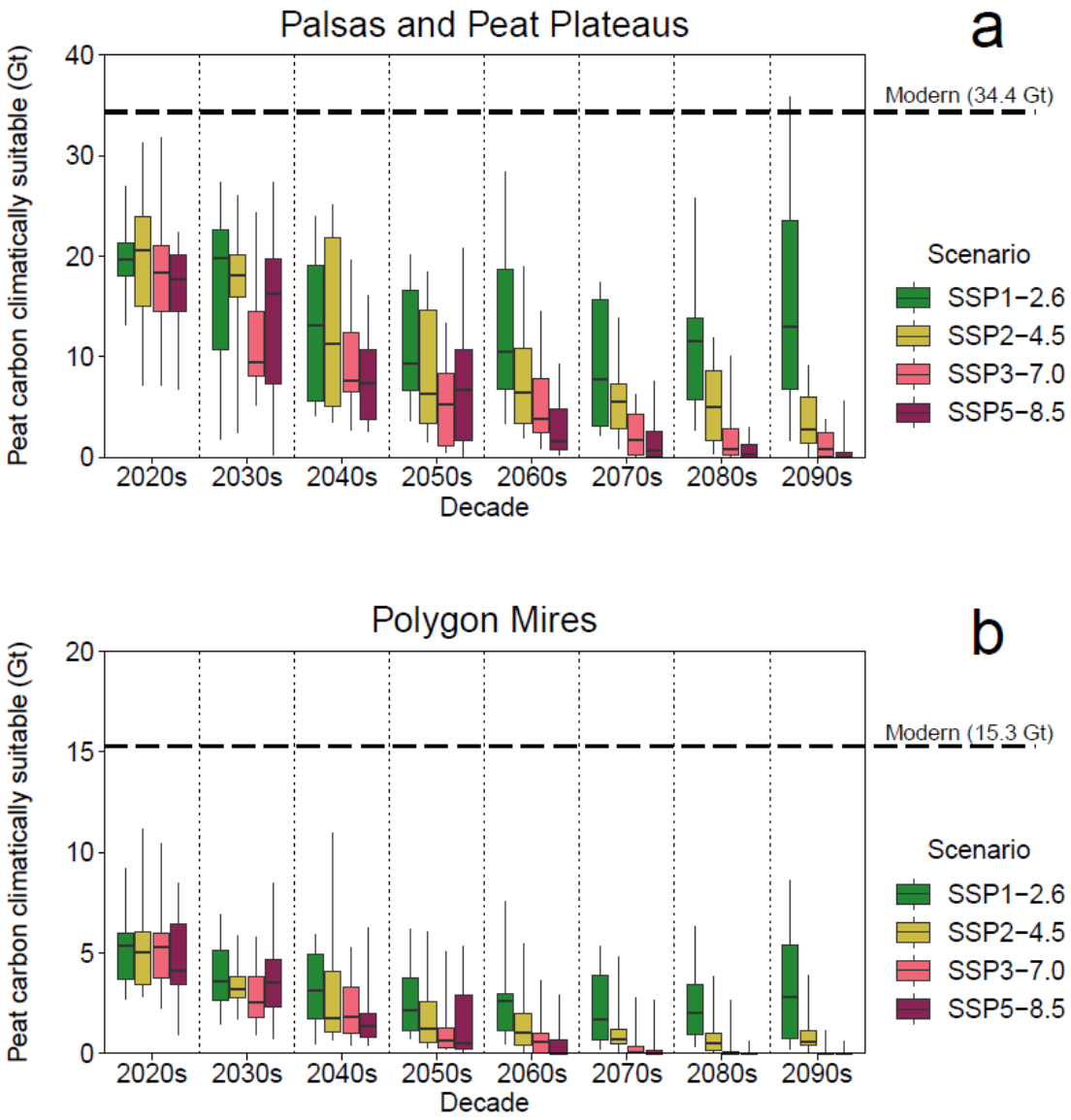

Figure 2.3. Comparisons of the total peat carbon (Gt) that is within the suitable climate envelopes for peatland permafrost in Europe and Western Siberia under four CMIP6 emission scenarios. Decadal time series showing for SSP1-2.6, SSP2-4.5, SSP3-7.0 and SSP5-8.5 the total peat soil organic carbon stock in Europe and Western Siberia that is: a) within the suitable climate envelope for palsas/peat plateaus; and b) within the suitable climate envelope for polygon mires. Whiskers indicate the full range of values from the 12 CMIP6 models in our ensemble, lower hinges indicate the 25th percentiles, upper hinges indicate the 75th percentiles, and centre lines indicate median values. Dashed lines represent the total peat soil organic carbon stock that is within the respective suitable climate envelopes during the modern baseline period (1961–1990). For comparisons of the total peatland area (km^2) that is within the suitable climate envelopes for peatland permafrost, see Figure S2.6.

Our results suggest that under SSP1-2.6 the suitable climate space for polygon mires in Western Siberia will contract to 99,000 km^2 by the 2070s, before recovering to 150,000 km^2 by the 2090s. The minimum extent reached by the 2070s represents an 83 % reduction in the modern climate envelope and would cause peatlands containing 13.7 Gt SOC to no longer exist under suitable climatic conditions for ice-wedge polygons. From the 2040s, however, the Yamal and Gyda peninsulas are predicted to fall within the northwards-moving climate envelope for palsas/peat plateaus, suggesting that new permafrost peatland landforms may begin to develop where suitable peat depths and *Sphagnum* moss communities exist (Zoltai, 1995; Fewster et al., 2020). The exact duration of palsa formation remains uncertain, but field experiments have observed nascent palsas developing after three years of snow clearances (Seppälä, 1982, 2011). Considering palsas/peat plateaus and polygon mires together, the climatic recovery projected for the 2090s under SSP1-2.6 would provide suitable climates for permafrost peatlands across 599,000 km^2, a 58 % reduction from 1961–1990. However, these suitable climate envelopes would exist further north than present, supporting Arctic peatlands that contain substantially less carbon than those at lower latitudes, because cold, dry climates have caused restricted plant productivity and peat accumulation rates there since the early-Holocene (Yu et al., 2010). These envelopes would therefore only support a combined permafrost peatland carbon stock of 14.9 Gt, a 62 % reduction from 1961–1990 (Figure 2.3).

2.2.4. Future changes under uninterrupted warming

The scenarios SSP2-4.5, SSP3-7.0 and SSP5-8.5 represent medium, high and very high 21st century emissions scenarios, resulting in global radiative forcings by 2100 of 4.5, 7.0, and 8.5 W m^{-2}, respectively (O'Neill et al., 2016). Overall, our CMIP6 climate model ensemble indicates that peatlands in Europe and Western Siberia will experience inter-model median *MAT* increases from the modern baseline period (1961–1990) to the 2090s of +4.0°C (SSP2-4.5; IQR = 3.3–4.2°C), +5.9°C (SSP3-7.0; IQR = 5.1–7.0°C), and +7.3°C (SSP5-8.5; IQR = 6.2–8.0°C), which are greater than the projected global increases

(Table 2.1). Northern high latitudes are projected to warm more quickly than other regions due to Arctic amplification (Serreze and Barry, 2011). By the 2050s, projected increases in *MAT* under SSP5-8.5 in some northern parts of Western Siberia, currently characterised by polygon mires, will surpass even the worst-case scenarios (+5.5–6°C warming) considered by recent equilibrium-climate modelling of permafrost peatlands (Hugelius et al., 2020a). Our ensemble also projects considerable increases in growing degree days, with warming winters leading to large increases in annual rainfall by the 2090s (Tables S2.8 and S2.9).

Our simulations indicate areal losses of the suitable climate envelope for palsas/peat plateaus across Europe and Western Siberia by the 2060s of 75 % (SSP2-4.5), 81 % (SSP3-7.0), and 93 % (SSP5-8.5) (equivalent to 0.85, 0.92, and 1.05 million km^2 respectively) (Figures S2.8–S2.10). By the 2090s, these projected losses have increased to 87 % (SSP2-4.5), 98 % (SSP3-7.0), and 100 % (SSP5-8.5) (equivalent to 0.99, 1.11, and 1.14 million km^2) (Figure 2.2) and the inter-model agreement is strong compared to SSP1-2.6 (Figure S2.6). Climate space is projected to contract most quickly before the 2070s. From the 2040s, suitable climates for palsas/peat plateaus are projected to be absent from Fennoscandia and persist only on the Yamal and Gyda peninsulas in Western Siberia, an area presently characterised by polygon mires (Minke et al., 2007; Peregon et al., 2008). However, continued warming under SSP3-7.0 and SSP5-8.5 would likely hinder any new palsa/peat plateau formation in these northernmost regions.

A shift towards warmer and wetter Arctic climates means that under continuous warming scenarios the modern climate envelope that supports polygon mires will have almost completely disappeared by the 2060s (with losses of 551,000–591,000 km^2, or 93–99.9 %, depending on scenario) (Figures S2.8–S2.10). By the 2090s, our simulations indicate that almost all of Europe and Western Siberia would be climatically unsuitable for permafrost peatlands under these scenarios, potentially leaving 37.0 (SSP2-4.5)–39.5 (SSP5-8.5) Gt of permafrost peatland carbon vulnerable to post-thaw decomposition (Figure 2.3). In comparison to SSP1-2.6, the combined suitable climate envelopes would support 12.1 (SSP2-4.5) to 14.9 (SSP5-8.5) Gt less

permafrost peatland carbon by the 2090s, equivalent to 61–75 % of the total carbon stored in European forests (Thurner et al., 2014).

We provide projections of the future climate spaces of palsas/peat plateaus and polygon mires in Europe and Western Siberia. Empirical modelling of ice-wedge polygons from all settings, including those formed in mineral soils, has suggested that some northern parts of Western Siberia could retain suitable climatic conditions during 2061–2080 under CMIP5's medium (RCP4.5) and very high (RCP8.5) warming scenarios (Karjalainen et al., 2020). Although this previous analysis demonstrated that ice-wedge distributions are primarily controlled by climate, these projections of suitable environmental space were also constrained by certain non-climatic predictors, including the availability of flat topography and coarse sediments (Karjalainen et al., 2020). Our modelling of broadly-equivalent CMIP6 scenarios indicates suitable climatic conditions for peatland polygons will exist only in the northernmost extremities of Western Siberia by the 2070s under medium warming (SSP2-4.5), and will be entirely absent from the region from the 2060s under very high warming (SSP5-8.5). Fennoscandia was previously projected to become climatically unsuitable for palsas during 2040–2069 under the CMIP2 scenario for very high warming (A2) (Fronzek et al., 2006), but our CMIP6 modelling now indicates that widespread losses of climate space will occur imminently even under low warming (SSP1-2.6).

2.2.5. Post-thaw possibilities for peatland carbon

Once a climatic threshold is surpassed, the presence of thick peat soils and peatland vegetation are thought to delay permafrost thaw by maintaining cool ground temperatures (Seppälä, 1986; Jorgenson et al., 2010). Local-scale negative feedbacks such as this may allow some peatland permafrost to endure for a considerable time after climates become unsuitable (Halsey et al., 1995). The magnitude of this time lag in degradation varies between years (Seppälä, 2011) and decades (Halsey et al., 1995; Mamet et al., 2017), although observations suggest that thaw rates have accelerated under recent temperature increases (Payette et al., 2004; Camill, 2005). Active-layer depths

of certain palsas/peat plateaus in northern Sweden (Åkerman and Johansson, 2008) and north-western Canada (Quinton and Baltzer, 2013) have increased at rates of 2.3–3.3 cm yr^{-1} during recent decades. Indeed, the magnitude of 21st century climate change projected by our CMIP6 model ensemble (Tables 2.1, S2.7–S2.10) may be sufficient to overcome these feedbacks, rendering climate-induced thaw of permafrost peatlands unavoidable**.** For example, the rainfall increases projected for Fennoscandia could encourage seasonal inundation, which can lead to the complete thawing of palsas within a single year and prevent refreezing (Seppälä, 2011). Future peatland permafrost thaw may occur more quickly under higher emission pathways, with our simulations showing twice as much warming in Western Siberia by the 2090s under SSP5-8.5 than under SSP2-4.5 (Table 2.1). We found no observational evidence of peatland permafrost persisting in Europe and Western Siberia under mean annual temperatures > 2.2°C during 1961–1990. However, under the SSP2-4.5, SSP3-7.0, and SSP5-8.5 scenarios only 29 %, 16 %, and 8 % of peat-containing grid cells are projected to remain below this *MAT* threshold by the 2090s.

Widespread thaw of northern permafrost peatlands will likely alter large-scale biosphere-atmosphere carbon fluxes, but the direction of the resulting radiative forcing remains an ongoing research question. On sub-decadal timescales, thaw of ice-rich palsas/peat plateaus and polygon mires often causes surface collapse and saturation as thermokarst ponds develop. Degrading permafrost peatlands can then transition into inundated Arctic fens (Swindles et al., 2015), which commonly exhibit high CH_4 emissions (Turetsky et al., 2002). If meltwaters drain away, enhanced aerobic decomposition are likely to provoke large CO_2 emissions (Schädel et al., 2016). Under warming climates, woody vegetation is expected to expand northwards (Myers-Smith and Hik, 2018), increasing the susceptibility of northern peatlands to wildfire. Active layer depths in recently burned peatlands can be 30–90 cm deeper than in neighbouring unburned sites, which can greatly increase respiration of deep peat carbon (Gibson et al., 2018, 2019), although such losses are inhibited by thermokarst (Estop-Aragonés et al., 2018). Conversely, the projected onset of warmer, wetter climates would increase plant productivity in Arctic peatlands

and eventually drive new surface peat accumulation, for example through terrestrialisation of thermokarst ponds (Payette et al., 2004; Magnússon et al., 2020), which could offset losses of deep peat carbon by 40 to > 100 % (Treat et al., 2021a).

The expected simultaneous increases to peat decomposition and accumulation make it highly unlikely that entire peatland carbon stocks would be lost following thaw. Empirical modelling of post-thaw chronosequences suggests that deep peat carbon losses by respiration would occur rapidly (e.g. < 10 years), and would take several centuries to be replaced by new peat accumulation (Jones et al., 2017; Hugelius et al., 2020a; Turetsky et al., 2020). Modelled net carbon losses only exist for a small number of sites and vary widely (-35 to +2.7 kg C m^{-2} $century^{-1}$) (Jones et al., 2017; Heffernan et al., 2020), depending on relative timings of peat initiation and permafrost aggradation (Treat et al., 2021a). An analysis of five permafrost peatland chronosequences of varying permafrost histories from Alaska and north-western Canada has reported an average net carbon loss of 19 % during the first 100 years post-thaw (Hugelius et al., 2020a; Turetsky et al., 2020), but similar analyses do not exist for peatlands in Europe or Western Siberia.

Previous hemispheric-scale modelling of CMIP5 simulations has suggested that northern peatlands will remain a weak carbon sink until the end of the 21st century (Gallego-Sala et al., 2018; Chaudhary et al., 2020; Qiu et al., 2020), but these assessments should now be revised to incorporate the climate changes projected by CMIP6 ensembles. For example, DGVM simulations forced by CMIP6 climate projections indicate that northern peatlands will become net carbon sources by 2100, even under SSP1-2.6 (Müller and Joos, 2021). Here, our own CMIP6 modelling projects imminent, widespread losses of suitable climate space for permafrost peatlands in Europe and Western Siberia, which would have important implications for the future net carbon balance of northern peatlands.

Our modelling, which uses the latest generation of CMIP6 future climate projections, suggests that the suitable climate envelopes for palsas/peat plateaus and polygon mires in Europe and Western Siberia are close to a

tipping point. We project the widespread loss of climate space in Fennoscandia within the coming decade, and across the entire study region by 2100. Under the full range of future emission pathways, only 8,000–16,000 km^2 of Fennoscandia will retain climatically suitable conditions for palsas/peat plateaus by the 2030s, a reduction of 89–94 % compared to 1961–1990. In Western Siberia, even under the most optimistic climate scenario (SSP1-2.6) 93 % of current palsas/peat plateaus and 79 % of polygon mires will fall outside their suitable climate envelope by the 2070s, as both envelopes move northwards. Further warming projected by the 2090s under SSP3-7.0 and SSP5-8.5 would cause all of Europe and Western Siberia to become climatically unsuitable for peatland permafrost. Peatlands projected to no longer climatically support permafrost by the 2090s contain 24.9 (SSP1-2.6), 37.0 (SSP2-4.5), 39.2 (SSP3-7.0) and 39.5 (SSP5-8.5) Gt peat C. The onset of substantially warmer, wetter climates at these sites could accelerate permafrost thaw and exacerbate greenhouse gas emissions. However, probable increases in plant productivity and peat accumulation mean that the net effect upon radiative forcing warrants further investigation. SSP1-2.6, characterised by strict climate change mitigation, is the only scenario where our models project a partial recovery of the suitable climate envelope for palsas/peat plateaus by 2100.

2.3. Methods

2.3.1. Catalogue of Permafrost Peatland landforms

We collated all recorded locations of palsas/peat plateaus and polygon mires across the northern hemisphere using a structured literature search (supplementary dataset S2.1). We searched for the terms “palsa”, “peat plateau”, “polygon mire”, “high-centre polygon”, “low-centre polygon”, and “permafrost peatland” alongside the names of selected regions (e.g. “Fennoscandia), countries (e.g. “Canada”), states (e.g. “Alaska”), Russian federal subjects (e.g. “Yamalo-Nenets Autonomous Okrug”), provinces and territories (e.g. “Quebec”) in Google Scholar. Other permafrost peatland types,

such as permafrost fens (Olefeldt et al., 2013), have been less readily observed and were not considered here. We prioritised research literature for which permafrost peatlands were the primary focus, but also scrutinised broader research publications that provided sufficient evidence to determine the type and location of individual landforms. Terminologies vary between regions, so where possible we used site descriptions and photographs to verify permafrost peatland classifications. The terms “palsa” and “peat plateau” are used interchangeably by some authors, so we combined these landforms into a single category. The focus of our study is permafrost peatlands. We did not consider permafrost landforms in non-peat soils (for example lithalsas, mineral palsas, or ice-wedge polygons in mineral soils) because such landforms are likely to respond differently to modern climate (Pissart, 2002; Wolfe et al., 2014).

The original coordinates of each site were converted to a 0.5° × 0.5° spatial resolution, to match the spatial grid of the modern baseline climate data (see below) (supplementary dataset S2.2). Sources varied in spatial resolution from site-specific studies to gridded 0.5° supervised classifications. Where landforms were reported without exact coordinates, we used site maps to record their location as the nearest 0.5° grid cell. Distributions of permafrost peatland landforms appear to be more fully defined in Fennoscandia, Western Siberia, and northern Alaska due to the availability of broad-scale gridded datasets (Luoto et al., 2004; Peregon et al., 2008; Terentieva et al., 2016; Lara et al., 2018), which were lacking for Canada, and eastern and central Siberia. Polygon mire presence in northern Alaska was principally identified using a remotely-sensed classification of polygonal tundra (Lara et al., 2018), with the presence of peat verified by local surface lithology descriptions (Jorgenson and Grunblatt, 2013). Our final catalogue presents a binary map for the presence of palsas/peat plateaus and polygon mires across the northern hemisphere. Our catalogue expands on the North American catalogue of palsas/peat plateaus by Fewster et al. (2020), with 1,199 additional sites from Europe and Siberia, and 553 observations of polygon mires from across the pan-Arctic (2,102 total sites) (see Figure S2.4 and supplementary dataset

S2.1). We set the southern limit of our study domain to be 44°N to encompass all observed permafrost peatland landforms.

2.3.2. Modern Distribution of Northern Peatlands

To estimate the modern distribution of northern peatlands, we primarily used the PEATMAP database (Xu et al., 2018). PEATMAP shapefiles were rasterised, reclassified, and sampled in ArcMap v.10.6.1 (ESRI, 2018) to produce a binary map of peatland presence/absence for each 0.5° × 0.5° grid cell north of 44°N. We improved our estimate of modern peat coverage in northern Alaska using the peat distribution map constructed by Fewster et al. (2020), and reclassified a small portion of grid cells that were classified as non-peat containing by these peatland maps, but which contained observations of palsas/peat plateaus or polygon mires.

2.3.3. Study Domain

Our study domain consists of European and Western Siberian peatlands, which we define as all terrestrial 0.5° × 0.5° grid cells that contain evidence of peat, and which are located north of 44°N and between 25°W and 95°E (4,615 grid cells in total). We focused our analyses on Europe and Western Siberia because the spatial extents of palsas, peat plateaus and polygon mires are much better constrained here than in other northern areas. Our study domain omits most of central Siberia, and all of eastern Siberia. Our literature search returned only 10 observations of permafrost peat landforms east of 95°E, which we believe severely underestimates their true extent. Although the number of records in Canada and Alaska was higher (367 grid cells contained permafrost peatland observations), the density of these observations was low compared to Europe and Western Siberia (where 934 grid cells contained permafrost peatland observations) and their distribution was patchy (Figure S2.4). Previous broad-scale mapping products indicate that several parts of Canada that lack observations are extensively covered by peatlands (Xu et al., 2018) and permafrost (Brown et al., 2002), suggesting that the locations of

some permafrost peatland landforms in North America are missing from published records (Fewster et al., 2020). For this reason, our study domain also omits North America. We only considered grid cells in Europe and Western Siberia that presently contain peat, because any new peat deposits that form outside of this domain are unlikely to reach a sufficient thickness to support permafrost peatland landforms before 2100. The remaining 4,615 grid cells in our study domain therefore represent plausible locations for permafrost peatland landforms to exist during the 21st century.

2.3.4. Estimation of Northern Peatland SOC stocks

We analysed the soil organic carbon (SOC) maps of histels and histosols by Hugelius et al. (2020) in QGIS v.3.12 (QGIS.org, 2020) to produce gridded estimates of peatland soil carbon (available from: https://bolin.su.se/data/hugelius-2020). These maps combined core-based analyses with machine-learning methods and showed greater spatial coverage than previous products (Hugelius et al., 2013). The maps estimate that histosols north of 23°N contain 230 ± 81 Gt SOC, whilst histels contain 185 ± 66 Gt SOC (see Hugelius et al. (2020) for details on agreement with previous estimates). These SOC stocks have high associated uncertainties caused by high spatial variation in peat depths and sampling densities, but represent the best gridded estimates of northern peat carbon currently available. Although histel and histosol maps include peatlands, they may also include other organic soils, such as mucks that are more heavily decomposed than peat (Everett, 1983). To improve confidence in our estimates, we therefore used our mapped extent of northern peatlands (described above) to only calculate SOC values for grid cells that are known to contain peat. This does necessarily assume that for grid cells where peat is present, the carbon mass of histosols and histels refers solely to peat soils, which may lead to some overestimation where non-peat organic soils are also present.

To estimate the peat soil organic carbon mass (SOCM) (hg) of each 0.5° grid cell, we first converted the soil organic carbon content (SOCC) (hg m^{-2}) maps by Hugelius et al. (2020) from rasters to polygons, and intersected any

polygons that extended across more than one grid cell. We calculated the surface area of each SOCC polygon and grid cell using the data's original World Azimuthal Equidistant projection. We then multiplied the surface area of each polygon by its SOCC and aggregated these values to the 0.5° grid cell in which they were located. To provide SOCC estimates at 0.5° spatial resolution, we divided our gridded estimates for SOCM by the surface area of each 0.5° grid cell. SOC data were available for all 4,615 peat containing grid cells in our study area for Europe and Western Siberia, equating to a total SOC stock of 141.1 Gt.

2.3.5. Modern climate data

We used a custom Python script (available from https://github.com/refewster/Imminent-loss-of-climate-space-for-Eurasian-permafrost-peatlands-) to extract and average mean monthly temperature and precipitation values during 1961–1990 from the gridded CRU TS 4.04 climatology (Harris et al., 2020) to represent modern baseline climate. We selected the period 1961–1990 to reduce any disequilibrium (Halsey et al., 1995) between landform distributions and the modern climate data, because the magnitude of anthropogenic climate change was less than at present (Fewster et al., 2020). The use of an earlier time period was deemed unsuitable because climate station coverage at high latitudes increased substantially during the second half of the 20th century, particularly in Eastern Europe and the Arctic where several regions previously lacked observational precipitation data (Harris et al., 2020). Furthermore, previous climate envelope modelling of North American palsas/peat plateaus found models fitted to climate data from 1961–1990 performed better than equivalent models fitted to general circulation model (GCM) simulations of preindustrial climate (Fewster et al., 2020). We obtained modern baseline climate data for all 4,615 grid cells within our study domain.

2.3.6. Future climate simulations

We obtained projected decadal 21st century climate projections from an ensemble of 12 GCMs included in the Coupled Model Intercomparison Project 6 (CMIP6) (Eyring et al., 2016), to represent future climates. To build our ensemble, we selected one CMIP6 GCM from each of the model groupings by Brunner et al. (2020) to ensure that our GCMs were independent from one another (i.e., without shared components or a common origin). Where multiple candidate GCMs were available, we selected the model from each grouping which displayed the highest native spatial resolution, and which simulated historical climates for our study region that most closely reproduced the mean temperature and precipitation values from our modern observational climatology for the period 1961–1990 (see above). Some CMIP6 models have a very high equilibrium climate sensitivity (ECS) of > 5°C, but none of these models were chosen by our model selection criteria and they were therefore not included in this study. Some studies have shown that CMIP6 model ensembles project lower warming when constrained by historical observational trends (Tokarska et al., 2020) or model weighting metrics (Brunner et al., 2020), but such constraints were not applied to our simulations. We obtained our CMIP6 climate projections from the Earth System Grid Federation (https://esgf-node.llnl.gov/search/cmip6/). Our final ensemble has an equilibrium climate sensitivity range of 1.9–4.8°C (median of 3.0°C) (Table S2.2), which closely aligns with the IPCC Assessment Report 6 “very likely” range of 2.0–5.0°C (best estimate = 3.0°C) (Forster et al., 2021). Our ensemble presents greater warming than CMIP5 ensembles, but slightly less warming than if all CMIP6 models were included (Flynn and Mauritsen, 2020).

We used a custom Python script (available from https://github.com/refewster/Imminent-loss-of-climate-space-for-Eurasian-permafrost-peatlands-) to extract and average projected mean monthly temperature and precipitation values for each decade during 2020–2099. We first converted temperature values from Kelvin (K) to degrees Celsius (°C) and converted precipitation values from mean precipitation flux (kg m^{-2} s^{-1}) to mean monthly totals (mm). We then downscaled and bias-corrected CMIP6 outputs to a 0.5° × 0.5° spatial resolution, following an almost identical method to

(Morris et al., 2018). This downscaling procedure retains terrestrial climates for islands and coastlines by initially extrapolating terrestrial climate data across the domain using a Poisson equation solver with overrelaxation. To downscale our climate data to a 0.5° × 0.5° spatial resolution, we favoured the use of bilinear interpolation over the bicubic spline approach used by Morris et al. (2018), because this approach is more widely used in climate science, and because bicubic interpolation can cause unrealistically high climatic variability (Latombe et al., 2018). We then used the CRU TS 4.04 land-sea mask to remove all oceanic 0.5° grid cells, resulting in an output that matched the spatial domain of the modern baseline climate data. We corrected for spatial biases in our downscaled CMIP6 future climate projections, again using the method of Morris et al. (2018). For temperature, we calculated the anomaly in simulated temperatures between the historical (1961–1990) and future time periods (from 2020–2029 to 2090–2099), and added this anomaly to the relevant observational mean (covering 1961–1990). For precipitation, we multiplied our simulated future precipitation values by a correction factor, derived from simulated and observational precipitation values for the historical baseline period (1961–1990) (see Morris et al. (2018) for full details).

2.3.7. Statistical Modelling and Evaluation

We fitted two climate envelope models to statistically predict the modern baseline (1961–1990) and future distributions of climates suitable for palsas/peat plateaus and polygon mires in Europe and Western Siberia (see above for study domain details). We used one-vs-all (OVA) binary logistic regression to fit our climate envelope models, where the two landform classes (palsas/peat plateaus, and polygon mires) were considered as a separate binary response (Galar et al., 2011). Logistic regression models relate binary observations to continuous predictors and have previously predicted palsa/peat plateau distributions in North America (Fewster et al., 2020) and Fennoscandia (Luoto et al., 2004). Multinomial logistic regression was unsuitable for this purpose because this method requires mutually exclusive classes (Petrucci, 2009) and our study domain included 76 grid cells where both palsas/peat plateaus and polygon mires were present. We then drove our

climate envelope models with projections of future climate from 12 CMIP6 models (Table S2.2) and calculated the median agreement of predicted presence/absence.

To fit our bioclimatic models, we selected five candidate climate variables that have previously been linked to permafrost peatland distributions in Fennoscandia (Luoto et al., 2004; Fronzek et al., 2006, 2011; Parviainen and Luoto, 2007; Aalto and Luoto, 2014; Aalto et al., 2017) and North America (Fewster et al., 2020): mean annual temperature (*MAT)*; annual temperature range *(TRANGE)*; growing degree days (GDD_5); rain precipitation (*RAINFALL*); and snow precipitation (*SNOWFALL*) (see Table S2.11 for variable descriptions). We calculated each climate variable from mean monthly temperature and precipitation values, following Fewster et al. (2020). We did not constrain our modelling with other non-climatic factors, such as the composition of peatland vegetation or peat cover thickness, because suitable geospatial data were unavailable. Multicollinearity was evident in our modern baseline climate dataset, with all five climatic predictor variables found to be significantly correlated with one another ($p < 0.025$) according to a Spearman's Rank correlation matrix (Table S2.12). Multicollinearity of climatic predictors was present in grid cells with and without landform observations (Tables S2.13 and S2.14). Whilst climate variables are often highly correlated, the presence of multicollinearity means that individual predictor coefficients in our models should be interpreted with caution, even if the model predictions as a whole can be considered robust (Graham, 2003). Additionally, strong correlations between predictors can, in some cases, cause significant predictors to be incorrectly excluded during model calibration and can impact model performance where predictions are extrapolated to a different time or place (Dormann et al., 2013; Graham, 2003). To limit multicollinearity, we omitted several similar variables from our modelling at an early stage. The frost number (*FROST*) has previously been linked to permafrost distributions at broad spatial scales (Anisimov and Nelson, 1997), but was too closely correlated with *MAT* for both variables to be included reliably. We experimented with preliminary models fitted with each variable separately and found that those models that included *MAT* consistently outperformed those fitted with *FROST*.

Furthermore, we included seasonal rather than annual precipitation metrics so that the insulating properties of snow cover (Aalto et al., 2017) and dry soils (Seppälä, 2011) could be represented individually in our modelling. Cross-validated evaluation statistics, generated by splitting the data randomly into separate calibration and evaluation subsets, are almost identical to those from models fitted to the full domain (Table S2.5), giving us confidence in the predictive capabilities of our final models (see below for full details).

We fitted our logistic regression models (Tables S2.3 and S2.4) in IBM SPSS Statistics 23 following the method of Fewster et al. (2020). We entered all five climatic predictors simultaneously (block entry), alongside the squared form of each variable (*MAT**, $TRANGE^2$, $RAINFALL^2$, $SNOWFALL^2$ and GDD_5^2). We calculated *MAT** as the product of *MAT* and its absolute value, |*MAT*|, to retain the sign of negative temperatures in its quadratic term. We sequentially removed non-significant pairs of predictors (e.g., *TRANGE* and $TRANGE^2$) using a stepwise backwards-deletion approach, until all remaining untransformed predictors significantly contributed to the model's predictive performance (based on deviance scores). Where untransformed predictor variables were found to be significant predictors of landform presence, we retained their quadratic terms irrespective of their significance, because previous studies have shown that permafrost peatland landforms exist within optimum climatic windows and do not relate linearly to climate (Luoto et al., 2004; Fewster et al., 2020). We used Bonferroni correction to select a stricter significance criterion for predictor removal (Student's t; $p < 0.025$ threshold) than Fewster et al., (2020), to limit the occurrence of Type I errors (i.e., non-significant variables falsely appearing to be significant) when fitting two models to the same training set (Armstrong, 2014). We then tested the addition of several first-order interaction terms (i.e., two variables multiplied together to form a single, combined predictor). To prevent spurious predictions where future climates exceeded modern climatic ranges, we added a plausibility criterion to nullify model predictions in grid cells where *RAINFALL* exceeded 1,500 mm yr^{-1}, which is more than twice the maximum rainfall (729 mm yr^{-1}) under which palsas/peat plateaus or polygon mires presently exist (Fewster et

al., 2020). We calculated standardised parameter coefficients (β_s) for each predictor variable following Menard (2011).

To make predictions with a logistic regression model, the continuous response variable (predicted probability) is classified into a binary prediction of presence/absence according to a threshold probability, which we refer to as the classification threshold. Positive cases (observations of landform presence) in our training set for Europe and Western Siberia were relatively rare (only 934 or 20 % of the 4,615 grid cells contained permafrost peatland landforms). We therefore selected an optimised classification threshold for each of our models that maximised model informedness (see below), a metric that is unaffected by case prevalence (Powers, 2011; Fewster et al., 2020). Our final climate envelope model for palsas/peat plateaus has an optimised classification threshold of 0.273, and our model for polygon mires has an optimised classification threshold of 0.130 (outputs shown in Figures 2.1 and 2.2).

We evaluated the predictive classifications of our logistic regression models using three complementary evaluation metrics: accuracy, informedness, and the area under the curve (AUC) of a receiver operating characteristic plot (Powers, 2011; Fewster et al., 2020) (Table S2.5). Accuracy evaluates the proportion (0–1) of correctly classified cases (both presence and absence) (Powers, 2011). Informedness evaluates both presence and absence to assess how informed a model's prediction is compared to chance, and how consistently a model can correctly predict a case, with values ranging from 1 (all cases classified correctly) through 0 (random predictions) to -1 (all cases classified incorrectly) (Powers, 2011). AUC is also unaffected by case prevalence but compares predictions across all possible classification thresholds, with scores ranging from 0.5 (random classification) to 1 (perfect classification) (Pearce and Ferrier, 2000).

To assess the predictive performance of our climate envelope modelling for predicting data points outside of the model calibration setting, we used five-fold cross-validation. We split our modern climate dataset into five random subsets of similar size. For palsas/peat plateaus and polygon mires in turn, we

used four subsets to calibrate a model, which we then used to predict landform presence/absence in a fifth, unused validation subset. From this prediction, we calculated model accuracy, informedness, and AUC. We repeated this process five times for palsas/peat plateaus and polygon mires respectively, each time omitting a different subset from the calibration set to be used for model evaluation. We then used these validation set predictions to calculate the cross-validated mean and standard error of each performance metric for each model type (palsas/peat plateaus and polygon mires) (Table S2.5). Final parameter estimates for both climate envelope models were calibrated from the full modern climate dataset, and not from cross-validation subsets.

2.4. Acknowledgements

R.E.F. is in receipt of a UK Natural Environment Research Council Training Grant (NE/S007458/1). A.P. is grateful for support of the Russian Science Foundation, grant 20-67-46018. The work of A.P. was carried out according to the State assignment of ISSA SB RAS. C.J.S. was supported by a NERC/IIASA Collaborative Research Fellowship (NE/T009381/1).

2.5. Supplementary material for Chapter 2

Table S2.2. General circulation models included in our CMIP6 model ensemble. Outputs from these models were used to represent future climates. Transient climate response (TCR) (°C) and equilibrium climate sensitivity (ECS) (°C) scores are taken from Meehl et al. (2020).

Model	TCR (°C)	ECS (°C)
INM-CM5-0	-	1.9
CAMS-CSM1-0	1.7	2.3
MIROC6	1.6	2.6
GFDL-ESM4	1.6	2.6
MPI-ESM1-2-HR	1.7	3.0
FGOALS-f3-L	2.1	3.0
BCC-CSM2-MR	1.7	3.0
MRI-ESM2-0	1.6	3.2
IPSL-CM6A-LR	2.3	4.6
ACCESS-CM2	2.1	4.7
CESM2-WACCM	2.0	4.8
CNRM-CM6-1	2.1	4.8

Table S2.3. Summary of the logistic regression model which describes the modern climate envelope of palsas/peat plateaus in Europe and Western Siberia. *βs* are standardised coefficients, according to the method of Menard (2011).

Variable	Coefficient	Standard error	*βs*	*t*	Significance
Constant	7.091×10^{1}	8.719	-	8.133	< 0.001
MAT	-4.616	3.369×10^{-1}	-9.708×10^{-1}	-13.703	< 0.001
*MAT**	3.030×10^{-1}	2.286×10^{-2}	5.251×10^{-1}	13.254	< 0.001
TRANGE	-4.371	3.863×10^{-1}	-1.493	-11.314	< 0.001
$TRANGE^2$	4.221×10^{-2}	3.941×10^{-3}	7.948×10^{-1}	10.709	< 0.001
GDD_5	2.232×10^{-2}	2.871×10^{-3}	6.646×10^{-1}	7.776	< 0.001
GDD_5^2	-7.653×10^{-6}	1.013×10^{-6}	-9.621×10^{-1}	-7.556	< 0.001
RAINFALL	-1.169×10^{-1}	1.930×10^{-2}	-1.290	-6.054	< 0.001
$RAINFALL^2$	1.998×10^{-5}	4.760×10^{-6}	4.394×10^{-1}	4.198	< 0.001
SNOWFALL	-2.291×10^{-2}	4.850×10^{-3}	-9.405×10^{-2}	-4.723	< 0.001
$SNOWFALL^2$	1.925×10^{-5}	6.961×10^{-6}	4.777×10^{-2}	2.765	0.006
RAINFALL × *TRANGE*	3.804×10^{-3}	5.299×10^{-4}	4.266×10^{-1}	7.179	< 0.001

Table S2.4. Summary of the logistic regression model which describes the modern climate envelope of polygon mires in Europe and Western Siberia. *βs* are standardised coefficients, according to the method of Menard (2011).

Variable	Coefficient	Standard error	*βs*	*t*	Significance
Constant	-3.066×10^{1}	3.372	-	-9.092	< 0.001
MAT	-6.739	5.384×10^{-1}	-9.316×10^{-1}	-12.517	< 0.001
*MAT**	3.865×10^{-1}	3.251×10^{-2}	4.404×10^{-1}	11.888	< 0.001
SNOWFALL	6.271×10^{-2}	2.122×10^{-2}	1.693×10^{-1}	2.955	0.003
$SNOWFALL^2$	-2.153×10^{-4}	4.905×10^{-5}	-3.512×10^{-1}	-4.388	< 0.001

Table S2.5. Cross-validated model performance statistics and optimised classification thresholds for our climate envelope models of palsas/peat plateaus and polygon mires for Europe and Western Siberia (from 25°W to 95°E). Mean values (and standard errors) for each evaluation metric were calculated from predictions generated from five validation subsets. We optimised the classification thresholds for each model, because of the imbalance of landform presence and absence in our training datasets (see methods for further details).

Metric	Palsas/peat plateaus	Polygon Mires
Accuracy	94.1 % (± 0.004)	96.1 % (± 0.005)
Informedness	0.886 (± 0.006)	0.936 (± 0.003)
AUC	0.982 (± 0.002)	0.991 (± 0.002)
Optimised classification threshold	0.273	0.130

Table S2.6. Predicted climate envelopes for palsas/peat plateaus and polygon mires in Europe and Western Siberia (from 25°W to 95°E), estimated using our logistic regression models (Tables S2.3 and S2.4) for the modern baseline period (1961–1990). Spatial minima, medians and maxima are presented, calculated from climatically suitable grid cells. Hyphens represent non-significant climate variables.

Climate Envelope		*MAT* (°C)	*TRANGE* (°C)	GDD_5 (°C days)	*RAINFALL* (mm yr^{-1})	*SNOWFALL* (mm yr^{-1})
Palsas/peat plateaus	Min	-9.4	11.6	0	141	130
	Median	-4.7	38.2	1246	283	222
	Max	2.6	43.5	1672	471	751
Polygon Mires	Min	-12.1	-	-	-	108
	Median	-8.3	-	-	-	209
	Max	-5.2	-	-	-	297

Table S2.7. Median projected values of regional annual temperature range (*TRANGE*) by 2090–2099; the change from the modern baseline period (1961–1990) (Δ *TRANGE*); and standard deviations of *TRANGE* across our CMIP6 model ensemble (Std. dev). *TRANGE* values were averaged across all grid cells that were classified to be climatically suitable for palsas/peat plateaus and polygon mires during the modern baseline period (Figure 2.2), for Fennoscandia and Russia. Our Russia region excludes the Kola Peninsula and Karelia, which are included in Fennoscandia.

Scenario	*TRANGE* (Δ *TRANGE*, Std. dev) (°C)		
	Palsas/peat plateaus in Fennoscandia	Palsas/peat plateaus in Russia	Polygon mires in Russia
SSP1-2.6	27.1 (-0.7, ±1.9)	37.9 (-0.6, ±1.7)	35.5 (-1.4, ±2.1)
SSP2-4.5	26.5 (-1.3, ±1.9)	37.3 (-1.2, ±1.5)	35.1 (-1.7, ±1.7)
SSP3-7.0	25.6 (-2.2, ±2.2)	36.1 (-2.3, ±2.4)	33.1 (-3.7, ±2.4)
SSP5-8.5	26.2 (-1.6, ±2.0)	35.0 (-3.5, ±3.0)	32.6 (-4.2, ±3.6)

Table S2.8. Projected regional growing degree days (GDD_5) for 2090–2099, with comparisons to the modern baseline period (1961–1990). See Table S2.7 caption for full details.

Scenario	GDD_5 (Δ GDD_5, Std. dev) (°C days)		
	Palsas/peat plateaus in Fennoscandia	Palsas/peat plateaus in Russia	Polygon mires in Russia
SSP1-2.6	1419 (+496, ±208)	1615 (+322, ±160)	1249 (+428, ±168)
SSP2-4.5	1639 (+716, ±155)	1876 (+583, ±213)	1442 (+621, ±209)
SSP3-7.0	1892 (+968, ±227)	2167 (+874, ±307)	1648 (+827, ±241)
SSP5-8.5	1970 (+1046, ±349)	2591 (+1298, ±425)	2049 (+1227, ±391)

Table S2.9. Projected regional rainfall for 2090–2099, with comparisons to the modern baseline period (1961–1990). See Table S2.7 caption for full details.

Scenario	*RAINFALL* (Δ *RAINFALL*, Std. dev) (mm yr^{-1})		
	Palsas/peat plateaus in Fennoscandia	Palsas/peat plateaus in Russia	Polygon mires in Russia
SSP1-2.6	357 (+69, ±27)	317 (+35, ±29)	230 (+33, ±20)
SSP2-4.5	407 (+118, ±29)	362 (+80, ±34)	250 (+53, ±37)
SSP3-7.0	445 (+156, ±39)	374 (+91, ±39)	308 (+111, ±48)
SSP5-8.5	472 (+183, ±58)	418 (+136, ±52)	328 (+131, ±58)

Table S2.10. Projected regional snowfall for 2090–2099, with comparisons to the modern baseline period (1961–1990). See Table S2.7 caption for full details.

Scenario	*SNOWFALL* (Δ *SNOWFALL*, Std. dev) (mm yr^{-1})		
	Palsas/peat plateaus in Fennoscandia	Palsas/peat plateaus in Russia	Polygon mires in Russia
SSP1-2.6	243 (-29, ±25)	234 (+14, ±25)	224 (+15, ±21)
SSP2-4.5	243 (-30, ±17)	219 (-1, ±22)	233 (+24, ±21)
SSP3-7.0	233 (-40, ±22)	226 (+6, ±22)	225 (+16, ±26)
SSP5-8.5	233 (-39, ±27)	217 (-3, ±33)	215 (+6, ±34)

Table S2.11. Description of candidate climate variables.

Variable	Description	Units
Mean annual temperature (*MAT*)	Average annual air temperature	°C
Temperature range (*TRANGE*)	Difference between maximum and minimum monthly air temperatures	°C
Growing degree days (GDD_5)	Annual time integral of monthly air temperatures above 5°C	°C days
Rain precipitation (*RAINFALL*)	Total annual precipitation in months with average air temperatures > 0°C	mm yr^{-1}
Snow precipitation (*SNOWFALL*)	Total annual precipitation in months with average air temperatures < 0°C	mm yr^{-1}

Table S2.12. Spearman's Rank correlation matrix for candidate climate variables included in our climate envelope modelling of Europe and Western Siberia. Correlation coefficients, r_s, and significance values, p, are presented. See Table S2.11 for variable descriptions.

	MAT	*TRANGE*	*GDD*$_5$	*RAINFALL*	*SNOWFALL*
MAT	-	$p < 0.001$	$p < 0.001$	$p < 0.001$	$p < 0.001$
TRANGE	$r_s = -0.783$	-	$p < 0.001$	$p < 0.001$	$p < 0.001$
GDD$_5$	$r_s = 0.897$	$r_s = -0.473$	-	$p < 0.001$	$p < 0.001$
RAINFALL	$r_s = 0.877$	$r_s = -0.773$	$r_s = 0.732$	-	$p < 0.001$
SNOWFALL	$r_s = -0.627$	$r_s = 0.390$	$r_s = -0.707$	$r_s = -0.438$	-

Table S2.13. Spearman's Rank correlation matrix for candidate climate variables for grid cells in Europe and Western Siberia where observations of palsas/peat plateaus are present (n = 671) and absent (n = 3,944). Correlation coefficients, r_s, and significance values, p, are presented. See Table S2.11 for variable descriptions.

		MAT	*TRANGE*	*GDD$_5$*	*RAINFALL*	*SNOWFALL*
MAT	*Presence*		$p = 0.213$	$p < 0.001$	$p < 0.001$	$p = 0.036$
	Absence		$p < 0.001$	$p < 0.001$	$p < 0.001$	$p < 0.001$
TRANGE	*Presence*	$r_s = -0.048$		$p < 0.001$	$p < 0.001$	$p = 0.014$
	Absence	$r_s = -0.787$		$p < 0.001$	$p < 0.001$	$p < 0.001$
GDD$_5$	*Presence*	$r_s = 0.390$	$r_s = 0.825$		$p < 0.001$	$p = 0.011$
	Absence	$r_s = 0.879$	$r_s = -0.455$		$p < 0.001$	$p < 0.001$
RAINFALL	*Presence*	$r_s = 0.712$	$r_s = 0.385$	$r_s = 0.668$		$p = 0.056$
	Absence	$r_s = 0.857$	$r_s = -0.816$	$r_s = 0.670$		$p < 0.001$
SNOWFALL	*Presence*	$r_s = -0.081$	$r_s = 0.095$	$r_s = -0.098$	$r_s = 0.074$	
	Absence	$r_s = -0.636$	$r_s = 0.359$	$r_s = -0.724$	$r_s = -0.413$	

Table S2.14. Spearman's Rank correlation matrix for candidate climate variables for grid cells in Europe and Western Siberia where observations of polygon mires are present (n = 339) and absent (n = 4,276). Correlation coefficients, r_s, and significance values, p, are presented. See Table S2.11 for variable descriptions.

		MAT	*TRANGE*	*GDD$_5$*	*RAINFALL*	*SNOWFALL*
MAT	*Presence*		$p < 0.001$	$p < 0.001$	$p < 0.001$	$p < 0.001$
	Absence		$p < 0.001$	$p < 0.001$	$p < 0.001$	$p < 0.001$
TRANGE	*Presence*	$r_s = 0.802$		$p < 0.001$	$p < 0.001$	$p = 0.001$
	Absence	$r_s = -0.810$		$p < 0.001$	$p < 0.001$	$p < 0.001$
GDD$_5$	*Presence*	$r_s = 0.983$	$r_s = 0.864$		$p < 0.001$	$p < 0.001$
	Absence	$r_s = 0.874$	$r_s = -0.473$		$p < 0.001$	$p < 0.001$
RAINFALL	*Presence*	$r_s = 0.797$	$r_s = 0.555$	$r_s = 0.800$		$p < 0.001$
	Absence	$r_s = 0.854$	$r_s = -0.807$	$r_s = 0.676$		$p < 0.001$
SNOWFALL	*Presence*	$r_s = 0.401$	$r_s = 0.181$	$r_s = 0.408$	$r_s = 0.835$	
	Absence	$r_s = -0.696$	$r_s = 0.414$	$r_s = -0.786$	$r_s = -0.488$	

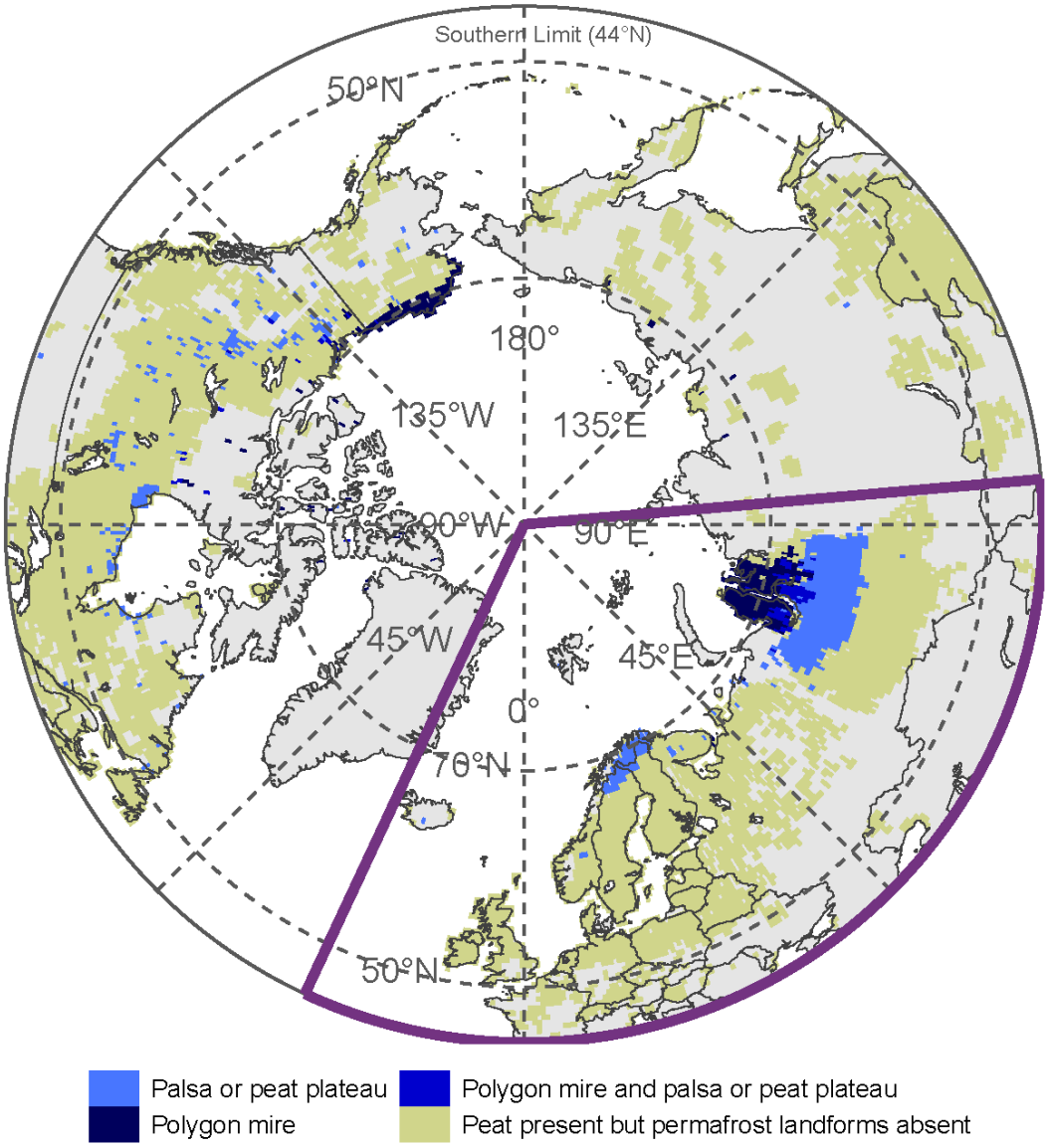

Figure S2.4. Distribution of observed permafrost peatland landforms in our catalogue of published records (supplementary dataset S2.1). Dark purple box indicates our study domain (north of 44°N and between 25°W and 95°E). Map outlines are from Brownrigg (2022).

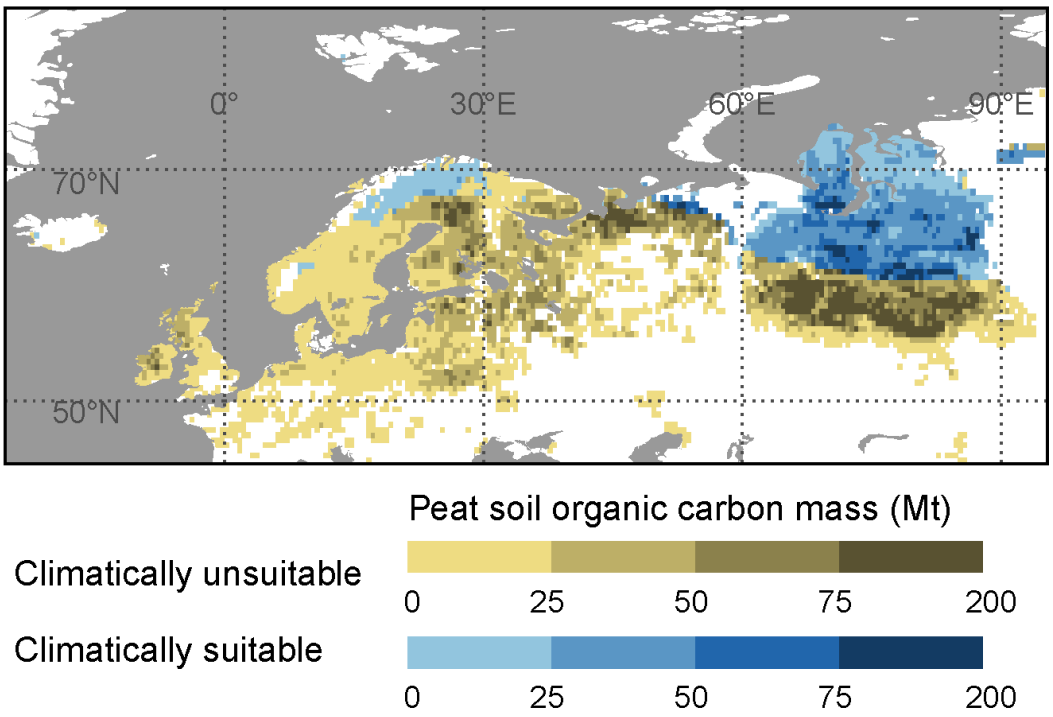

Figure S2.5. The distribution of gridded peat soil organic carbon mass (Mt), based on recent soil maps (Hugelius et al., 2020a, 2020b) (see methods for details) and coloured according to the predicted presence and absence of suitable climatic conditions for permafrost peatlands. Map outlines are from Brownrigg (2022).

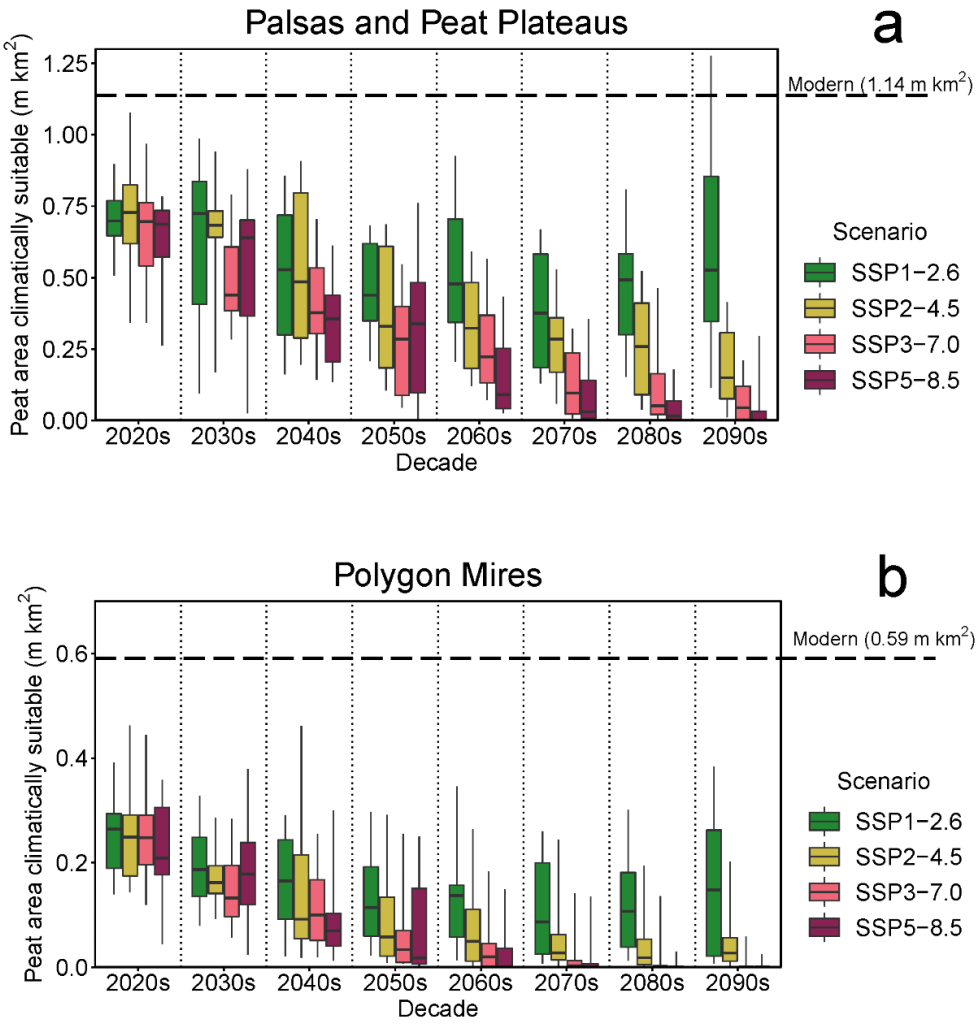

Figure S2.6. Comparisons of the total peatland area (m km^2) that is within the suitable climate envelopes for peatland permafrost in Europe and Western Siberia under four CMIP6 emission scenarios. Decadal time series showing for SSP1-2.6, SSP2-4.5, SSP3-7.0 and SSP5-8.5 the total peatland area in Europe and Western Siberia that is: a) within the suitable climate envelope for palsas/peat plateaus; and b) within the suitable climate envelope for polygon mires. Whiskers indicate the full range of values from the 12 CMIP6 models in our ensemble, lower hinges indicate the 25th percentiles, upper hinges indicate the 75th percentiles, and centre lines indicate median values. Dashed lines represent the total peatland area that is within the respective suitable climate envelopes during the modern baseline period (1961–1990).

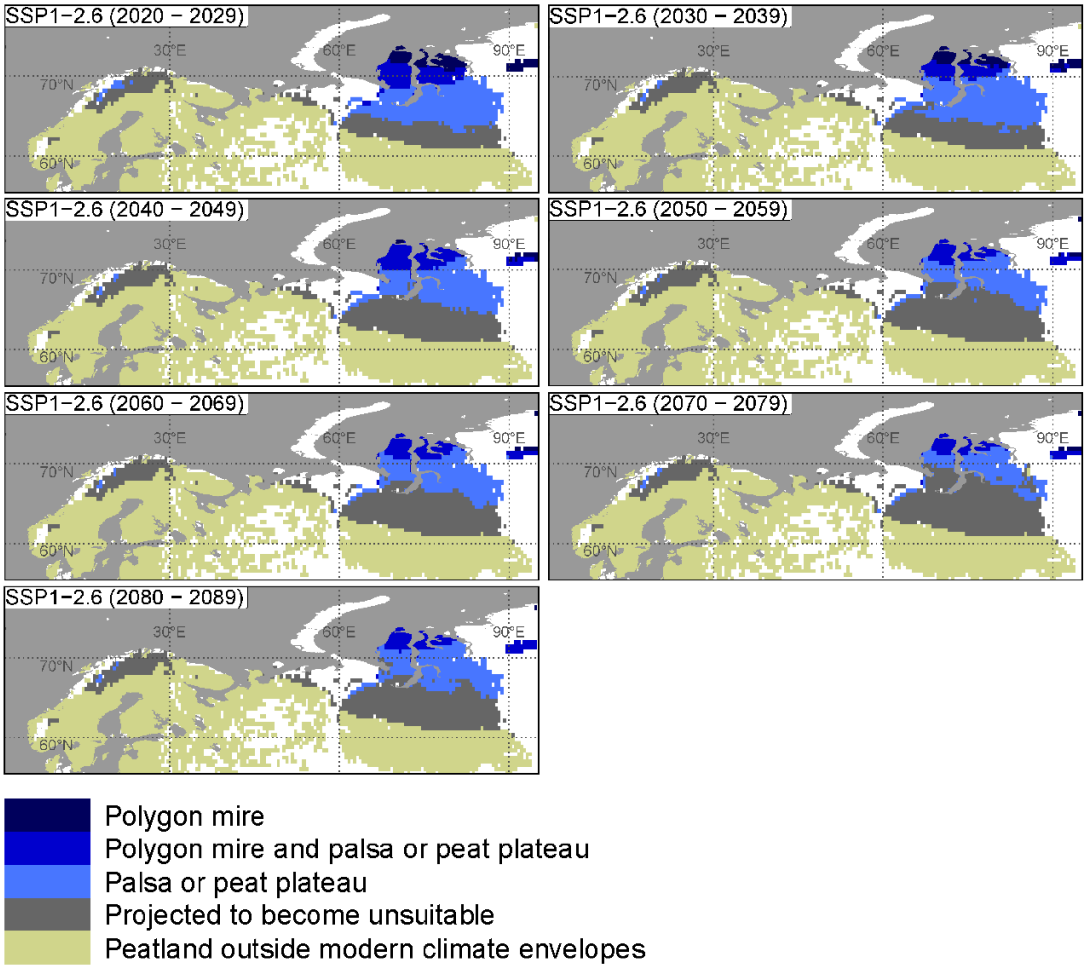

Figure S2.7. Projected decadal distributions of the suitable climate envelopes for palsas/peat plateaus and polygon mires in Europe and Western Siberia under SSP1-2.6 (strong climate change mitigation) from 2020–2029 to 2080–2089. Map outlines are from Brownrigg (2022).

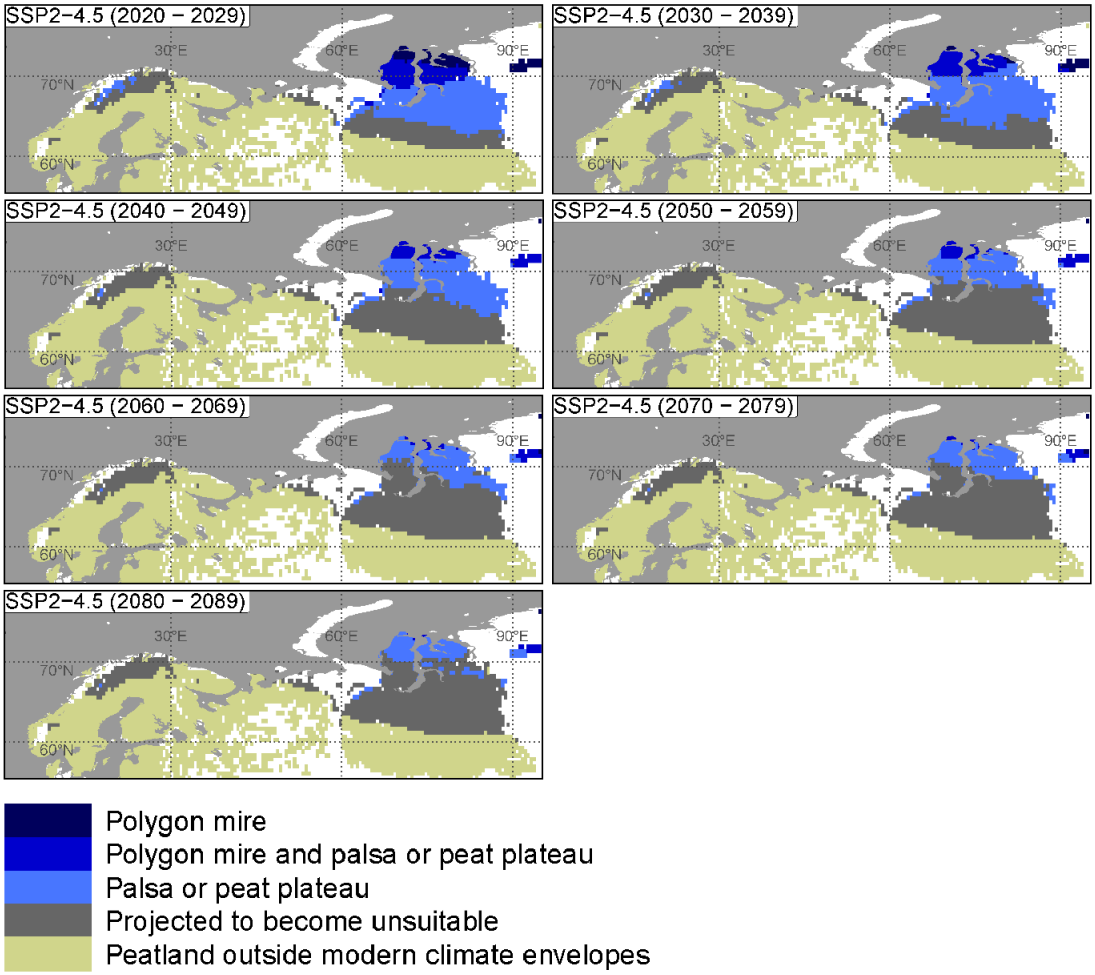

Figure S2.8. Projected decadal distributions of the suitable climate envelopes for palsas/peat plateaus and polygon mires in Europe and Western Siberia under SSP2-4.5 (moderate mitigation) from 2020–2029 to 2080–2089. Map outlines are from Brownrigg (2022).

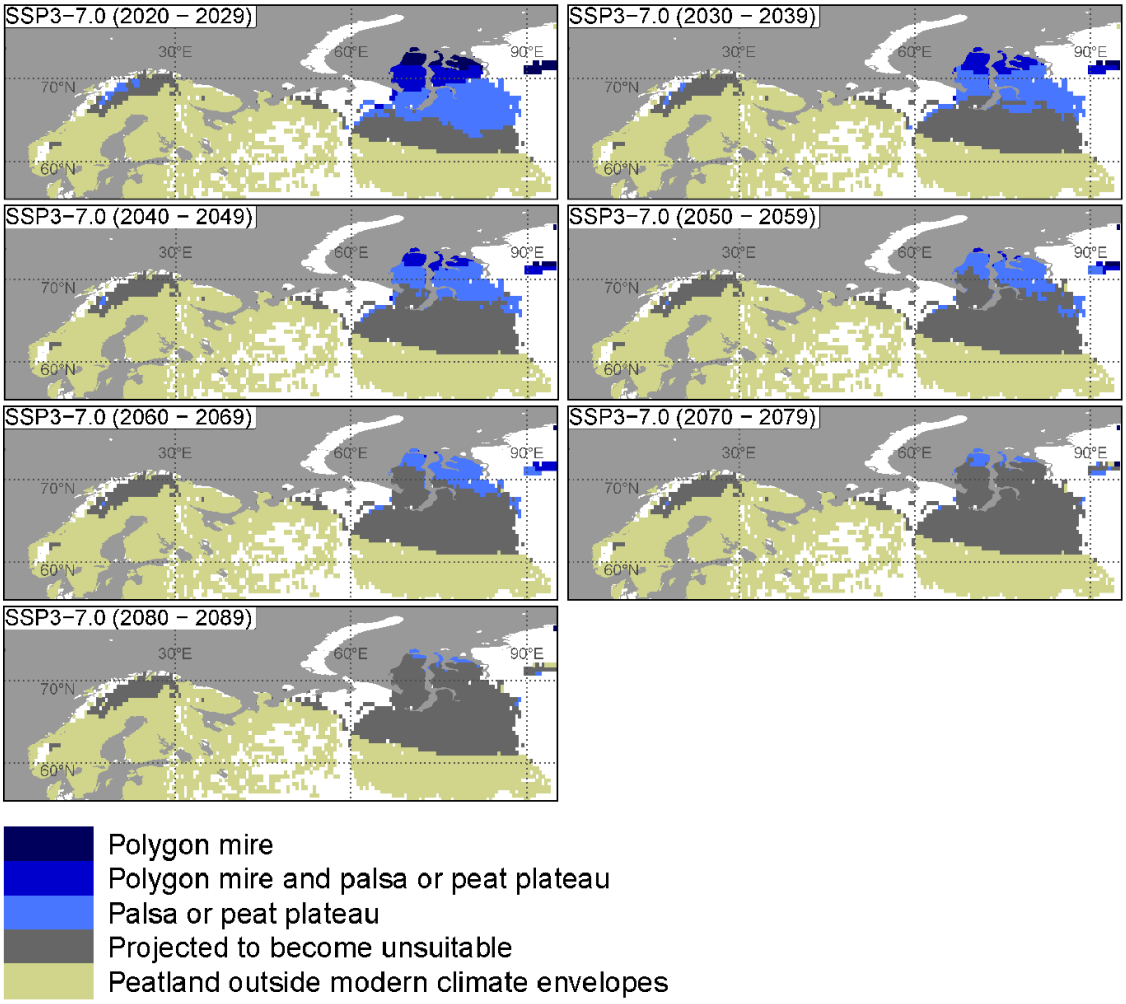

Figure S2.9. Projected decadal distributions of the suitable climate envelopes for palsas/peat plateaus and polygon mires in Europe and Western Siberia under SSP3-7.0 (no mitigation baseline) from 2020–2029 to 2080–2089. Map outlines are from Brownrigg (2022).

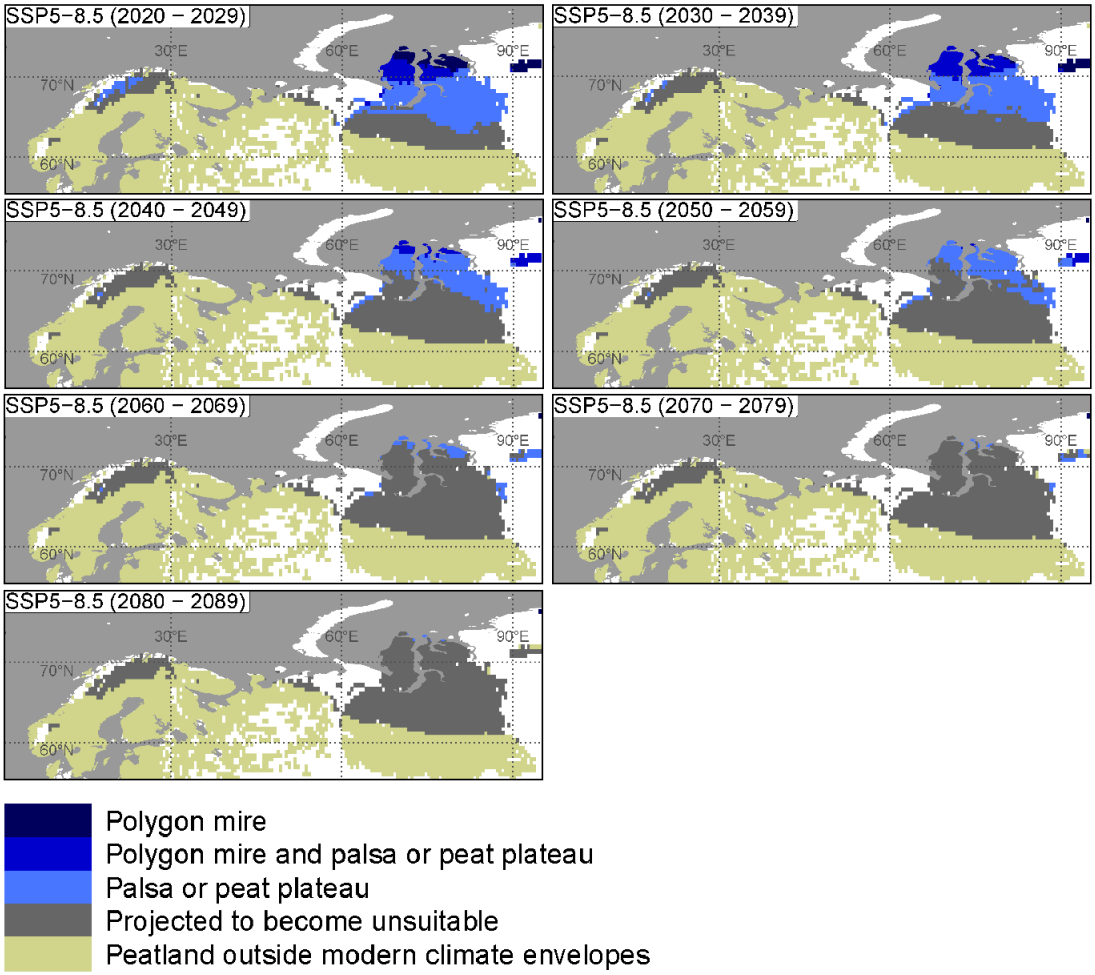

Figure S2.10. Projected decadal distributions of the suitable climate envelopes for palsas/peat plateaus and polygon mires in Europe and Western Siberia under SSP5-8.5 (no mitigation, worst-case) from 2020–2029 to 2080–2089. Map outlines are from Brownrigg (2022).

2.6. Supplementary data for Chapter 2

Any remaining data used to produce this research are included in the supplementary datasets S2.1 and S2.2 (uploaded alongside this thesis).

Chapter 3
Holocene vegetation dynamics of circum-Arctic permafrost peatlands

3.1. Abstract

Vegetation shifts in circum-Arctic permafrost peatlands drive feedbacks with important consequences for peatland carbon budgets and the extent of permafrost thaw under changing climate. Recent shrub expansion across Arctic tundra environments has led to an increase in above-ground biomass, but the long-term spatiotemporal dynamics of shrub and tree growth in circum-Arctic peatlands remain unquantified. We investigate changes in peatland vegetation composition during the Holocene using previously-published plant macrofossil records from 76 sites across the circum-Arctic permafrost zone. In particular, we assess evidence for peatland shrubification at the continental scale. We identify increasing abundance of woody vegetation in circum-Arctic peatlands from ~8,000 years BP to present, coinciding with declining herbaceous vegetation and widespread *Sphagnum* expansion. Ecosystem shifts varied between regions and present-day permafrost zones, with late-Holocene shrubification most pronounced where permafrost coverage is presently discontinuous and sporadic. After ~600 years BP, we find a proliferation of non-*Sphagnum* mosses in Fennoscandia and across the present-day continuous permafrost zone; and rapid expansion of *Sphagnum* in regions of discontinuous and isolated permafrost as expected following widespread fen-bog succession, which coincided with declining woody vegetation in eastern and western Canada. Since ~200 years BP, both shrub expansion and decline were identified at different sites across the pan-Arctic, highlighting the complex ecological responses of circum-Arctic peatlands to post-industrial climate warming and permafrost degradation. Our results suggest that shrubification of circum-Arctic peatlands has primarily occurred alongside surface drying, resulting from Holocene climate shifts, autogenic peat accumulation, and permafrost aggradation. Future shrubification of

circum-Arctic peatlands under 21st century climate change will likely be spatially heterogeneous, and be most prevalent where dry microforms persist.

3.2. Introduction

Twenty-first century climate change is projected to drive widespread vegetation shifts in permafrost peatlands, which presently cover 1.7 ± 0.5 million km^2 and contain 185 ± 70 Gt carbon (C) (Hugelius et al., 2020a). Permafrost (perennially frozen ground) renders these vast, fragile carbon stores vulnerable to warming, because thaw-induced surface collapse can drive peatland inundation, which strengthens methane emissions (Heffernan et al., 2022; Holmes et al., 2022). Future peat carbon release may be partially offset by increased plant productivity under warming climates and a poleward shift in woody vegetation, termed shrubification (Myers-Smith et al., 2015; Mekonnen et al., 2021). Shrubification has been widely recognised across upland tundra in response to late-20th century climate change by decadal observations and satellite imagery (Myers-Smith and Hik, 2018; Chen et al., 2021; Mekonnen et al., 2021), although permafrost thaw in lowland tundra has driven thermokarst formation and succession towards graminoid-dominated vegetation (Magnússon et al., 2021; Heijmans et al., 2022). Peatlands represent poorly-drained environments that are often resistant to succession until ecohydrological thresholds are surpassed (Belyea, 2009; Swindles et al., 2015) and may therefore exhibit less linear vegetation transitions under warming climates than mineral-soil tundra. Experimental studies suggest that climate warming and drought increase peatland suitability for shrub and tree encroachment owing to deeper water tables, longer growing seasons, thicker active layers, and restricted moss growth (Heijmans et al., 2013; Limpens et al., 2014b, 2021; Holmgren et al., 2015). Shrubs and trees also survive most effectively on raised peatland surfaces, such as hummocks formed of *Sphagnum* sect. *Acutifolia* (Pouliot et al., 2011; Holmgren et al., 2015). During recent decades, many circum-Arctic peatlands have evidenced surface drying (Zhang et al., 2022), while abundances of *Sphagnum* sect. *Acutifolia* have

rapidly increased in Canadian permafrost regions (Magnan et al., 2018, 2022) and the European sub-Arctic (Piilo et al., 2023), providing potentially suitable environments for peatland shrubification. Indeed, some core-based palaeoreconstructions of the recent past have identified shrubs expanding in high-latitude peatlands in North America following late-20th century warming (Gałka et al., 2018; Sim et al., 2019), but no study has yet quantified the broader spatial extent of shrubification in circum-Arctic peatlands, or its long-term context.

Peatland vegetation shifts have important implications for carbon cycling, peat decomposition, and permafrost dynamics (Loisel et al., 2014; Treat et al., 2016). Herbaceous-dominated fens generally exhibit high methane emissions and decay rates (Treat et al., 2021b), meaning that *Sphagnum*-dominated bogs are overall more effective carbon sinks (Loisel and Bunsen, 2020; Holmes et al., 2022; Magnan et al., 2022). Tree and shrub establishment on peatlands can substantially increase aboveground biomass and, like *Sphagnum*, woody material is highly resistant to decay (van Breemen, 1995; Camill et al., 2001; Moore et al., 2007). Conversely, peatland shrubification also increases fuel for wildfires, which can combust deep peat carbon in dry sites (Turetsky et al., 2015) and accelerate peat permafrost thaw (Zoltai, 1993; Gibson et al., 2018). Thaw can reverse hydroseral succession (the transition from open waterbodies to fens and bogs), creating saturated depressions that restrict growth of woody vegetation and become recolonised by hydrophilic *Sphagnum* and sedges (Camill, 1999; Minke et al., 2009; Varner et al., 2022), although ice-wedge degradation can also increase lateral drainage (Olefeldt et al., 2021). Therefore, a clear understanding of both recent and long-term successional trends is vital for predicting the future vulnerability of circum-Arctic peatlands.

Plant macrofossils record the past composition of *in situ* plant communities, and enable the study of past changes in peatland vegetation composition (Mauquoy et al., 2010). In a recent compilation by Treat et al. (2016), more than half of the 280 studied peatlands showed fen–bog transitions (FBTs) during the Holocene, while permafrost aggradation in boreal and tundra peatlands resulted in vegetation communities akin to permafrost-free bogs and

fens, respectively. A subsequent reanalysis by Treat and Jones (2018) of the same catalogue showed that permafrost aggraded most rapidly in northern peatlands during neoglaciation and the Little Ice Age (LIA), which has been linked to a 20 % reduction in methane emissions (Treat et al., 2021b). However, these studies did not analyse compositional changes in Holocene peatland vegetation, but rather identified changes in wetland types and primary vegetation, based on the dominant macrofossil component (> 30 %) or lithological description of peat layers (Treat et al., 2016; Treat and Jones, 2018). Woody vegetation rarely comprised the dominant peat-forming material in any of the studied wetland types (Treat et al., 2016), so past peatland shrubification trends may have been concealed by this approach. Magnan et al. (2022) collated data on plant macrofossil composition from peatlands in Quebec for the last ~200 years and found no evidence of enhanced peatland shrubification under late 20th-century warming, but rather a rapid, northwards expansion of *Sphagnum*. The findings from this study in Quebec contrast recent palaeoecological reconstructions of shrub expansion in other areas, such as northern Alaska (Gałka et al., 2018) and High Arctic Canada (Sim et al., 2019); therefore, the spatiotemporal dynamics of late-Holocene peatland shrubification warrant further investigation.

Existing palaeoecological syntheses have not yet analysed Holocene peatland shrubification at continental scales, and many recently published plant macrofossil records have not been included in previous palaeoecological compilations. Here, we compile and analyse a catalogue of 76 previously-published plant macrofossil records from peatlands across the circum-Arctic permafrost region to explore proportional changes in peatland vegetation during the Holocene. Our analysis provides long-term context for recent observations of shrubification and *Sphagnum* expansion in circum-Arctic peatlands.

3.3. Methods

3.3.1. Dataset compilation

We used a structured literature search to collate published plant macrofossil records from peatlands across the circum-Arctic permafrost region. We searched Google Scholar for the terms “permafrost”, “peatland”, “plant macrofossil”, “paleoecology” in conjunction with names of selected regions (e.g., Fennoscandia), countries (e.g., Sweden), states (e.g., Alaska), and provinces and territories (e.g., Nunavut) until June 2022. We selected peat core records from peer-reviewed studies that: i) were located within the circum-Arctic permafrost zone (Brown et al., 2002); ii) contained peat depth and proportional plant macrofossil composition (%) information; and iii) reported uncalibrated radiocarbon (^{14}C) dates. We only considered cores with at least two radiometric dates. We prioritised cores for which raw data are available in the public domain. To reduce bias towards peatlands where multiple plant macrofossil records existed, we selected a single core for each site based on a combination of chronological detail, sampling resolution, core length, proximity to the peatland’s centre, and an absence of obvious disturbances in the palaeoecological record (e.g. water-filled voids and stratigraphic unconformities). We grouped cores into broad regional subgroups according to geographical boundaries and core locations (Figure 3.1) and determined the zone of contemporary permafrost coverage for each site using the Circum-Arctic Map of Permafrost and Ground-Ice Conditions, Version 2 (Brown et al., 2002). Contemporary permafrost coverage is categorised as continuous (90–100 %), discontinuous (50–90 %), sporadic (10–50 %), or isolated (< 10 %) (Brown et al., 2002). Plant macrofossils represent *in situ* peatland vegetation (Mauquoy et al., 2010), so our approach does not seek to characterise the full spatial heterogeneity found within complexes of circum-Arctic peatlands. Rather, we explore broad-scale trends in Holocene peatland vegetation change using a subset of well-dated, directly-comparable plant macrofossil records from across the circum-Arctic permafrost region.

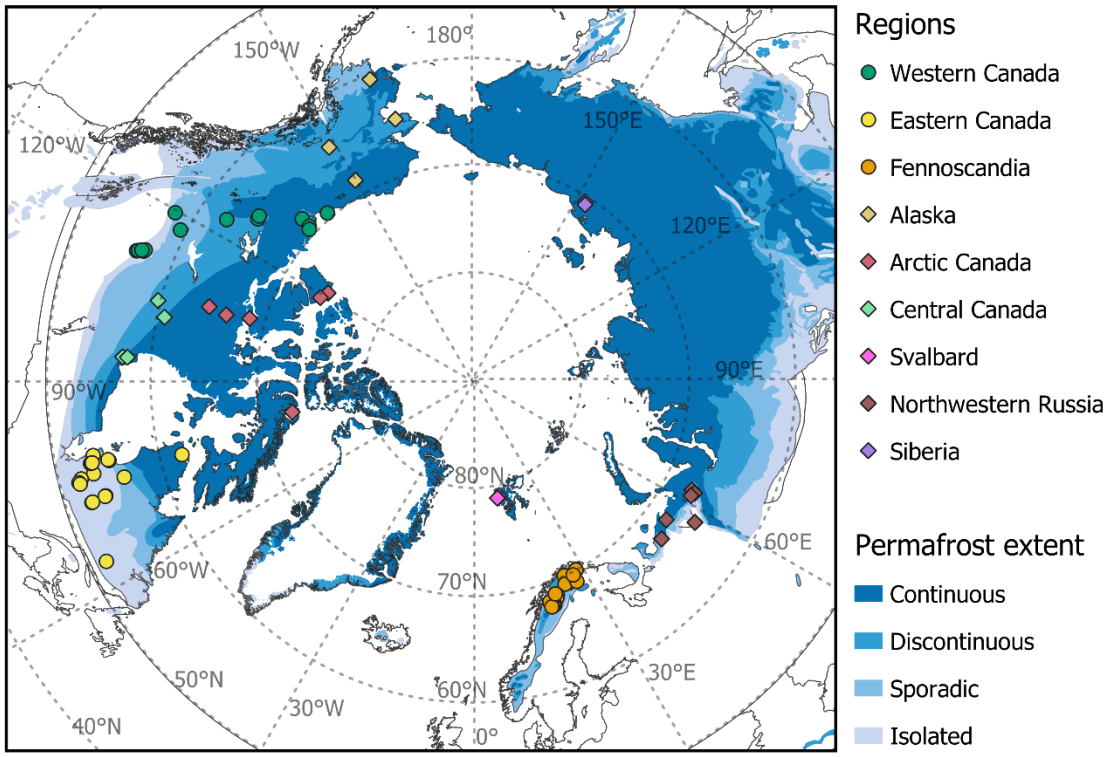

Figure 3.1. Distribution of the 76 compiled cores across the circum-Arctic permafrost region, coloured by regional grouping. Circles represent sites used in the regional analyses in Figures 3.3 and S3.7. Extent of contemporary permafrost coverage derived from Brown et al. (2002).

From our selection criteria, we assembled published Holocene plant macrofossil data from 76 peat cores (supplementary dataset S3.1), including 35 cores not included in previous meta-analyses; and 41 cores previously analysed by Treat and Jones (2018) and/or Magnan et al. (2022). Published site descriptions indicate that our selected cores were sampled from a broad range of permafrost and permafrost-free peat types. However, in common with previous peatland syntheses (Loisel et al., 2014; Treat et al., 2016; Magnan et al., 2022), suitable records from fens (*n* = 11) were less readily available than for bogs (*n* = 19) and palsas/peat plateaus (peat-covered frost mounds) (*n* = 36), likely due to the difficulty of recovering useable samples from saturated fen peats. The collated plant macrofossil records were primarily extracted from *Sphagnum* microhabitats (e.g., hummocks, lawns), partly because shrub and

tree roots are more difficult to core through, which may cause some underestimation of recent peatland shrubification in our analyses. Additionally, only nine cores are from polygon mires, which are found in remote northern extremes in cold climates (Fewster et al., 2022). Reconstructions from permafrost peatlands can be hindered by slow net peat accumulation, and even net peat loss during some periods (Väliranta et al., 2021). The temporal lengths of records from permafrost peatlands can also be limited where only unfrozen, active-layer peats are sampled above the local frost table (Zhang et al., 2020; Sim et al., 2021b). The peat cores in our dataset are from North America (*n* = 47) and Eurasia (*n* = 29), and span contemporary zones of permafrost coverage (continuous, *n* = 19; discontinuous, *n* = 21; sporadic, *n* = 16; isolated, *n* = 20) (Figure 3.1). However, the spatial representation of suitable plant-macrofossil records varied across the circum-Arctic, with a majority of cores located in western Canada (*n* = 14), eastern Canada (*n* = 19), and Fennoscandia (*n* = 19). Conversely, published records of relative plant-macrofossil compositions were rare across Alaska (*n* = 4), Arctic Canada (*n* = 6), and Siberia (*n* = 2), where polygon mires are most abundant (Minke et al., 2007; Peregon et al., 2008).

For each core, we compiled information on peat sampling depth, radiometric chronological controls, plant macrofossil proportions (%) at the taxonomic resolution reported by the original authors, and relevant in-text site descriptions. Plant macrofossil assemblages were recorded by the original authors using standard techniques. We omitted plant macrofossil counts from our analyses (e.g., numbers of fruits and seeds), because these counts cannot be compared directly to relative abundance data, which summarise the major peat forming components through time. Our analyses may therefore underestimate some phases of peatland shrubification where the presence of woody vegetation was only indicated in count data. Additionally, we omitted plant macrofossil data from basal, non-peat sediments. Where numerical plant macrofossil datasets were unavailable in the public domain, we extracted plant macrofossil information from stratigraphic diagrams using WebPlotDigitzer v.4.5 (Rohatgi, 2021).

To enable comparisons of peatland vegetation between cores, we grouped the plant macrofossil data into four plant functional types (PFTs) previously used by Treat et al. (2016): woody (e.g., shrubs, trees, ligneous roots), herbaceous (e.g., grasses, *Equisetum*, and Cyperaceae), non-*Sphagnum* mosses (e.g., brown and feather mosses), and *Sphagnum* spp.. Because not all plant macrofossil records were recorded to species level, we did not differentiate between *Sphagnum* functional types (hummock, lawn, hollow) in our analyses. We included an additional group "other" to quantify the combined proportion of ambiguous material (e.g., uncategorised roots) and unidentified organic matter (UOM) resulting from decomposition. When summed, the collated plant macrofossil proportions did not always total 100 %, even when we extracted data directly from published datasets. For these samples, we rescaled the relative abundances of each plant macrofossil group recorded by the original authors to a 0-100 % scale, by dividing by the sample total. Our final catalogue contains plant macrofossil records for 2,581 distinct samples from 76 cores, and includes 1,076 samples compiled into a synthesis dataset for the first time (see supplementary dataset S3.2).

3.3.2. Age-depth modelling

We constructed new age-depth models for each core to ensure our peatland chronologies were standardised against the latest radiocarbon calibration curve, IntCal20 (Reimer et al., 2020). For all cores, we collated uncalibrated ^{14}C dates and their associated laboratory errors. We used reported dates of core extraction as surface ages, but for seven cores without such information we estimated surface ages to be three years prior to study publication dates. For 26 cores, near-surface peat layers were dated by high-precision lead-210 (^{210}Pb) chronologies, and where possible we collated calibrated ^{210}Pb ages and errors. We interpret the most recent changes in the 37 cores from present-day sporadic and discontinuous permafrost zones with some caution, because only 10 of these 37 cores were dated with ^{210}Pb chronologies, while 23 of 37 were missing data for the most recent part of the record (1975–2022 C.E.). By comparison, 28 of the 39 cores from regions of isolated and continuous permafrost included data for this recent period.

For the majority of cores (*n* = 58/76), where at least four uncalibrated radiocarbon dates were available, we constructed Bayesian age-depth models using the rbacon package (v.2.5.7) (Blaauw and Christen, 2011) in R v.4.1.3 (R Core Team, 2022). For six cores, where calibrated ^{210}Pb dates were unavailable but sufficient data on ^{210}Pb activity, laboratory errors, and bulk density were accessible, we derived age-depth models using the rplum package (v.0.2.2) (Aquino-López et al., 2018). A Bayesian approach was deemed unsuitable for cores with fewer than four dates, and so for the 12 cores that reported only two or three radiocarbon dates we instead developed classical age-depth models, using the clam package (v.2.4.0) (Blaauw, 2010). Of the 12 age-depth models we constructed in clam, 10 were for cores located in regions of present-day continuous and discontinuous permafrost. We calculated the calibrated age of each sample according to the probability estimates provided by each age-depth model, and do not therefore include chronological uncertainties in our subsequent analyses. Information on the prior settings used for our Bayesian age-depth models, and the regression functions used for our classical models, are presented in Figures S3.9–S3.84 (see supplementary material S3.2, uploaded alongside this thesis).

3.3.3. Statistical analysis

To investigate long-term trends of peatland vegetation change during the Holocene, we binned the plant macrofossil relative abundance data (%) into non-overlapping 200-year age bins using calibrated dates derived from the age-depth models described in section 3.3.2., above. To ensure that cores with greater temporal sampling frequency did not distort the binned mean across sites, we calculated the mean of any samples from the same core in the same timestep prior to binning, following Magnan et al. (2022). To identify shorter-term shifts, we also binned the plant macrofossil assemblages into 50-year bins, although the binned data rarely comprised a continuous record for every 50-year timestep. Because our 200-year binned data exhibited greater site replication for each timestep (see Figures S3.6–S3.8 for the temporal distribution of core records), we conducted all time-series analyses at a 200-

year resolution and present the equivalent 50-year data as supplementary scatter plots.

We also calculated normalised binned plant macrofossil records for each core, which emphasised the direction of change in PFT relative abundance rather than the absolute magnitude. This approach was useful for identifying subtle but potentially important shifts in PFTs with low abundance, because the coexistence of several PFTs at the time of peat formation may obscure trends in non-dominant PFTs in data averaged across multiple sites. For example present-day treed peat plateaus often exhibit an understory of *Sphagnum*, non-*Sphagnum* mosses and lichens (Jones et al., 2017), meaning woody vegetation rarely comprises a dominant peatland-forming component in these sites (Treat et al., 2016), except in rootlet peat layers (Sannel and Kuhry, 2008). Our normalisation approach rescaled the maximum binned relative abundance of each PFT within each core to 100 %, and was calculated as:

$$N_{i,j,t} = \frac{A_{i,j,t}}{A_{i,j,max}} \times 100 \quad (1)$$

where $N_{i,j,t}$ is the normalised binned relative abundance of PFT *i* in core *j* at timestep *t*; $A_{i,j,t}$ *is* the non-normalised binned relative abundance of PFT *i* in core *j* at timestep *t*; and $A_{i,j,max}$ is the maximum non-normalised binned relative abundance of PFT *i* in core *j* throughout the core record.

We then combined $N_{i,j,t}$ and $A_{i,j,t}$ values between multiple cores to establish trends at different spatial scales. We considered: i) the circum-Arctic (Figures 3.2 and S3.6), ii) geographical regions with at least 10 cores (i.e., western Canada, eastern Canada, and Fennoscandia) (Figures 3.3 and S3.7); and iii) present-day permafrost zones (Brown et al., 2002) (Figures 3.4 and S3.8). Within each grouping of cores, for each PFT *i* at each 200-year timestep *t*, we calculated the between-core sum of $A_{i,j,t}$; the between-core mean of $N_{i,j,t}$, which we refer to as the mean normalised relative abundance ($MNRA_{200}$); and the between-core standard error of $N_{i,j,t}$. We also calculated the between-core mean of $N_{i,j,t}$ for each 50-year timestep, which we refer to as $MNRA_{50}$ (presented in Figures S3.6–3.8). We excluded three cores from our normalised 200-year trends that only contained data for the most recent 200-year

timestep, but included these cores in our normalised 50-year analysis. To show the effect of our data normalisation, we also present the between-core mean of $A_{i,j,t}$ at 50-year and 200-year intervals for each core grouping in Figures S3.6–S3.8.

We define Holocene subdivisions as early (~11,700–~8,200 years BP), middle (~8,200–~4,200 years BP), and late (~4,200 years BP–present) (Walker et al., 2019). Henceforth, we report ages as 200-year bin midpoints, unless otherwise specified, and abbreviate “calibrated years BP” to “years BP”.

To identify associations between PFTs, we conducted a non-metric multidimensional scaling (NMDS) analysis with the Bray-Curtis dissimilarity index using the vegan library v2.6-2 in R (Oksanen et al., 2022) (Figure 3.5). For this analysis, we assessed the between-core mean of $A_{i,j,t}$ for each PFT i at 50-year intervals, averaged across all available cores during the Holocene (since ~11,700 years BP) (Figure S3.6c), because these data provided a much greater sample size (n = 228) than our equivalent 200-year binned data (n = 59). We limited our ordination to two dimensions to aid interpretability, while ensuring the ordination stress of our final solution was < 0.2, following Clarke (1993).

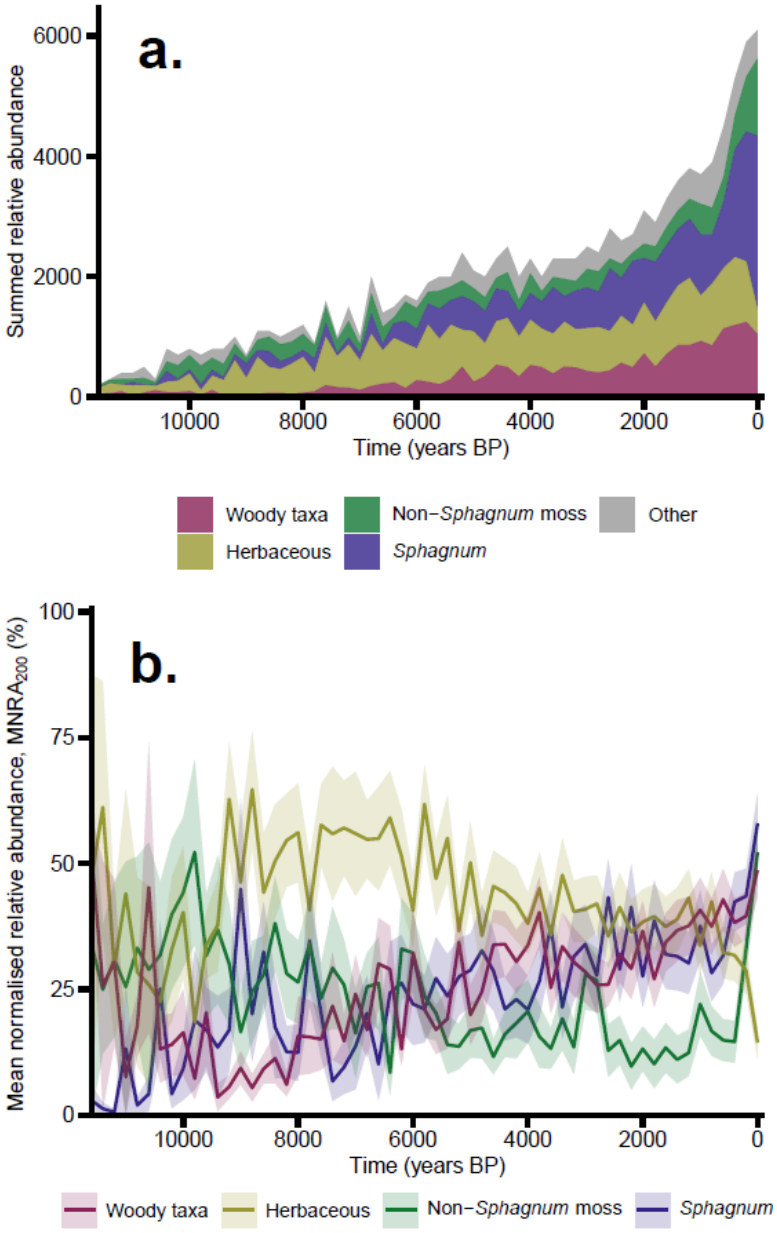

Figure 3.2. Holocene vegetation shifts in the studied circum-Arctic peatlands presented in 200-year bins as: (a) the between-core summed relative abundance of plant functional types (PFTs); and (b) the between-core mean normalised relative abundance (%) of PFTs, $MNRA_{200}$, with shading representing the standard error of $MNRA_{200}$. Other refers to unidentified organic matter or ambiguous material. Increasing summed data over time reflects continued peatland initiation (see Figure S3.6a for core distribution through time). For details of data normalisation, see methods section 3.3.3., and for the between-core mean normalised relative abundance in 50-year bins, $MNRA_{50}$, see Figure S3.6d.

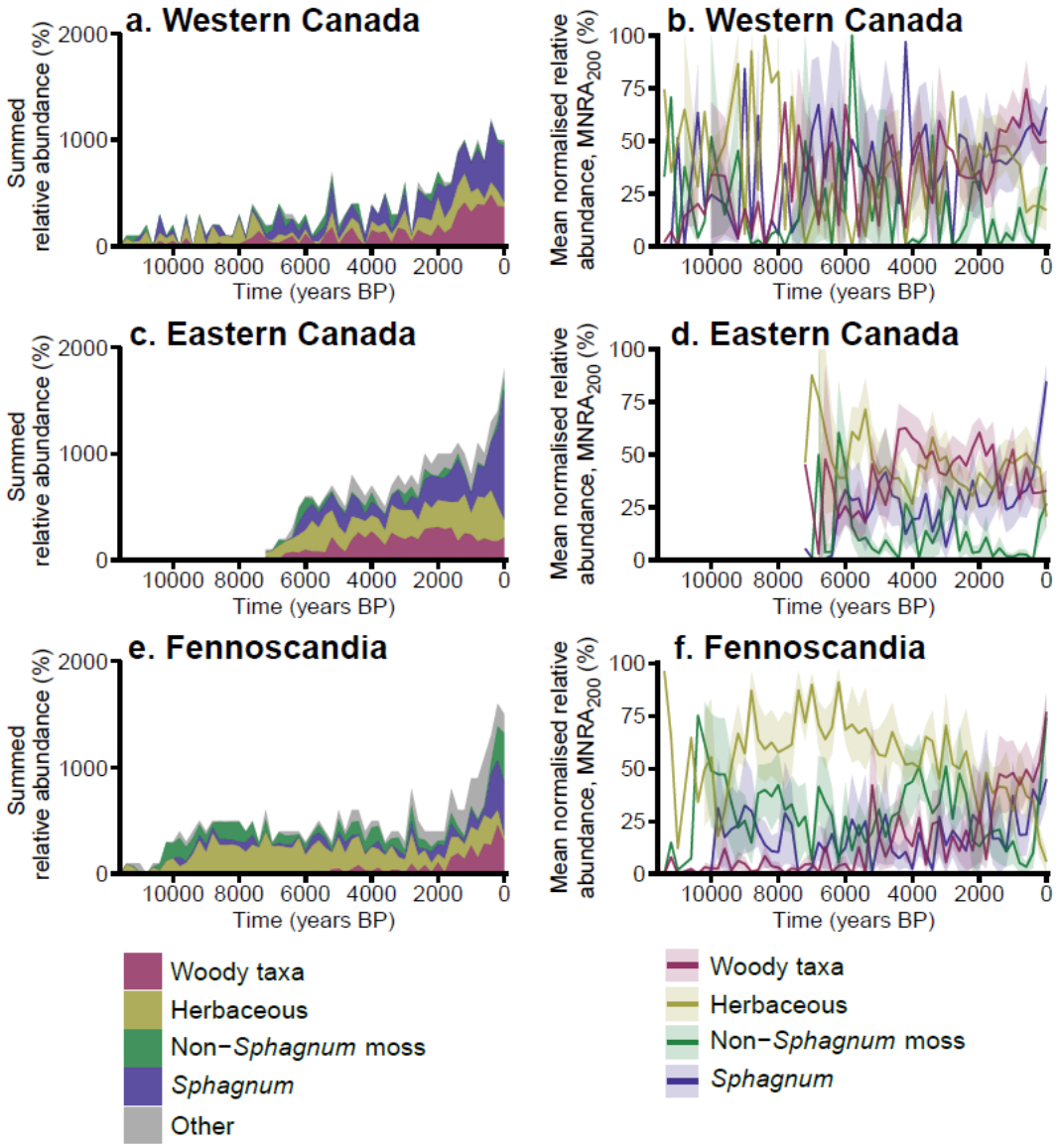

Figure 3.3. Spatiotemporal variation in Holocene peatland vegetation shifts between geographic regions (see Figure 3.1 for details). The between-core summed relative abundance of plant functional types (PFTs) in 200-year bins for cores from (a) western Canada, (c) eastern Canada, and (e) Fennoscandia. Other refers to unidentified organic matter or ambiguous material. Increasing summed data over time reflects continued peatland initiation (see Figure S3.7a–c for core distribution through time). The between-core mean normalised relative abundance (%) of PFTs in 200-year bins, $MNRA_{200}$, for cores from (b) western Canada, (d) eastern Canada, and (f) Fennoscandia. Shading represents the standard error of $MNRA_{200}$. For details of data normalisation, see methods section 3.3.3., and for the between-core mean normalised relative abundance in 50-year bins, $MNRA_{50}$, see Figure S3.7j–l.

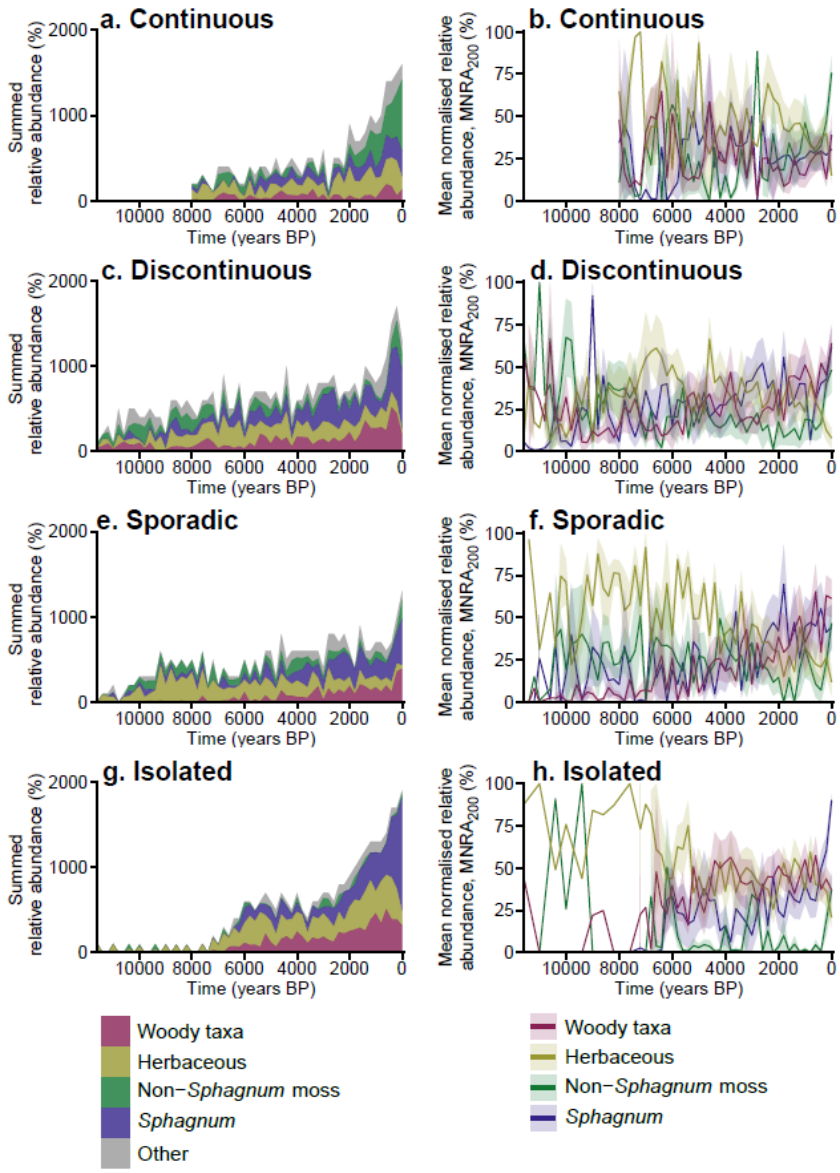

Figure 3.4. Spatiotemporal variation in Holocene peatland vegetation shifts between present-day permafrost zones. The between-core summed relative abundance of plant functional types (PFTs) in 200-year bins for cores from the (a) continuous, (c) discontinuous, (e) sporadic, and (g) isolated permafrost zones. Other refers to unidentified organic matter or ambiguous material. Increasing summed data over time reflects continued peatland initiation (see Figure S3.8a–d for core distribution through time). The between-core mean normalised relative abundance (%) of PFTs in 200-year bins, $MNRA_{200}$, for cores from the (b) continuous, (d) discontinuous, (f) sporadic, and (h) isolated permafrost zones. Shading represents the standard error of $MNRA_{200}$. For details of data normalisation, see methods section 3.3.3., and for the between-core mean normalised relative abundance in 50-year bins, $MNRA_{50}$, see Figure S3.8m–p.

3.4. Results

3.4.1. Overall spatiotemporal changes in vegetation

The number of peatland sites represented by our binned 200-year timesteps increased throughout the Holocene from four cores at ~11,000 years BP to 61 cores at ~0 years BP (Figure S3.6a). Relative changes in peatland vegetation during the early-Holocene should be interpreted with some caution because of the low availability of core records, particularly in regions of present-day continuous and isolated permafrost (Figure S3.8a,d). We therefore focus our interpretations primarily on changes to vegetation composition during the mid- and late-Holocene, when the number of core records increased (Figure S3.6a). Additionally, 11 cores in our database contain no data before ~400 years BP. During the full length of peat core records, the 200-year binned relative abundance of herbaceous taxa decreased in 59 cores, while woody vegetation and *Sphagnum* increased in 44 and 41 cores, respectively. Proportions of woody vegetation and *Sphagnum* predominantly increased in cores extracted from palsas/peat plateaus (woody, n = 24/36; *Sphagnum*, n = 21/36) and bogs (woody, n = 13/19; *Sphagnum*, n = 13/19).

Overall, circum-Arctic peatlands evidenced a shift from communities dominated by herbaceous taxa prior to ~4,000 years BP, to those composed primarily of *Sphagnum,* non-*Sphagnum* mosses and woody vegetation at ~0 years BP (Figures 3.2 and S3.6). Transitions from herbaceous communities to assemblages dominated by *Sphagnum* and non-*Sphagnum* mosses accelerated from ~600 years BP, although woody expansion continued more gradually (Figure 3.2b), reflecting heterogeneity between geographical regions and present-day permafrost zones (see section 3.4.2 below). The $MNRA_{200}$ of PFTs averaged across all sites indicates a consistent expansion of woody vegetation from ~8,200 years BP to present (Figure 3.2b). However, recent increases to woody material were often of a smaller magnitude than *Sphagnum* and non-*Sphagnum* mosses, possibly due to the bias in field sampling towards *Sphagnum*-dominated microhabitats, which resulted in a slight decline in non-normalised mean woody abundance at ~0 years BP (Figures 3.2a and S3.6b). The $MNRA_{200}$ of woody vegetation increased

steadily during ~8,200–3,800 years BP and since ~1,800 years BP, although a temporary decline occurred during ~3,600–2,600 years BP. Our results indicate a substantial increase in the $MNRA_{200}$ of *Sphagnum* between ~7,400 and 3,600 years BP, when *Sphagnum* became the dominant PFT for the first time (Figure S3.6), following a steady reduction in herbaceous taxa across the same period (Figure 3.2b). *Sphagnum* expansion in circum-Arctic peatlands occurred in three main phases during the mid- to late-Holocene: during ~7,400–4,800 years BP, ~3,400–2,600 years BP, and since ~800 years BP. *Sphagnum* expansion temporarily slowed during ~1,600–800 years BP, enabling herbaceous taxa to briefly re-emerge as the dominant PFT (Figure S3.6). However, following a recent rapid decline, herbaceous taxa became the least abundant PFT at ~0 years BP, while the $MNRA_{200}$ of *Sphagnum* increased sharply after ~600 years BP. Non-*Sphagnum* mosses evidenced comparatively low $MNRA_{200}$ during ~5,800–400 years BP, but increased rapidly thereafter, with the greatest expansion occurring in cores from the continuous permafrost zone (see section 3.4.3 below).

Our NMDS ordination highlighted the underlying dissimilarity between PFTs in circum-Arctic peatlands and presented a temporal gradient of vegetation succession along Axis 1 (Figure 3.5). Binned mean assemblages from before ~6,000 years BP were commonly distributed to the right of the ordination space, alongside the herbaceous and non-*Sphagnum* moss PFTs. All binned mean assemblages since ~2,000 years BP recorded negative Axis 1 scores and were closely clustered, with low Axis 1 scores evidencing close association with *Sphagnum* and woody vegetation. Axis 2 indicated further dissimilarity between the PFTs, with *Sphagnum* and non-*Sphagnum* mosses shown to be strongly dissimilar across both axes.

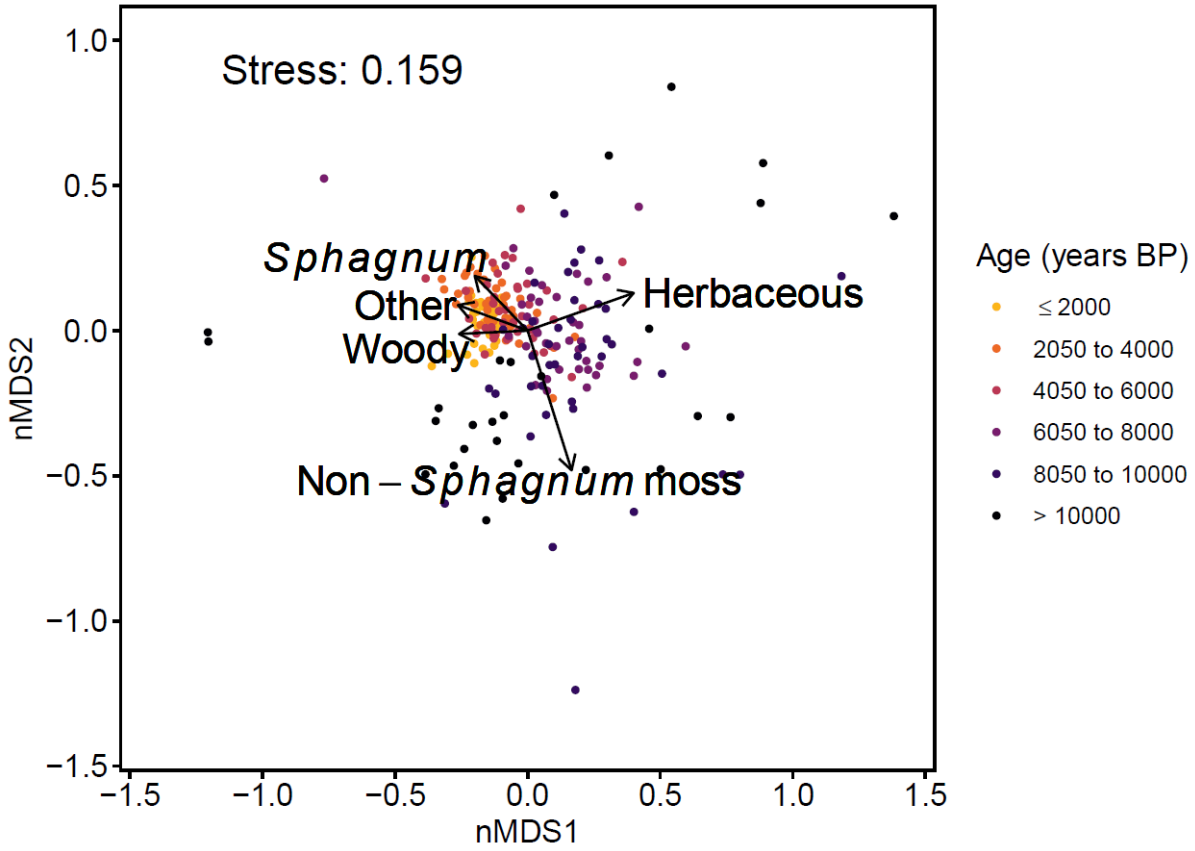

Figure 3.5. Non-metric multidimensional scaling (NMDS) plot showing Bray-Curtis dissimilarities between the mean relative abundance (%) of plant functional types in 50-year bins, averaged across all available cores. Other refers to unidentified organic matter or ambiguous material. For the time-series of these data, see Figure S3.6c. Binned samples are colour-coded by age (years BP).

3.4.2. Spatiotemporal variation in Holocene shrubification

The $MNRA_{200}$ of woody vegetation gradually increased through the mid- to late-Holocene across the present-day discontinuous, sporadic, and isolated permafrost zones (Figures 3.4 and S3.8), with late-Holocene increases prominent in cores from Fennoscandia and western Canada (Figure 3.3). In the discontinuous permafrost zone, woody vegetation in some cores peaked prior to ~10,000 years BP (Figure 3.4d), for example in early deglaciated regions of Alaska (Hunt et al., 2013) and northwestern Russia (Oksanen et al., 2001). However, during ~9,400–8,000 years BP the $MNRA_{200}$ of woody vegetation in this zone was generally low. After ~6,000 years BP, the $MNRA_{200}$

of woody vegetation in the discontinuous permafrost zone greatly increased, although large fluctuations occurred during this period, with lower abundances particularly evident during ~3,600–2,200 years BP. Similarly, cores from the sporadic permafrost zone evidenced a consistent expansion of woody vegetation after ~5,000 years BP, in parallel with *Sphagnum* increases (Figure 3.4f). In the isolated permafrost zone, the $MNRA_{200}$ of woody vegetation primarily increased before ~4,000 years BP and remained high throughout the late-Holocene, despite a steady decline after ~600 years BP (Figure 3.4h).

The late-Holocene expansion of woody vegetation in the contemporary discontinuous and sporadic permafrost zones was largely driven by increases in Fennoscandia, where 49 % (*n* = 18/37) of cores from these permafrost zones are located. The $MNRA_{200}$ of woody vegetation was low in Fennoscandia throughout the early- and mid-Holocene, but increased rapidly during ~1800–1400 years BP and after ~400 years BP (Figure 3.3f). A comparable increase in the $MNRA_{200}$ of woody vegetation occurred in western Canada during ~1,800–600 years BP, although proportions in this region have subsequently declined (Figure 3.3b). Our results for the isolated permafrost zone were dominated by cores located in eastern Canada (*n* = 14/20), where a longer-term decline in the $MNRA_{200}$ of woody vegetation was indicated from ~2,000 years BP to present (Figure 3.3d).

In contrast, five cores from the present-day continuous permafrost zone exhibited maximum values for the 200-year binned relative abundance of woody vegetation between ~6,600 and 3,000 years BP (Figure 3.4b), while four cores from this zone exhibited no woody material throughout the entire core record (Ellis and Rochefort, 2004; Nakatsubo et al., 2015; Sim et al., 2019). The density of core records for the continuous permafrost zone in each 200-year timestep prior to ~2,000 years BP was low, but increased thereafter (Figure S3.3a). Between ~2,000 and ~200 years BP the $MNRA_{200}$ of woody vegetation persisted at relatively low levels in the continuous permafrost zone, but noticeably increased at ~0 years BP when six cores recorded maximum 200-year binned relative abundances of woody vegetation.

Of the 52 cores that contained data for both the ~200 and ~0 years BP timesteps, a comparable number evidenced recent woody expansion (*n* = 23) and decline (*n* = 24), with both trajectories evident across all permafrost zones. Very recent shifts in vegetation composition should be interpreted with some caution, because relatively undecomposed organic matter may be present in some near-surface samples. Despite this, a greater number of cores in eastern Canada between ~200 and ~0 years BP evidenced reductions in woody vegetation (*n* = 8) than increases (*n* = 5), coinciding with rapid *Sphagnum* expansion (see section 3.4.3 below). Considering all records, we found that maximum values for the 200-year binned relative abundance of woody vegetation were reached at ~0 years BP in 16 cores, of which a majority were located northwards of 65°N (*n* = 11/16), for example in Fennoscandia (Sim et al., 2021b), Arctic Canada (Sim et al., 2019), Alaska (Gałka et al., 2018), and Siberia (de Klerk et al., 2011).

3.4.3. Holocene moss expansion in permafrost peatlands

Peatlands in regions of contemporary discontinuous, sporadic and isolated permafrost exhibited late-Holocene shifts from herbaceous- to *Sphagnum*-dominated assemblages, while peatlands in the continuous permafrost zone indicated rising abundances of non-*Sphagnum* mosses from ~1,800 years BP (such as *Calliergon* spp., *Dicranum* spp. and *Scorpidium* spp.) (Figure 3.4). During the early- and mid-Holocene, the $MNRA_{200}$ of herbaceous taxa was high across the circum-Arctic, but declined steadily in regions of continuous, discontinuous and sporadic permafrost from ~2,400 years BP, ~4,600 years BP, and ~5,800 years BP, respectively. Conversely, the $MNRA_{200}$ of herbaceous taxa remained stable in the isolated permafrost zone until ~400 years BP, but decreased sharply thereafter. Our dataset indicates a steady expansion in the $MNRA_{200}$ of *Sphagnum* in regions of discontinuous and sporadic permafrost during ~4,600–2,600 years BP and ~2,800–1,800 years BP, respectively. The $MNRA_{200}$ of *Sphagnum* in the discontinuous and sporadic permafrost zones subsequently declined until ~800 years BP and ~1,200 years BP, respectively, when herbaceous communities temporarily recovered (Figure 3.4c-f). In the isolated permafrost zone, the $MNRA_{200}$ of

Sphagnum has increased consistently since ~3,000 years BP and rapidly since ~600 years BP. Continued late-Holocene expansion of *Sphagnum* meant that at ~0 years BP, *Sphagnum* was the dominant PFT in the studied cores from regions of discontinuous, sporadic, and isolated permafrost (Figure 3.4c,e,g).

Conversely, in the continuous permafrost zone non-*Sphagnum* mosses were the dominant PFT at ~0 years BP (Figure 3.4a), following consistent increases from ~1,800 years BP, which accelerated after ~400 years BP (Figure 3.4b). By comparison, the $MNRA_{200}$ of *Sphagnum* in the continuous permafrost zone has persisted at low levels since ~2,400 years BP. Rapid increases to the $MNRA_{200}$ of non-*Sphagnum* mosses also occurred after ~400 years BP in cores from the discontinuous, sporadic, and isolated permafrost zones, although absolute increases in relative abundance in these cores were lesser than those from the continuous permafrost zone (Figures 3.4 and S3.8).

Our regional analyses indicate moderate *Sphagnum* abundance in cores from eastern Canada from ~6,000 years BP, while *Sphagnum* expansion in Fennoscandian cores primarily occurred during ~2,400–1,800 years BP and after ~1,200 years BP (Figure 3.3). After ~1,000 years BP, the $MNRA_{200}$ of *Sphagnum* increased steadily in western Canada and rapidly in eastern Canada, with eight cores from these regions exhibiting maximum values for the 200-year binned relative abundance of *Sphagnum* at ~0 years BP. In Fennoscandia, a steady decline in the $MNRA_{200}$ of herbaceous taxa from ~6,200 years BP accelerated from ~400 years BP, when the $MNRA_{200}$ of non-*Sphagnum* mosses substantially increased (Figure 3.3f).

3.5. Discussion

3.5.1. Drivers of Holocene peatland vegetation dynamics

3.5.1.1. *Early succession (prior to ~6,000 years BP)*

Cores in our plant macrofossil compilation with basal dates indicate distinct spatial patterns of peat initiation prior to ~6,000 years BP, when peatlands primarily established in early-deglaciated regions of Fennoscandia (Kjellman

et al., 2018; Sannel et al., 2018), northwestern Russia (Oksanen et al., 2001, 2003; Väliranta et al., 2003), western Canada (Vardy et al., 1997, 1998; Kettles et al., 2003; Bauer and Vitt, 2011) and Alaska (Hunt et al., 2013). Although only seasonally-thawed peats from the active layer were sampled from some permafrost peatland sites, these spatiotemporal patterns of peatland development corroborate previous findings (MacDonald et al., 2006; Morris et al., 2018; Treat et al., 2021b). Early peat initiation in these regions occurred during warming growing seasons (Morris et al., 2018) following the onset of the Holocene Thermal Maximum (HTM) at ~11,000–8,000 years BP (Kaufman et al., 2004; Weckström et al., 2010; Salonen et al., 2011), with proxy records indicating that generally warm, stable climates continued in these regions until ~5,000 years BP (Korhola et al., 2002; Salonen et al., 2011; Kaufman et al., 2016; Sejrup et al., 2016). In Fennoscandian cores, high abundances of herbaceous taxa and non-*Sphagnum* mosses from inception (Figure 3.3e–f) have been inferred to represent direct peat establishment onto wet mineral substrates (Kjellman et al., 2018; Sannel et al., 2018). Conversely, cores compiled from northwestern Russia and western Canada indicated peat initiation by terrestrialisation (infilling of waterbodies), with aquatic plants pre-dating fen species (Vardy et al., 1997, 1998; Oksanen et al., 2001, 2003), or paludification of existing forests, indicated by woody basal materials (Oksanen et al., 2001; Väliranta et al., 2003). Extensive peat initiation is thought to have started later in eastern Canada between ~8,000 and ~4,000 years BP (Payette, 1984; MacDonald et al., 2006; Fewster et al., 2020), following the final deglaciation of the Laurentide Ice Sheet during ~8,200–6,700 years BP (Ullman et al., 2016). Core records for eastern Canada in our synthesis begin from ~7,200 years BP (Figure 3.3c–d) and indicate peat initiation through paludification (Robitaille et al., 2021) and terrestrialisation (Beaulieu-Audy et al., 2009; Langlais et al., 2021).

Our dataset contains limited evidence for woody expansion in circum-Arctic peatlands prior to ~6,000 years BP, despite existing evidence that treelines were located farther north than present in early-deglaciated regions during the HTM (Payette and Lavoie, 1994; MacDonald et al., 2000). High peaks in the $MNRA_{200}$ of woody vegetation prior to ~10,000 years BP in the contemporary

discontinuous permafrost zone more likely indicate early paludification or alder fen formation than peatland shrubification, because abundances quickly declined and remained low during 9,400–8,000 years BP (Figure 3.4c–d). A previous review of subfossil peatland tree chronologies suggested that a scarcity of tree subfossils for the early-Holocene resulted from an absence of ombrotrophic peatlands (Edvardsson et al., 2016), likely owing to the generally long timescales required for FBTs (centuries to several millennia) (Beaulieu-Audy et al., 2009; Väliranta et al., 2017; Sannel et al., 2018), although some later-forming cores indicate *Sphagnum fuscum* presence since initiation (Sannel and Kuhry, 2008). Alternatively, woody vegetation may have grown in alder fens, but these wetlands are uncommon in permafrost regions. Indeed, the $MNRA_{200}$ of herbaceous taxa was high across the circum-Arctic prior to ~6,000 years BP (Figure 3.2), particularly in cores from Fennoscandia (Figure 3.3e–f), where several of the studied peatlands persisted as sedge-dominated fens throughout this period (Kjellman et al., 2018; Sannel et al., 2018). Even alongside the favourable warm climates of the HTM, shrub growth in minerotrophic fens would have been complicated by continuously high water tables, which reduce oxygen availability for roots (Leuschner et al., 2002). However, proportions of woody vegetation did increase in several herbaceous-dominated sites before ~6,000 years BP (Oksanen et al., 2001; Väliranta et al., 2003; Vardy et al., 1998, 2005; van Bellen et al., 2011), for example where isolated hummocks provided suitably dry substrates for ligneous root growth (Kjellman et al., 2018).

3.5.1.2. *Mid- to late-Holocene (~6,000–~1,000 years BP)*

After ~6,000 years BP, circum-Arctic peatland communities experienced a widespread shift towards *Sphagnum* and woody vegetation (Figure 3.2), particularly in regions of present-day discontinuous, sporadic and isolated permafrost (Figure 3.4c–f). Across the Arctic, this period is characterised by neoglacial climate cooling (Seppä and Birks, 2001; Gajewski, 2015; McKay et al., 2018). Multiproxy analyses indicate that the onset of neoglacial cooling was spatially variable, beginning earliest in Fennoscandia and Russia from ~7,000 years BP where cooling accelerated after ~2,000 years BP (McKay et al.,

2018), when binned assemblages in our analyses were primarily associated with *Sphagnum* and woody vegetation (Figure 3.5). Treelines retracted to their contemporary geographical limit at ~3,500 years BP across much of the Arctic (Payette and Lavoie, 1994; MacDonald et al., 2000), but continued to retreat southwards in Fennoscandia and European Russia after ~3,000 years BP (Seppä and Birks, 2001; Fang et al., 2013).

The sharp decline in herbaceous vegetation after ~6,000 years BP, and rising abundances of *Sphagnum* across all permafrost zones, is indicative of widespread FBTs and permafrost aggradation across the circum-Arctic from ~7,500 years BP (Treat et al., 2021b)**.** Autogenic peat accumulation occurred rapidly during the HTM (Jones and Yu, 2010; Yu et al., 2010; Loisel et al., 2014), causing peat surfaces in many sites to rise above local water tables, which facilitated growth of hummock-forming *Sphagnum* and shifts to ombrotrophic conditions during the mid-Holocene (Kuhry, 2008; Beaulieu-Audy et al., 2009; Langlais et al., 2021; Robitaille et al., 2021). These raised, ombrotrophic surfaces likely provided more suitable environments for shrub and tree colonisation than preceding wet fens. The persistence of high herbaceous abundances during ~4,000–1,200 years BP in regions of present-day continuous permafrost (Figure 3.4a–b) may partly be attributed to the initiation of several new peatlands, exhibiting initially wet conditions that favoured growth of sedges and brown mosses (Fritz et al., 2016; Teltewskoi et al., 2016; Gałka et al., 2018). Furthermore, herbaceous-dominated communities persisted in several Fennoscandian cores until ~2,400 years BP (Figure 3.3e–f), with ombrotrophication of these sites likely delayed by cold and moist neoglacial climates (Seppä and Birks, 2001) and the late aggradation of permafrost in this region (Kjellman et al., 2018; Sannel et al., 2018; Treat and Jones, 2018). Temporary reversions to fen vegetation also occurred in some established *Sphagnum*-dominated peatlands after ~6,000 years BP, in response to water table fluctuations (Robitaille et al., 2021) or permafrost degradation (Sannel and Kuhry, 2008), highlighting that peatland succession is not a unidirectional process.

The continued expansion of woody vegetation may also have been facilitated by early peat permafrost aggradation. Previous syntheses indicate steady

rates of permafrost aggradation in peatlands across the circum-Arctic from ~9,000 years BP, and peat permafrost became widespread in high latitude regions of Alaska, western Canada and Siberia by ~2,500 years BP (Treat and Jones, 2018; Treat et al., 2021b). In a similar manner to ombrotrophication, permafrost aggradation can create raised surfaces that are conducive to shrub colonisation, for example atop palsas/peat plateaus that exhibit deeper water tables than neighbouring fens (Zoltai and Tarnocai, 1975). Considering all cores in our dataset, original author interpretations suggest that peat permafrost aggradation occurred earliest in cores from western and central Canada (before ~4,000 years BP) (Vardy et al., 1998; Sannel and Kuhry, 2008; Bauer and Vitt, 2011), as indicated by alternating *Sphagnum fuscum* and rootlet layers, and rising abundances of Ericaceae. Although evidence exists for peat permafrost occurrence in some parts of northeastern Quebec from ~5,500 years BP (Treat and Jones, 2018), pollen records suggest that warm, moist climates persisted in Quebec until ~2,000 years BP (Kaufman et al., 2004; Viau and Gajewski, 2009), and most cores compiled for eastern Canada appear to have been permafrost-free throughout the Holocene. Increases to the $MNRA_{200}$ of *Sphagnum* and woody vegetation in eastern Canada after ~6,000 years BP were therefore more likely driven by FBTs, accelerated by rapid peat accumulation under favourable climates (Beaulieu-Audy et al., 2009; Robitaille et al., 2021). Furthermore, previous research indicates that peat permafrost aggradation in Fennoscandia and northwestern Russia primarily occurred after ~1,000 years BP (Kjellman et al., 2018; Sannel et al., 2018; Treat and Jones, 2018).

The declining $MNRA_{200}$ of woody vegetation in western Canada during ~3,200–1,800 years BP (Figure 3.3a–b) may indicate that cooling climates across the MacKenzie River Basin after ~5,000 years BP (Viau and Gajewski, 2009) eventually restricted peatland shrubification through reduced growing season temperatures or rising water tables. Simultaneous increases in *Sphagnum* perhaps reflects their broader tolerance to wet, anoxic conditions, low temperatures, and low nutrient availability (van Breemen, 1995; Gajewski et al., 2001). Alternatively, this temporary woody decline may be explained by peatland wildfires, which increased in frequency and severity in parts of

western and central Canada after ~4,000 years BP (Zoltai, 1993; Camill et al., 2009; Pelletier et al., 2017), and some cores from these regions evidenced a recurrence of charcoal and burnt materials after ~3,600 years BP (Kettles et al., 2003; Sannel and Kuhry, 2008).

3.5.1.3. *Last millennium (since ~1,000 years BP)*

Peatland vegetation succession accelerated in circum-Arctic peatlands after ~1,000 years BP, when late-Holocene climate shifts increased rates of ombrotrophication (Magnan et al., 2022) and peat permafrost aggradation and thaw (Treat and Jones, 2018). In common with previous suggestions by Treat et al. (2016), we identified differing successional pathways between peatlands in boreal and tundra ecoregions, with peatlands in the continuous permafrost zone evidencing a rapid expansion of non-*Sphagnum* mosses from ~1,800 years BP (Figure 3.4b). Although this late-Holocene expansion of non-*Sphagnum* mosses primarily occurred in polygon mires (Ouzilleau Samson et al., 2010; de Klerk et al., 2011; Teltewskoi et al., 2016; Sim et al., 2019), several cores from palsas/peat plateaus and bogs in Fennoscandia also indicated increased proportions of non-*Sphagnum* mosses in recent centuries (Kjellman et al., 2018; Sannel et al., 2018; Sim et al., 2021b) (Figure 3.3e–f). In contrast to other permafrost regions, the $MNRA_{200}$ of *Sphagnum* in the continuous permafrost zone remained comparatively low during the last millennium, perhaps indicating that growing seasons at high northern latitudes have been too cold for enhanced *Sphagnum* productivity (Gajewski et al., 2001; Loisel et al., 2012). Alternatively, in some High Arctic wetlands *Sphagnum* growth may have been restricted by high calcium concentrations (Vicherová et al., 2015), which can develop in shallow Arctic peats that overlie carbonate landscapes and that are seasonally inundated by snowmelt and ground-ice melt (Woo and Young, 2006). Recent peatland succession in the studied polygon mires appears to have been strongly influenced by shifts in local hydrology, resulting from permafrost-driven changes to microtopography (Ellis and Rochefort, 2004; de Klerk et al., 2011; Teltewskoi et al., 2016). Recent non-*Sphagnum* moss growth was primarily attributable to hydric moss expansion (e.g., *Calliergon* spp. or *Drepanocladus* spp.) in cores extracted

from wet polygon depressions or thawed trenches (Ouzilleau Samson et al., 2010; de Klerk et al., 2011; Sim et al., 2019), and mesic moss expansion (e.g., *Aulacomnium turgidum* and *Dicranum* spp.) in cores from drier, high-centred polygons and ridges (Ellis and Rochefort, 2004; Vardy et al., 2005; Teltewskoi et al., 2016).

Although six cores from the continuous permafrost zone recorded maximum values for the 200-year binned relative abundance of woody vegetation at ~0 years BP, non-normalised woody proportions remained low (≤ 11 %) at this time in many of the available cores from this zone (*n* = 13/16) (Figure S3.8a). This may suggest that permafrost peatlands in the High and Low Arctic have not, as yet, undergone the widespread shrubification observed in tundra environments (Mekonnen et al., 2021; Heijmans et al., 2022). Notable examples of recent peatland shrubification in regions of continuous permafrost were identified in cores from northern Alaska (Gałka et al., 2018) and a coastal fen in High Arctic Canada (Sim et al., 2021b), where binned woody abundances have greatly increased since ~200 years BP. In the latter fen site, woody vegetation was subsequently replaced by non-*Sphagnum* mosses after 2,000 C.E., a transition previously attributed to the preferential herbivory patterns of Arctic geese (Sim et al., 2019). Phases of increased shrubification also occurred in some polygon mire sites during recent millennia, but predominantly in cores extracted from elevated high-centred polygons and ridges (Vardy et al., 1997, 2005; Teltewskoi et al., 2016), supporting previous observational studies of polygon mire succession (Minke et al., 2009; Wolter et al., 2016). Conversely, core assemblages from low-centred polygons and troughs were dominated by herbaceous taxa and non-*Sphagnum* mosses throughout the Holocene (de Klerk et al., 2011; Sim et al., 2019). These localised depressions commonly exhibit persistent wet conditions, because neighbouring polygon rims create strong hydraulic gradients and act as hydrological barriers within the landscape (Helbig et al., 2013). Furthermore, vegetation compositions in low-centred polygons are more greatly influenced by the hydraulic properties of the underlying mineral soil, particularly where active-layers have deepened, because these sites exhibit shallower peat

layers than high-centred polygons and palsas/peat plateaus (Zoltai and Tarnocai, 1975).

Considering all cores in our dataset, the $MNRA_{200}$ of woody vegetation was consistently highest after ~1,000 years BP (Figure 3.2b), following the warm summer temperatures of the Medieval Climate Anomaly (MCA) in the Arctic during ~1,030–890 years BP (Werner et al., 2018). Temperatures varied across the northern hemisphere during the MCA, becoming mild in eastern Canada and northern Europe, but remaining cool across much of Siberia (Mann et al., 2009; Werner et al., 2018). Climatic conditions in Fennoscandia during the MCA were favourable for shrubification, as evidenced by altitudinal upshifts in the *Pinus sylvestris* treeline in Fennoscandia (Hiller et al., 2001; Kullman, 2015). The $MNRA_{200}$ of woody vegetation in the discontinuous and sporadic permafrost zone generally stabilised after ~1,000 years BP (Figure 3.4c–f), but evidenced continued increases in Fennoscandia after ~400 years BP (Figure 3.3e–f). Woody growth in these regions therefore continued during the coldest temperatures of the LIA (~550–100 years BP) (Mann et al., 2009; Werner et al., 2018), when peatland permafrost reached its most southerly extent (Halsey et al., 1995; Treat and Jones, 2018). LIA cooling deepened water tables in some peatlands in western Canada and Fennoscandia, often through climate-induced permafrost aggradation, which resulted in drier peat surfaces favourable for *Sphagnum* and woody encroachment (Magnan et al., 2018; Zhang et al., 2018). By contrast, the declining $MNRA_{200}$ of woody vegetation in eastern Canada after ~2,000 years BP coincided with regional increases to precipitation (Viau and Gajewski, 2009; Rodysill et al., 2018) and recent peatland surface wetting (Zhang et al., 2022). For example, reduced evapotranspiration during the LIA caused water tables to rise in some poor fen sites in Quebec, resulting in an expansion of hydrophilic *Sphagnum* (Van Bellen et al., 2013). Furthermore, recent woody decline has occurred in 24 cores across the circum-Arctic since ~200 years BP, during the peak period of Holocene peat permafrost thaw (Magnan et al., 2018; Treat and Jones, 2018).

In agreement with previous studies by (Magnan et al. (2018, 2022) and Piilo et al. (2023) our results demonstrated a rapid, concurrent expansion of

Sphagnum during recent centuries in peatlands from western and eastern Canada and Fennoscandia (Figure 3.3), coinciding with the end of the LIA and the onset of recent anthropogenic climate change. Magnan et al. (2018; 2022) demonstrated that peatlands from regions of sporadic and isolated permafrost in eastern Quebec and Alberta widely transitioned from fens to bogs during the 20th century and experienced a rapid expansion of *Sphagnum* sect. *Acutifolia* after 1980 CE in response to recent climate warming and increased evapotranspiration. Our data compilation includes 17 cores from eastern and western Canada that were included in these two studies, a majority of which are located in the isolated permafrost zone (*n* = 15), which explains why our results for this permafrost zone show similarly rapid increases to *Sphagnum* abundance after ~200 years BP (Figure 3.4g–h). In some alternative cores from the James Bay Lowlands, Quebec, that were not previously analysed by Magnan et al. (2022), there is evidence of earlier shifts towards *Sphagnum* sect. *Acutifolia* (Beaulieu-Audy et al., 2009; van Bellen et al., 2011), while *Sphagnum fuscum* developed from ~760 years BP in a palsa near Duncan Lake, Quebec (Tremblay et al., 2014). We interpret very recent changes in the isolated permafrost zone with greater confidence than other regions, because 65 % of our age-depth models from this permafrost zone (*n* = 13/20) included ^{210}Pb dating profiles for near-surface peats in addition to ^{14}C chronologies, compared to 23 % of cores from all other permafrost zones (*n* = 13/56). Slow peat accumulation rates, low sampling resolutions, and intermixing of deceased plant material can also sometimes disrupt near-surface ^{14}C dating (Goslar et al., 2005). Given such chronological limitations, we refrained from making conclusions on recent peatland vegetation trends at sub-centennial timescales. However, at the broad ~200-year resolution of our analyses, we identified similar, recent shifts to high *Sphagnum* abundance in well-dated cores from regions of discontinuous and sporadic permafrost. For example, several cores from Fennoscandia (Sim et al., 2021b) and the Seward Peninsula, Alaska (Hunt et al., 2013) exhibited increased *Sphagnum* abundance after ~400 years BP in response to 20th century climate warming and late-Holocene permafrost aggradation and thaw.

3.5.2. The importance of peatland hydrology for shrubification

Our catalogue of plant macrofossil records provides further evidence that Holocene tree and shrub growth on circum-Arctic peatlands has predominantly coincided with shifts to raised and drier peatland surfaces, resulting from autogenic peat accumulation, warming climates, and peat permafrost aggradation. However, recent shrubification signals were often concealed in non-normalised trendlines, because increases to binned relative abundances of woody vegetation were comparatively smaller during recent centuries than increases to *Sphagnum* (Figures S3.6–S3.8), which accelerated following late-Holocene FBTs and peat permafrost expansion. Woody vegetation and *Sphagnum* showed strong dissimilarity to wet-favouring herbaceous taxa (Figure 3.5) and both PFTs expanded through time as herbaceous vegetation declined (Figure 3.2). Herbaceous species presently dominate water-saturated fens and thermokarst wetlands (Vitt, 2006; Treat et al., 2016), with high water tables and anoxic conditions that restrict shrub and tree root growth (Szumigalski and Bayley, 1996; Jones et al., 2013). Our findings generally concur with recent experimental studies that have shown increased seedling survival on raised *Sphagnum* hummocks (Holmgren et al., 2015) and that increased evapotranspiration from newly-established trees may provide a positive feedback that further encourages woody encroachment (Limpens et al., 2014a). However, woody decline was also identified in several palsas/peat plateaus and bogs experiencing rapid, recent *Sphagnum* expansion (van Bellen et al., 2011; Tremblay et al., 2014; Magnan et al., 2018; Sim et al., 2021b), suggesting that *Sphagnum* can sometimes outcompete ligneous species through rapid vertical growth (Ohlson et al., 2001) or by engineering conditions that are slowly-draining, acidic, and nutrient-poor (van Breemen, 1995). While our study sought to establish between-site trends in past peatland vegetation change across the circum-Arctic, future studies could further investigate the importance of local hydrology and peatland microhabitat on the within-site variability of vegetation succession through analyses of closely-sampled, replicate cores (e.g., Piilo et al., 2023).

We found limited evidence of woody-herbaceous communities developing during recent centuries, although this may partly reflect a sampling bias in

existing palaeoecological studies towards *Sphagnum*-dominated microhabitats, and shrubified fens presently exist in some boreal permafrost regions (e.g., Davies et al. (2022)). Future palaeoecological analyses of cores from such fen sites may reveal alternative mechanisms for recent peatland shrubification. During the mid- and late-Holocene, woody vegetation developed in some herbaceous-dominated cores in eastern Canada, prior to major *Sphagnum* establishment (Loisel and Garneau, 2010; Tremblay et al., 2014; Primeau and Garneau, 2021; Robitaille et al., 2021) (Figures 3.3 and S3.7). Climate drying may have facilitated this temporary shrubification of fens by deepening water tables (Loisel and Garneau, 2010; Robitaille et al., 2021), because abundances of woody vegetation subsequently declined as regional precipitation increased in Quebec and Labrador after ~5,000 years BP (Viau and Gajewski, 2009). Available peatland water-table depth reconstructions, for example using testate amoebae, from boreal and coastal peatlands in eastern Canada indicate increased hydrological variability in the region from ~3,000 years BP (van Bellen et al., 2011; Magnan and Garneau, 2014; Primeau and Garneau, 2021). However, similar palaeohydrological reconstructions have currently only been synthesised since the LIA for permafrost regions (Zhang et al., 2022), which prevented detailed comparisons with our findings. The development of additional, long-term palaeohydrological records for circum-Arctic peatlands would further elucidate the relative importance of water tables and climate for past peatland shrubification.

The widespread Holocene expansion of *Sphagnum* in our dataset is consistent with previous syntheses of northern peat core records (Treat et al., 2016; Treat and Jones, 2018; Magnan et al., 2022), but unravelling the implications of the shift to *Sphagnum*-dominated assemblages was complicated by an absence of species-level records for more than a quarter of our compiled cores. *Sphagnum* mosses occupy wide environmental gradients, from minerotrophic, poor fens (e.g., *S. riparium* and *S. lindbergii*) to ombrotrophic bogs (e.g., *S. fuscum*, *S. rubellum* or *S. capillifolium*) (Treat and Jones, 2018; Magnan et al., 2022). Relative abundance data at a species-level is therefore required to determine wetland types from plant macrofossil records (Treat et al., 2016). It may also be possible to infer environmental niches of Holocene *Sphagnum*

communities through correlations with other PFTs, but the closed compositional nature of our dataset made such analyses unsuitable. Where species-level *Sphagnum* data were available, we found that *Sphagnum* expansion in the vast majority of cases was associated with eventual shifts to ombrotrophic indicators (*n* = 31 cores), while only three cores transitioned towards hydrophilic *Sphagnum*. However, this finding should be interpreted cautiously, and we reinforce previous recommendations that future studies should differentiate between *Sphagnum* species to improve palaeoecological reconstructions.

Our long-term palaeoecological analyses suggest that future peatland shrubification may occur heterogeneously in circum-Arctic peatlands under 21st century warming, and will likely be limited to sites where dry, ombrotrophic microhabitats persist. Warming climates can shift the hydrological balance of permafrost peatlands in divergent trajectories, as shown by recent palaeohydrological studies of changing peatland surface wetness since the LIA (Sim et al., 2021b; Zhang et al., 2022), with important implications for peatland vegetation composition. Projected future warming is expected to cause widespread peat permafrost degradation (Fewster et al., 2022) and peatland inundation (Olefeldt et al., 2016), but also increased surface drying through enhanced evapotranspiration (Swindles et al., 2015). Our Holocene dataset indicates that woody growth was initially restricted in sites that became saturated post-thaw, which resulted in rising abundances of sedges and hydrophilic *Sphagnum*. However, future plant productivity increases under warming climates could accelerate peat accumulation and FBTs, which previously drove increases to woody vegetation and *Sphagnum* sect. *Acutifolia* in the studied records. Furthermore, recent ice-wedge degradation has drained polygon depressions (Wolter et al., 2016), which may raise the likelihood of future shrub encroachment at northern high latitudes.

3.6. Conclusions

Our synthesis of plant macrofossil records from peatlands in the circum-Arctic permafrost region indicates a consistent, widespread expansion of woody vegetation and *Sphagnum* in circum-Arctic peatlands from ~8,000 years BP to present, as herbaceous vegetation declined. Transitions from herbaceous vegetation to *Sphagnum* accelerated after ~1,000 years BP, coinciding with continued neoglacial cooling and extensive peat permafrost aggradation. *Sphagnum* expanded rapidly after ~800 years BP in sites located in present-day regions of discontinuous and isolated permafrost, while non-*Sphagnum* mosses have become dominant in the continuous permafrost zone. Peatland shrubification during recent centuries was highly spatially variable, with our dataset evidencing widespread increases in Fennoscandia but a general decline in western and eastern Canada. Our findings suggest that shrub and tree growth will not occur as widely in circum-Arctic peatlands under 21st century climate warming as in upland tundra environments, and will more likely be restricted to peatlands experiencing surface drying.

3.7. Acknowledgements

R.E.F. is in receipt of a UK Natural Environment Research Council Training Grant (no. NE/S007458/1). C.C.T. is supported by a European Research Council Horizon 2020 grant (no. 851181) and the Helmholtz Impulse and Networking Fund. M.C.J. is funded by the USGS Climate Research and Development Program.

3.8. Supplementary material (S3.1) for Chapter 3

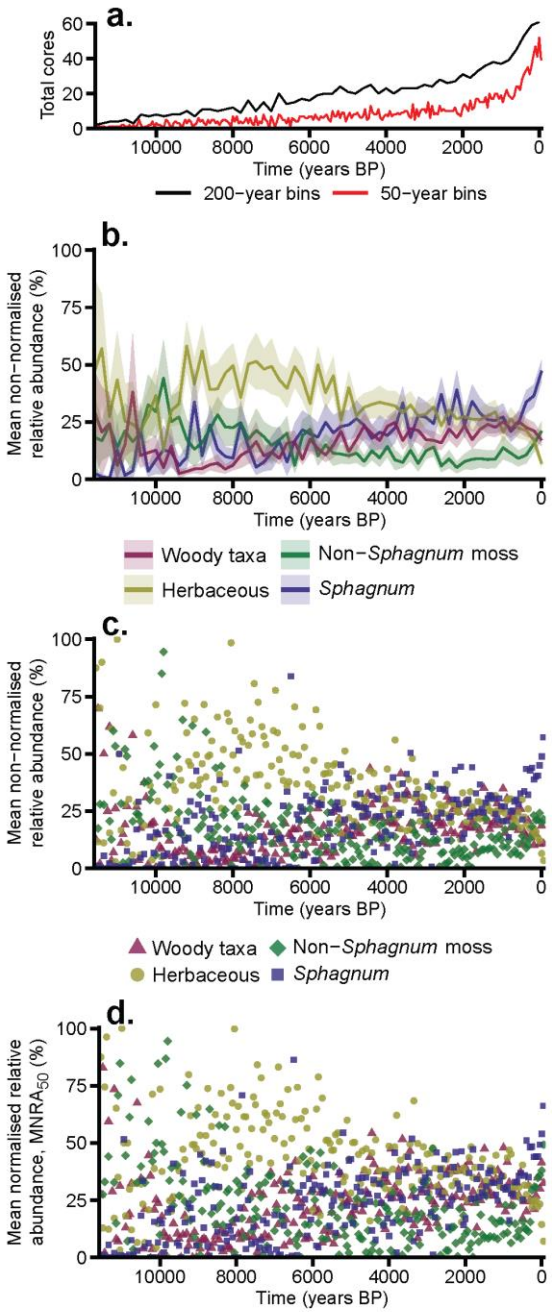

Figure S3.6. Holocene vegetation shifts in the studied circum-Arctic peatlands presented as: (a) the total cores included in each 200-year (black) and 50-year bin (red); (b) the between-core mean non-normalised relative abundance (%) of plant functional types (PFTs) in 200-year bins, with shading representing the standard error; (c) the between-core mean non-normalised relative abundance of PFTs in 50-year bins; and (d) the between-core mean normalised relative abundance of PFTs in 50-year bins, $MNRA_{50}$.

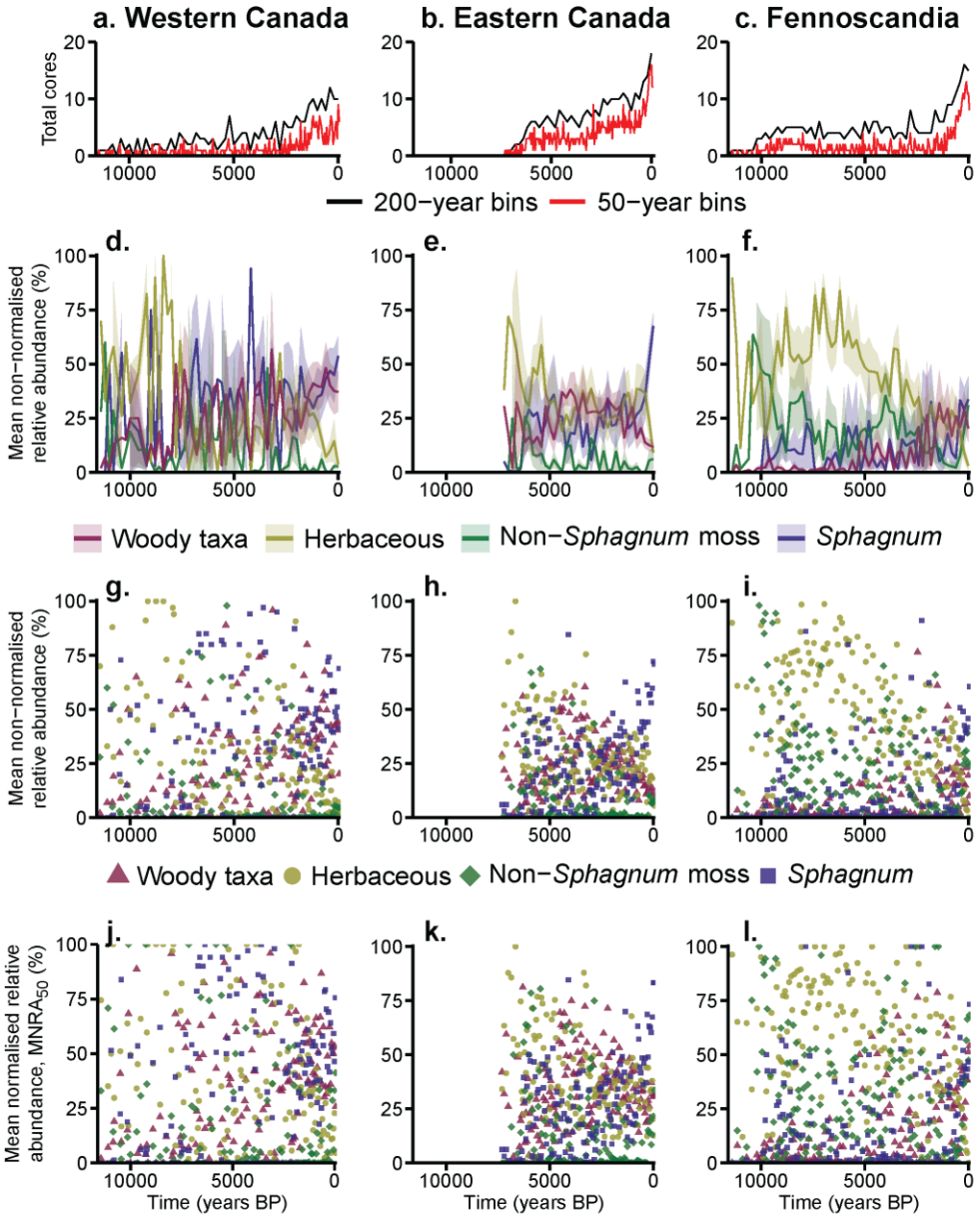

Figure S3.7. Spatiotemporal variation in Holocene peatland vegetation shifts between geographic regions (see Figure 3.1 for details). The total cores included in each 200-year (black) and 50-year bin (red) for (a) western Canada, (b) eastern Canada, and (c) Fennoscandia. The between-core mean non-normalised relative abundance (%) of plant functional types (PFTs) in 200-year bins for cores from (d) western Canada, (e) eastern Canada, and (f) Fennoscandia, with shading representing the standard error. The between-core mean non-normalised relative abundance of PFTs in 50-year bins for cores from (g) western Canada, (h) eastern Canada, and (i) Fennoscandia. The between-core mean normalised relative abundance of PFTs in 50-year bins, $MNRA_{50}$, for cores from (j) western Canada, (k) eastern Canada, and (l) Fennoscandia.

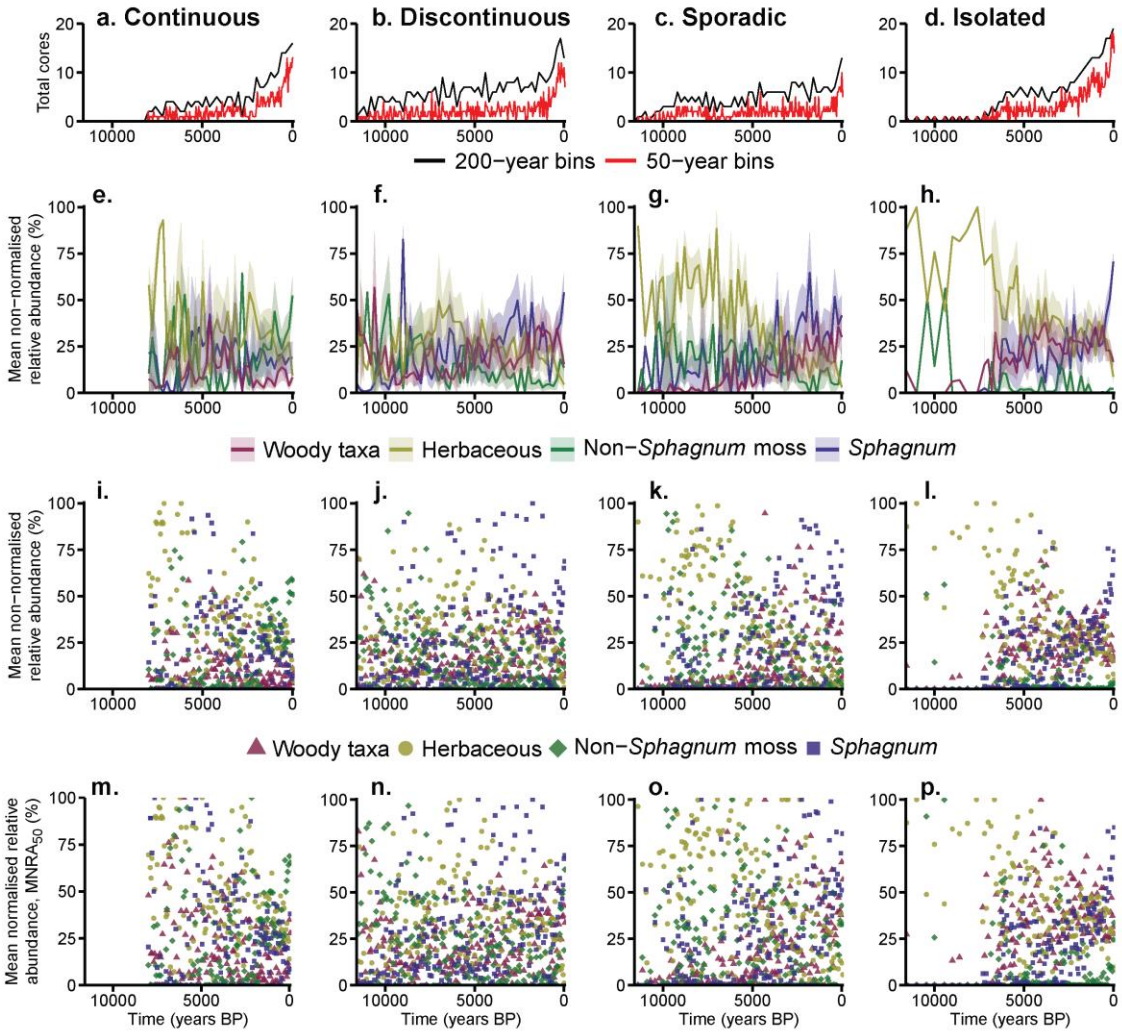

Figure S3.8. Spatiotemporal variation in Holocene peatland vegetation shifts between present-day permafrost zones. The total cores included in each 200-year (black) and 50-year bin (red) for the (a) continuous, (b) discontinuous, (c) sporadic, and (d) isolated permafrost zones. The between-core mean non-normalised relative abundance (%) of plant functional types (PFTs) in 200-year bins for cores from the (e) continuous, (f) discontinuous, (g) sporadic, and (h) isolated permafrost zones, with shading representing the standard error. The between-core mean non-normalised relative abundance of PFTs in 50-year bins for cores from the (i) continuous, (j) discontinuous, (k) sporadic, and (l) isolated permafrost zones. The between-core mean normalised relative abundance of PFTs in 50-year bins, $MNRA_{50}$, for cores from the (m) continuous, (n) discontinuous, (o) sporadic, and (p) isolated permafrost zones.

3.9. Supplementary material (S3.2) and supplementary data for Chapter 3

Any remaining data used to produce this research, including all age-depth models, are included in supplementary material S3.2 and supplementary datasets S3.1 and S3.2 (uploaded alongside this thesis).

Chapter 4
Controls on saturated hydraulic conductivity in a degrading permafrost peatland complex

4.1. Abstract

Permafrost peatlands are vulnerable to rapid structural changes under climatic warming, including vertical collapse. Peatland water budgets, and therefore peat hydraulic properties, are important determinants of vegetation and carbon fluxes. Measurements of hydraulic properties exist for only a limited number of permafrost peatland locations, primarily concentrated in North America. The impacts of thaw-induced collapse upon properties such as horizontal saturated hydraulic conductivity (K_h), and thus lateral drainage, remain poorly understood. We made laboratory determinations of K_h from 82 peat samples from a degrading Swedish palsa mire. We fitted a linear mixed-effects model (LMM) to establish the controls on K_h, which declined strongly with increasing depth, humification and dry bulk density. Depth exerted the strongest control on K_h in our LMM, which demonstrated strong predictive performance (r^2 = 0.605). Humification and dry bulk density were influential predictors, but the high collinearity of these two variables meant only one could be included reliably in our LMM. Surprisingly, peat K_h did not differ significantly between desiccating and collapsed palsas. We compared our site-specific LMM to an existing, large-scale model, fitted primarily to boreal and temperate peatlands. The large-scale model made less skilful predictions (r^2 = 0.528) than our site-specific model, possibly due to latitudinal differences in peat compaction, floristic composition and climate. Nonetheless, low bias means the large-scale model may still be useful for estimating peat K_h at high latitudes. Permafrost peatlands remain underrepresented in large-scale models of peat hydraulic properties, and measurements such as ours could be used to improve future iterations.

4.2. Introduction

Permafrost peatlands represent a globally-important soil organic carbon (SOC) store of 185 ± 70 Gt (Hugelius et al., 2020a), which has accumulated under cold climates that restrict microbial decomposition (Fewster et al., 2020, 2022). This important carbon store is threatened by projected climate warming, because permafrost thaw enables microbial decomposition to resume (Schädel et al., 2016; Voigt et al., 2019) and drives threshold changes in peatland physical and hydraulic structures, including surface collapse and increased hydrological connectivity between near-surface peats and drainage outlets (Olefeldt et al., 2021). Once thawed, saturated conditions protect peat carbon from aerobic decomposition, thereby limiting carbon dioxide emissions, but coincidently increase methane emissions (Turetsky et al., 2008; Grosse et al., 2011; Holmes et al., 2022). Model projections currently disagree as to whether permafrost peatland degradation will exert a net climate cooling or warming effect by 2100 (Gallego-Sala et al., 2018; Chaudhary et al., 2022; Zhao and Zhuang, 2023), because post-thaw greenhouse gas emissions may be partially offset by increased ecosystem productivity and carbon sequestration under warming climates (Holmes et al., 2022). The future radiative forcing of permafrost peatlands is therefore closely tied to their water retention, and an improved understanding of the peat hydraulic properties that mediate groundwater flows is valuable for predicting the future trajectories of these ecosystems.

One of the most important peat hydraulic properties is saturated hydraulic conductivity (K_{sat}) (dimensions of L T^{-1}). In permafrost peatlands, the widespread presence of a shallow, impermeable frost table means that vertical exchanges between the peat and underlying aquifers are limited, and horizontal saturated hydraulic conductivity (K_h) is relevant to determining rates of subsurface drainage (Quinton et al., 2008); while vertical saturated hydraulic conductivity (K_v) is more relevant to surface-atmosphere exchanges of moisture and heat (Nagare et al., 2012; O'Connor et al., 2020). Peat K_{sat} has been widely measured in boreal and temperate regions and these data have been used to develop large-scale pedotransfer functions (Lennartz and Liu,

2019; Liu and Lennartz, 2019; Morris et al., 2022), the most skilful of which demonstrate strong predictive performance (cross-validated $r^2 = 0.747$) (Morris et al., 2022). However, peat K_{sat} has been rarely measured in permafrost peatlands outside of North America, and permafrost dynamics are not currently represented in pedotransfer functions of peat K_{sat} (Morris et al., 2022), so it is unclear whether such models can be reliably applied in permafrost regions.

Existing K_{sat} measurements from permafrost peatlands are concentrated in specific geographic locations, particularly around Scotty Creek Research Station, Northwest Territories, Canada (Quinton et al., 2008, 2019; Quinton and Baltzer, 2013; Nagare et al., 2013; Gharedaghloo et al., 2018; Ackley et al., 2021) and the North Slope of the Brooks Mountain Range, Alaska (O'Connor et al., 2019, 2020). Scotty Creek is located in the discontinuous permafrost zone where peat-covered frost mounds are prevalent, termed palsas or peat plateaus depending on their areal extent (Zoltai and Tarnocai, 1975). Analyses of these peat plateaus have identified strong, vertical variations in near-surface K_{sat} across several orders of magnitude: an upper zone (depth ≤ 0.1 m) of high K_{sat} and a deeper zone (depth ≥ 0.2 m) of consistently low K_{sat} (Quinton et al., 2008, 2019; Nagare et al., 2013). Vertical gradients in peat K_{sat} are driven by changes in properties such as dry bulk density and peat humification (Päivänen, 1973; Morris et al., 2022). Deeper, older peats have typically been subjected to more decomposition and compaction, which weakens cellular structures and causes pores to collapse and become less connected (Pichan and O'Kelly, 2012; Rezanezhad et al., 2016). Other Canadian permafrost sites have evidenced similar depth relationships (Quinton et al., 2000, 2004; Morison et al., 2017), and dry bulk density has been identified as a universally strong predictor of K_{sat} in organic soils (including peats) on the Alaskan North Slope (O'Connor et al., 2020). Palsas and peat plateaus are also susceptible to desiccation and burning, which can remove the most permeable, near-surface peats (Ackley et al., 2021). Furthermore, pore network structures in permafrost peatlands are likely to be influenced by peat floristic composition (McCarter et al., 2020) and annual freeze-thaw cycles (Liu et al., 2022). Thaw can reduce groundwater flows by lowering the water table into deep, low K_{sat} peats, decreasing

hydraulic gradients across permafrost landforms, and shifting the peat-forming vegetation towards more readily-decomposed sedges (Quinton and Baltzer, 2013; Olefeldt et al., 2021), although it remains unknown whether permafrost thaw has any direct impact on peat hydraulic properties.

Permafrost peatlands in Fennoscandia appear to be close to a climatic tipping point (Fewster et al., 2022) and often exhibit mosaics of desiccating, raised palsas and collapsed areas that are now permafrost-free (Swindles et al., 2015). Surface collapse would appear to have the potential to drive important changes in pore structure and peat permeability, and ongoing thaw in these sites provides an opportunity to study peat hydraulic properties at different stages of palsa degradation. To our knowledge, only Wetzel et al. (2003) have previously measured peat K_{sat} in permafrost peatlands in Fennoscandia. They identified high dry bulk densities (up to 0.3 g cm^{-3}) and declining K_v with increasing depth in nine samples from Norwegian palsas. However, peat K_h remains unstudied for palsas in this region, which limits our understanding for their hydrological functioning following thaw, and it remains unclear how generalisable existing, spatially-limited measurements from permafrost peatlands are to Fennoscandian palsas.

We aimed to characterise peat K_h, and to establish its controls, in a degrading European palsa mire. Specifically, we addressed the following research questions:

1. Can combinations of easily-measured properties, such as depth, dry bulk density and the von Post hand-squeeze test for degree of humification, be used to predict peat K_h in degrading palsas?
2. Can an existing model, trained primarily on boreal and temperate peats (Morris et al., 2022), reliably predict peat K_h in a degrading permafrost peatland?
3. Do desiccating and collapsed areas of the palsa mire exhibit characteristic differences in peat K_h?

4.3. Methods

4.3.1. Study site

Rensjön palsa mire, sometimes also known as ‘Railway Bog’, is a degrading permafrost peatland in northern Sweden (68.0868°N, 19.8314°E; 488 m above sea level) (Figure 4.1), bordered by a regional railway line to the east, a watercourse to the south, and forested, mineral-soil uplands to the west. The site contains a mosaic of desiccating palsas with remaining permafrost, and collapsed areas and inundated fens that are permafrost-free, which characterises the trajectory of permafrost peatland degradation in Fennoscandia (Swindles et al., 2015). Desiccating palsas have either bare peat surfaces, or surface vegetation primarily comprised of *Cladonia* sp., *Empetrum nigrum*, *Andromeda polifolia*, *Betula nana*, *Salix sp.* and *Rubus chamaemorus.* Collapsed palsas are dominated by brown mosses, feather mosses and *Rubus chamaemorus*, with some *Sphagnum* spp., *Empetrum nigrum*, *Andromeda polifolia*, and *Betula nana*. Thermokarst and open-fen areas contain *Eriophorum* spp., *Carex* spp., *Sphagnum* spp., brown mosses, and *Lycopodium* sp., while *Salix* sp. are prevalent along the site’s permafrost-free, eastern margin. Palsas from Rensjön palsa mire have previously been sampled for palaeohydrological reconstructions, which have indicated peatland surface drying and reduced local C accumulation during the late-20th century (Sim et al., 2021b). At the nearby Rensjön weather station (68.0730°N, 19.8351°E; 493 m above sea level), mean annual temperature is currently −0.7°C with monthly average temperatures ranging from −13.3°C in January to 13.0°C in July, while annual unfrozen precipitation is 508.1 mm yr^{-1} (10-year averaging period: 2013–2022) (Swedish Meteorological and Hydrological Institute, 2023).

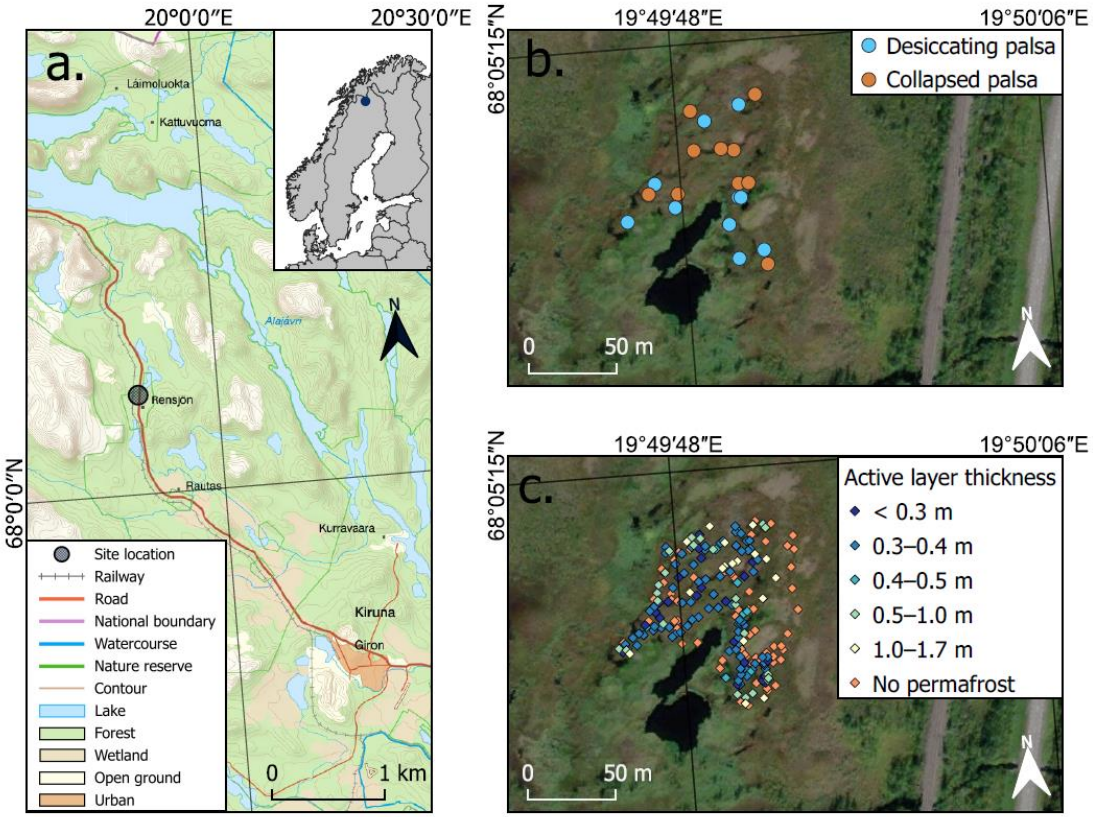

Figure 4.1. The Rensjön palsa mire study site: (a) the location of the site within Sweden (inset) and the Kiruna Municipality; and aerial imagery (August 2022) of the site overlain with (b) the 20 coring locations, coloured by the stage of palsa degradation; and (c) active-layer thickness across the site, measured using a ~2 m-long steel probe. Land cover data sourced from www.lantmateriet.se/. Aerial imagery sourced from ESRI (2023).

4.3.2. Field sampling

We extracted shallow peat cores from 20 locations across Rensjön palsa mire in July 2022, following a similar method to Morris et al. (2019). We inserted a cylindrical section of polyvinyl chloride (PVC) downpipe of 0.5 m length × 0.1 m diameter carefully into the peat using the scissor-cut method of Green and Baird (2012) to minimise sample compression. Each core was then carefully excavated using a spade. Cores were retained within their PVC cylinders during transport to the laboratory at the University of Leeds, UK, where they were stored in an upright, refrigerated state at ~4.0°C. To investigate whether peat hydraulic properties vary between different stages of palsa degradation, we collected 10 cores from desiccating palsas with intact, underlying

permafrost, and 10 cores from permafrost-free, collapsed palsas (Figure 4.1). Peat in inundated fen areas was too wet and loose to be recovered as intact samples.

At each coring location, we surveyed surface vegetation in a 0.5 × 0.5 m quadrat and measured the active-layer thickness adjacent to the coring location using a ~2 m-long steel probe. We also conducted a more extensive survey of active-layer thickness by taking 200 probe measurements across the site (Figure 4.1c). Active-layer thickness at coring locations on desiccating palsas ranged from 0.31–0.41 m (median = 0.36 m), which is similar to desiccating palsas across the site (0.22–0.46 m). No coring locations on collapsed palsas contained permafrost within the ~2 m reach of the steel probe, which enabled deeper samples to be collected for K_h determinations from collapsed areas than from desiccating palsa peats (Figure 4.2a). More broadly, some collapsed palsas across the site retained some permafrost at depths between 0.30 and 1.68 m, while 64 out of the 110 probed locations on collapsed palsas had no permafrost within ~2 m of the peat surface.

4.3.3. Laboratory analysis

We determined peat K_h in the laboratory using a custom-built permeameter method. We froze each peat core prior to our analysis at ~−18.0°C. We carefully cut open the PVC downpipes containing each frozen peat core using a thin-bladed angle grinder and checked the surface of each peat core for any cracks or voids. We used a pillar drill with a customised core drill bit to cut horizontal, cylindrical samples of 4.2 cm diameter from each frozen peat core. We then removed curved end faces from each subsample using a sharp knife. Samples were thawed overnight in cold storage at ~4.0°C and were then sealed inside an acrylic split-cylinder (4.0 cm internal diameter × 12.0 cm length), which consisted of two half cylinders that allowed the sample to be inserted without damage. We fastened a thin, neoprene gasket to the edge of one of these half cylinders, to form a water-tight seal when the sample was enclosed. We lined the acrylic cylinders with petroleum jelly to prevent preferential flow along the acrylic-peat interface and used tensioned rubber O-

rings to secure the two halves of the PVC split-cylinder together during K_h determinations (Figure S4.4).

Each enclosed subsample was saturated with pool water from a blanket bog in northern England (Keighley Moor) with a similar acidity (pH range: 3.91–4.13) to our studied palsa peats (pH range: 3.95–4.42).

Once saturated, a Mariotte regulator was positioned above the sample to generate a hydraulic gradient, with an outflow tube positioned into a measuring cylinder with a 'U' bend to control the outflow head (Figure S4.4). We took care at all times to ensure no air entered the saturated sample. We adjusted the height of the Mariotte regulator to ensure that the flow rate across the sample was similar for peats with different degrees of humification (e.g., shallow hydraulic gradients were required for highly permeable samples with open, connected pores). We ran pool water through the sample for an initial settling period of 30 minutes before running any tests. To measure peat K_h, we recorded the volume of water released through the split-cylinder during time intervals of between 10 and 20 minutes and calculated K_h from Darcy's Law, as described by Beckwith et al. (2003). Tests were repeated five times to evaluate any drift in measured K_h over time and we deemed K_h to have stabilised if at least three of the five K_h measurements were within ± 5 % of the median; any measurements outside this range were considered outliers and were removed. We temperature-corrected each K_h measurement to 20°C (Thomas et al., 2016), to account for the temperature-dependence of fluidity. For each sample, we then calculated the between-replicate harmonic mean of K_h from our standardised measurements (harmonic mean is appropriate in this situation, where the average is calculated from properties that have dimensions of velocity). In total, we measured peat K_h in 82 samples, comprising 35 from desiccating palsas and 47 from collapsed palsas (supplementary dataset S4.1).

We measured peat dry bulk density (g cm^{-3}) (DBD) by sampling known volumes of peat (between 1.0 and 2.5 cm^3) in peat offcuts immediately adjacent to each sample used for our K_h determinations, and oven-dried these samples at 105°C overnight, following Chambers et al. (2011). We repeated

this process three times for each sample and calculated the arithmetic mean of DBD. We also established the degree of peat humification for each sample using immediately adjacent peat offcuts, following the von Post classification method (Ekono, 1981).

4.3.4. Model development

Because we measured peat K_h at multiple depths in each core, it is possible that our dataset contains a hierarchical structure whereby measurements may exhibit greater variance between cores than within cores. Any such structured variance would violate the assumption of independent observations required by standard multiple regression. We therefore fitted a linear mixed-effects model (LMM) with core identity treated as the subject for a random intercept in an attempt to account for any between-core effects.

We developed a LMM to predict our measurements of peat K_h using: three continuous fixed-effect predictors (depth, DBD and von Post score); one categorical fixed-effect predictor describing the stage of palsa degradation (two levels: desiccating and collapsed); and the random effect describing core identity. We considered von Post score to be a continuous predictor, following the rationale of Morris et al. (2019). Our K_h measurements extended across four orders of magnitude, producing highly skewed, non-linear relationships with all continuous predictors. We therefore $\log_{10}$–transformed our measurements of peat K_h, following Morris et al. (2022). We also $\log_{10}$-transformed depth and DBD, because residuals from preliminary models fitted with transformed variables were more closely aligned with a Gaussian (normal) distribution. These transformations resulted in approximately linear, homoscedastic relationships between our continuous predictors and $\log_{10}(K_h)$.

During the model building process, we experimented with the inclusion of two-way, fixed-effect interactions between palsa degradation stage (desiccating or collapsed) and each continuous, fixed-effect predictor: $\log_{10}$(depth) × degradation stage; $\log_{10}$(DBD) × degradation stage; and von Post score × degradation stage. Additionally, we considered two-way interactions between

pairs of continuous, fixed-effect predictors: $\log_{10}$(depth) × $\log_{10}$(DBD); $\log_{10}$(depth) × von Post score; and $\log_{10}$(DBD) × von Post score.

We refined the specification of our LMM using a stepwise, forwards and backwards model building procedure, which balanced predictive performance with model parsimony, in R v.4.1.3 (R Core Team, 2022) using the *lmer* function from the *lme4* package (v.1.1-29) (Bates et al., 2014). We began by including all candidate fixed-effect predictors ($\log_{10}$(depth), $\log_{10}$(DBD), von Post score, and degradation stage), and core identity as a random effect. We then tested whether the addition of any interactions (see above) significantly improved model performance, before testing the removal of the remaining fixed effects. To evaluate the significance of each alteration, we followed the method of Morris et al. (2022) to calculate the difference in the corrected Akaike Information Criterion (AICc) (Hurvich and Tsai, 1989) for each model iteration. This approach considered AICc to be a Chi-squared statistic with degrees of freedom reflecting the difference in the number of predictors included in each model. We removed any predictor or interaction from our LMM where their omission led to a non-significant increase ($p > 0.05$) or decrease in AICc (lower AICc indicates improved model performance). Lastly, we assessed each pair of remaining predictors for any evidence of high collinearity, by calculating the Spearman's Rank correlation coefficient (r_s), and the generalised variance-inflation factor (GVIF) using the *vif* function from the R package *car* (v.3.1-0) (Fox and Weisberg, 2018). We deemed any predictor that exhibited a GVIF greater than $\sqrt{5}$ to be too highly collinear with at least one other predictor. In such cases, we excluded one of the affected predictors and recalculated GVIF. For our final LMM, we calculated standardised coefficients for each predictor by re-running our LMM with standardised predictors and response (Schielzeth, 2010), which we calculated using the *std* function in the *sjmisc* package (v.2.8.9) (Lüdecke, 2018).

4.3.5. Applicability of a model trained on boreal and temperate peats

We evaluated the ability of an existing pedotransfer function for peat K_{sat} by Morris et al. (2022), trained primarily on boreal and temperate peats, to predict our measurements of $\log_{10}(K_h)$ at Rensjön palsa mire. We tested the best performing model from Morris et al. (2022), which they termed Model 1, and which requires the continuous predictors $\log_{10}$(depth), $\log_{10}$(DBD), and von Post score (all measured in this study), and the categorical predictors trophic type (e.g., bog, fen), microform (e.g., hummock, hollow), and the Kerner Oceanity Index (KOI) (Morris et al., 2022). We initially classified the trophic type and microform of our samples as the unspecified category given by Morris et al. (2022), because palsa mires were not represented in the training data used to fit their model. However, given that our site exhibits ombrotrophic characteristics, including low peat pH (see section 4.3.3., above) and a prevalence of lichens, shrubs, and mosses at the coring locations, we also tested the use of the raised bog classification for trophic type. Following Morris et al. (2022), we calculated the KOI of Rensjön palsa mire from gridded mean monthly temperature data from the CRU TS 4.04 climatology (spatial resolution 0.5° latitude × 0.5° longitude) (Harris et al., 2020), averaged across the period 1961–1990. This classified the local climate to be oceanic (KOI = 10.8), albeit close to the KOI threshold for continental and subcontinental climates.

4.3.6. Evaluation of model performance

We evaluated the predictive performance of each model using the standard coefficient of determination (r^2), which we calculated from the linear relationship between measured and modelled values of $\log_{10}(K_h)$. We also adjusted this value (r^2_{adj}) to account for the number of predictors in each model, using the Wherry formula-1 in Yin and Fan (2001). We assessed bias in model predictions using Lin's concordance correlation coefficient (ρ_c), which has a range of −1 to 1, and which quantifies the agreement of the linear relationship between measured and modelled values to a line of perfect concordance.

Higher values of ρ_c indicate lower bias (i.e., closer agreement), while 0 indicates no agreement and −1 indicates perfect disagreement (Lin, 1989). We calculated ρ_c using the *CCC* function in the *DescTools* package (v0.99.47) (Signorell et al., 2022).

4.4. Results

4.4.1. Controls on peat K_h in degrading palsas

Measured values of peat K_h for Rensjön palsa mire varied from 4.85×10^{-7} to 3.61×10^{-4} m s^{-1}. Palsa peats evidenced varying degrees of humification (H1 to H8) and had higher bulk densities (median = 0.14 g cm^{-3}; range = 0.05–0.31 g cm^{-3}) than many boreal and temperate peats used to train existing, pedotransfer functions of peat K_{sat} (Morris et al., 2022). Inspection of simple bivariate plots indicates that $\log_{10}(K_h)$ is negatively related to $\log_{10}$(depth), $\log_{10}$(DBD) and von Post score (Figure 4.2a–c).

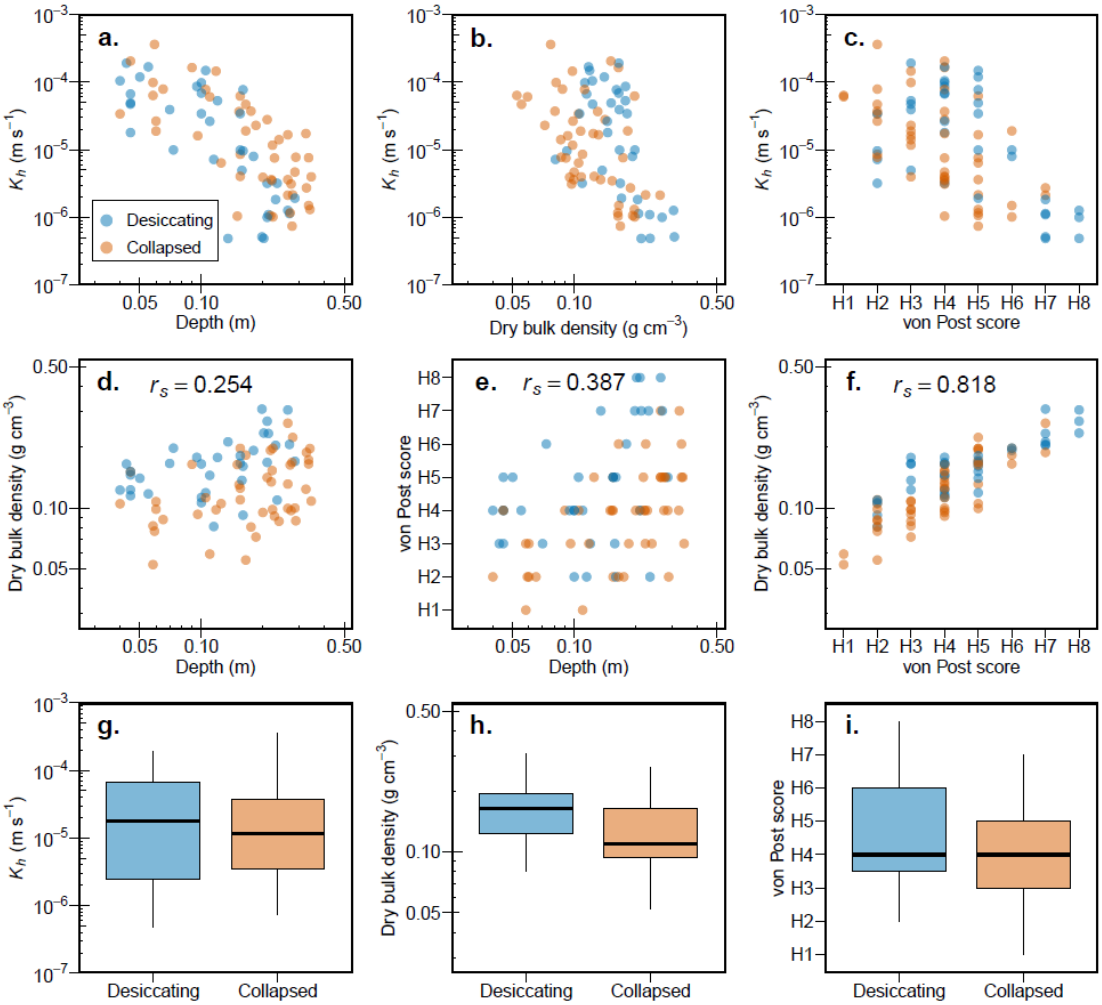

Figure 4.2. Peat hydraulic properties in degrading palsas. Top row: the response of K_h to (a) depth, (b) dry bulk density, and (c) von Post score. Middle row: bivariate correlation plots showing collinearity between continuous predictors (d–f); r_s is the Spearman's Rank correlation coefficient. Data points are coloured by the stage of palsa degradation. Bottom row: variation in (g) K_h, (h) dry bulk density, and (i) von Post score between stages of palsa degradation. K_h, depth and dry bulk density are presented on a $\log_{10}$ scale. In panels g–i: centrelines indicate median values; boxes indicate the interquartile range (IQR), and whiskers extend to 1.5 times the IQR beyond the upper and lower quartiles.

Our final LMM for Rensjön palsa mire indicates that $\log_{10}(K_h)$ declines significantly with increasing $\log_{10}$(depth) ($p < 0.001$) and von Post score ($p < 0.001$) (Table 4.1). The removal of either $\log_{10}$(depth) or von Post score leads to a significant increase in AICc (both $p < 0.001$), so both predictors were

retained. However, retaining both $\log_{10}$(DBD) and von Post score in our LMM resulted in GVIF scores greater than 3.4 for both predictors, indicating unacceptable levels of variance inflation in their parameter estimates. The predictors $\log_{10}$(DBD) and von Post score were strongly, positively correlated (r_s = 0.818) (Figure 4.2f), while lower levels of collinearity were evident between $\log_{10}$(depth) and von Post score (r_s = 0.387), and between $\log_{10}$(depth) and $\log_{10}$(DBD) (r_s = 0.254) (Figure 4.2d,e). The omission of either von Post score or $\log_{10}$(DBD) from our LMM did not lead to a significant increase in AICc, but the omission of both variables did. For this reason, it was necessary to omit one of $\log_{10}$(DBD) or von Post score from our final LMM. Residuals for a LMM fitted with von Post score were more closely aligned with a Gaussian (normal) distribution than an equivalent LMM fitted with $\log_{10}$(DBD), so we retained von Post score and omitted $\log_{10}$(DBD) for our final model. However, predictive performance is similar for these two LMMs, and either predictor could be used effectively for modelling peat K_{sat} in degrading palsas. During the backwards removal of fixed effects, we found that the stage of palsa degradation (desiccating or collapsed) did not have any significant, independent effect on $\log_{10}(K_h)$ and its removal caused AICc to decrease (see section 4.4.3., below).

Our final LMM has normally distributed, unstructured residuals with low GVIF scores for $\log_{10}$(depth) (1.4) and von Post score (1.4), indicating that the issue of multicollinearity has been resolved. The standardised parameter coefficient for $\log_{10}$(depth) (−0.587) suggests that it exerts a stronger influence on $\log_{10}(K_h)$ than von Post score does (−0.343). Model performance metrics indicate that our LMM explains a substantial proportion of the variance in measured $\log_{10}(K_h)$ (r^2 = 0.605; r^2_{adj} = 0.590) with low predictive bias (ρ_c = 0.756) (Figure 4.3a). Our LMM generally underestimates near-surface, high values of $\log_{10}(K_h)$ and overestimates deeper, low values (Figure 4.3a).

While testing the addition of two-way interactions in our model building process, we discounted the interaction between $\log_{10}$(DBD) and von Post score, because the inclusion of an interaction between these two highly correlated predictors (Figure 4.2f) risked introducing severe multicollinearity to our LMM. No addition of any interactions improved model performance, so

none were included in our final LMM. As expected, our dataset exhibits some evidence of within-core dependency, indicated by a significant increase in model AICc ($p < 0.05$) if the random subject for core identity is removed. Our final LMM therefore includes core identity as the subject of a random intercept term.

Table 4.1. Summary of fixed effects for our linear mixed-effects model to characterise $\log_{10}(K_h)$ in Rensjön palsa mire.

Predictor	Coefficient	Std. Error	Std. Coeff.	t	*p*
Constant	−5.62066	0.29293	-	−19.188	< 0.001
$\log_{10}$(depth) (m)	−1.60117	0.18781	−0.58673	−8.526	< 0.001
Von Post score	−0.15609	0.03702	−0.34339	−4.217	< 0.001

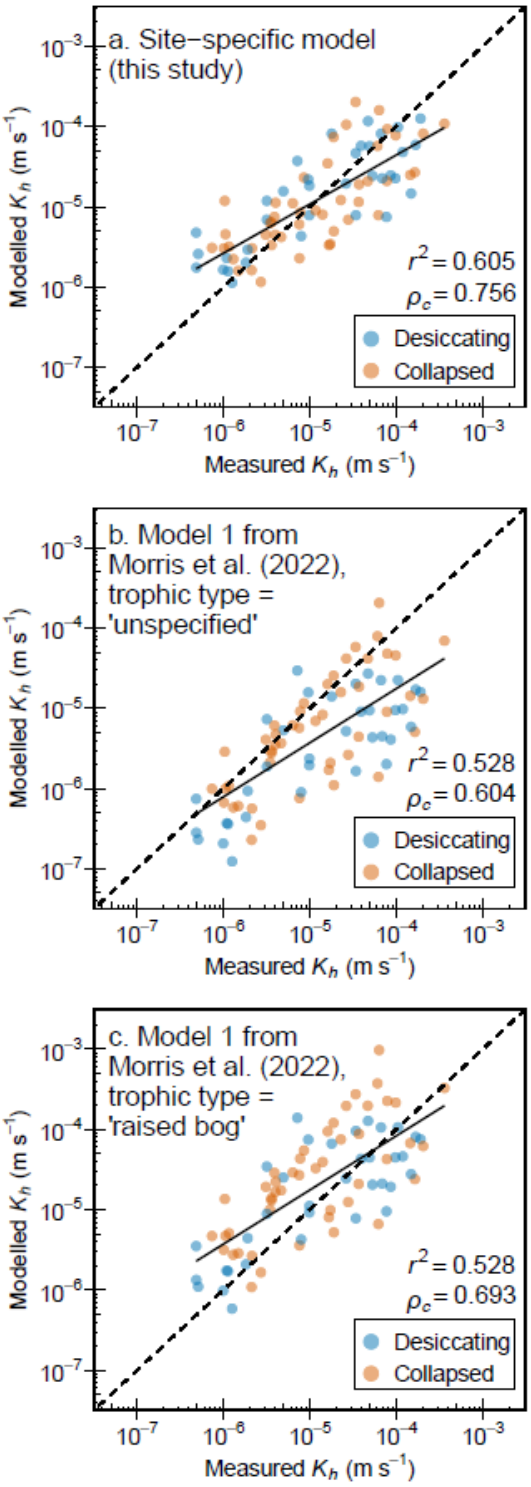

Figure 4.3. Performance plots showing measured values against modelled values for: (a) our linear mixed-effects model (LMM); and for an existing, large-scale model by Morris et al. (2022) with trophic type specified as (b) unspecified and (c) raised bog. Dashed line indicates perfect concordance between measured and modelled values; solid line indicates a linear regression between measured and modelled values; r^2 is the coefficient of determination; and ρ_c is Lin's concordance correlation coefficient, used to estimate model bias.

4.4.2. Performance of an existing K_{sat} model

The peat K_{sat} model by Morris et al. (2022) accounted for a lower proportion of the variance in $\log_{10}(K_h)$ at Rensjön palsa mire (r^2 = 0.528; r^2_{adj} = 0.429) than our site-specific LMM (see section 4.4.1., above). Setting the trophic type of the site to be unspecified resulted in model predictions that had substantial bias (ρ_c = 0.604) and consistently underestimated measured $\log_{10}(K_h)$, particularly for shallow peats with high $\log_{10}(K_h)$ (Figure 4.3b). Changing the trophic type to raised bog removed some of this bias, increasing ρ_c to 0.693 (Figure 4.3c). This level of bias is similar to that of our LMM (Figure 4.3a). For high measured values of $\log_{10}(K_h)$, the model by Morris et al. (2022) more commonly overpredicted values for collapsed palsas and underpredicted values for desiccating palsas, although no discernible trends were evident in predictions of lower $\log_{10}(K_h)$ values (Figure 4.3b–c).

4.4.3. The effect of palsa collapse on peat K_h

The stage of palsa degradation did not exert a significant, independent control on measured $\log_{10}(K_h)$ at Rensjön palsa mire. Measurements of K_h were similar between desiccating palsas (median = 1.79×10^{-5} m s^{-1}) and collapsed palsas (median = 1.17×10^{-5} m s^{-1}) (Figure 4.2g). Contrary to our expectations, DBD was generally higher in peats from desiccating than collapsed palsas (medians of 0.17 and 0.11 g cm^{-3}, respectively) (Figure 4.2h), and the most highly humified peats were also sampled from desiccating palsas (Figure 4.2i). However, when all fixed effects were included during the stepwise model building process, there was almost no evidence of the categorical variable for degradation stage exerting an effect on $\log_{10}(K_h)$ (p = 0.983) and the removal of this predictor caused model AICc to decline (an improvement in model performance). Furthermore, no interactions involving degradation stage ($\log_{10}$(depth) × degradation stage; $\log_{10}$(DBD) × degradation stage; or von Post score × degradation stage) gave any significant improvement in the performance of our LMM.

4.5. Discussion

4.5.1. Horizontal permeability of degrading palsas

Peat K_h in degrading palsas near Rensjön evidenced similar negative relationships with depth, humification and DBD to previous studies of northern peatlands, with our highest K_h values occurring in lightly decomposed, near-surface peats. While between-site comparisons of peat K_h are somewhat complicated by different measurement techniques (Morris et al., 2022), our measured values for the upper 0.1 m of peat were at least one order of magnitude lower than those reported for peat plateaus at Scotty Creek, Northwest Territories, Canada (Quinton et al., 2008; Gharedaghloo et al., 2018), perhaps due to the comparatively lower DBD of unburnt peats at that site (Ackley et al., 2021). The higher DBD values for Rensjön palsa mire are comparable to previous DBD measurements from Fennoscandian palsas (Wetzel et al., 2003; Sim et al., 2021b) and our maximum K_h value (3.61×10^{-4} m s^{-1}) is similar to the highest K_v value recorded for palsas near Kautokeino, Norway (2.94×10^{-4} m s^{-1}) (Wetzel et al., 2003). The minimum value of peat K_h measured in our study (4.85×10^{-7} m s^{-1}) is similar to some previous measurements from anoxic peats on the Alaskan North Slope (O'Connor et al., 2020).

Log_{10}(depth) exerted the strongest control on $log_{10}(K_h)$ in our LMM, as indicated by its high standardised coefficient, while the von Post measure of peat humification also exerted a highly significant control (Table 4.1). Peat depth accounts for some of the variation in both peat compaction and decay because the structural matrix of deeper, older peats is weakened by prolonged decomposition, which increases their susceptibility to compression under the weight of fresher, overlying peats (Ohlson, 1998; Branham and Strack, 2014). Alternatively, declining K_h with depth may relate to differences in peat hydraulic properties between the oxic and anoxic components of the peat profile (O'Connor et al., 2020), increased pore tortuosity, and loss of pore connectivity (Gharedaghloo et al., 2018). Peat desiccation can also drive a vertical displacement of the peat profile through peat shrinkage and compression (Hobbs, 1986; Ackley et al., 2021) or by rendering raised palsa surfaces

susceptible to aeolian erosion (Seppälä, 2003). Log_{10}(depth) was positively correlated with von Post score (Figure 4.2e), although low GVIF scores suggest that any collinearity is not great enough to destabilise parameter estimates and that each predictor exerts a strong, independent effect on $log_{10}(K_h)$ in our LMM.

The high collinearity of log_{10}(DBD) and von Post score (Figure 4.2f) was greater than reported for previous studies (Morris et al., 2019, 2022) and prevented us from including both predictors in our final LMM due to unacceptable inflation of parameter variance. However, even after omitting log_{10}(DBD), the high explanatory power of our LMM (r^2 = 0.605) suggests that only one of these predictors is required to explain this portion of variance for $log_{10}(K_h)$ in degrading palsas. Indeed, our preliminary analyses identified a similar level of predictive performance from an equivalent LMM fitted with log_{10}(DBD) instead of von Post score, and DBD has independently explained large portions of peat K_{sat} variance in other permafrost sites (O'Connor et al., 2020). The retention of log_{10}(depth) and von Post score, and removal of log_{10}(DBD), means that our LMM contains the same continuous predictors as Model 2 by Morris et al. (2022), which allows for rapid field estimation of peat K_{sat} without the need for any laboratory measurements.

Estimated slope coefficients for log_{10}(depth) and von Post score in our LMM (Table 4.1) closely align with those from the large-scale meta-analysis by Morris et al. (2022), providing some support for the assertion by Quinton et al. (2008) that peats with a similar degree of decomposition and compaction evidence similar K_{sat} irrespective of their geographic location. However, the generally high DBD of palsas at our study site means that our near-surface K_h determinations are towards the lower tail of values recorded for the upper 0.35 m of boreal and temperate peats (Morris et al., 2022). This may partly explain why the large-scale pedotransfer function by Morris et al. (2022) made less skilful predictions of $log_{10}(K_h)$ at Rensjön palsa mire than our site-specific LMM (Figure 4.3), and had less explanatory power (r^2 = 0.528) than for the boreal and temperate peatlands on which it was trained (cross-validated r^2 = 0.747). Alternatively, its reduced performance may relate to unrepresented processes specific to permafrost peatlands, such as their different floristic composition or

freeze-thaw dynamics (discussed below). Regardless, the large-scale model still explained approximately half of the total variance in unseen values of $\log_{10}(K_h)$ in degrading palsas and exhibited similar levels of bias to our site-specific model, which may be considered adequate depending on the application.

4.5.2. Permafrost thaw and peat hydraulic properties

Contrary to our expectations, we did not find any significant difference in peat K_h between desiccating and collapsed palsas (Figure 4.2g), nor any significant interaction involving the stage of palsa degradation. For the uppermost peat layers (< 0.1 m depth), the range of peat K_h was almost identical in desiccating and collapsed palsas (Figure 4.2a), despite samples from desiccating palsas often having higher DBD and slightly greater degrees of peat humification (Figure 4.2d,e,h,i). Alternative, unmeasured factors, such as macroporosity, may have reduced any differences in the K_h of these shallow peats (Holden et al., 2001), particularly because some deeper, lightly-humified samples from collapsed palsas did have higher K_h than comparably-deep, desiccating palsa peats (Figure 4.2a,e), although unequal sampling of deep peats may affect this comparison. Raised, desiccating palsa surfaces were more commonly inhabited by ligneous shrubs than collapsed areas, where saturated, anoxic conditions restrict root growth (Limpens et al., 2021; Olefeldt et al., 2021). Ligneous roots can increase K_{sat}, even in decayed and compacted peats, through the creation of macropores and relict root channels (Holden, 2009; Surridge et al., 2005; McCarter et al., 2020). Shallow, impenetrable frost tables in desiccating palsas force rooting zones to be near-surface and to extend laterally, meaning shrub roots may be less influential for the K_h of deeper peats or K_v. Alternatively, freeze-thaw cycles can increase the macroporosity of low K_{sat} peats through the formation of ice lenses in micropores, which produce cracks upon expansion that subsequently increase peat K_{sat} (Liu et al., 2022). Conversely, for peats with initially high K_{sat}, freeze-thaw processes generally reduce peat K_{sat}, because existing macropores can become blocked by the breakdown of large aggregates (Liu et al., 2022).

Given the similarity of peat K_h between desiccating and collapsed areas of the palsa complex, thaw-driven changes to the hydraulic functioning of the site will more likely be driven by increases to active layer thickness and reduced topographical gradients than any direct alterations to peat hydraulic properties. Currently, lateral runoff from desiccating palsas into neighbouring, collapsed areas and inundated fens is driven by the high K_h of the uppermost, seasonally-thawed peats, steep hydraulic gradients, and the prevalence of near-surface, impermeable permafrost. As palsas thaw and active layers thicken, water tables may be initially lowered into deeper peats with lower K_h, which could increase water retention as hydraulic gradients simultaneously decline (Quinton and Baltzer, 2013). A shift to persistently saturated, anaerobic conditions may explain why many collapsed palsa peats unexpectedly had lower humification and DBD, although this could also indicate that compaction following subsidence occurs deeper in the peat profile, below the active layer. Longer-term permafrost degradation may increase the hydrological connectivity of the site, because water tables in collapsed areas persist closer to the surface, where peat K_h is highest (Figure 4.2a), and thaw removes impermeable, frozen barriers to groundwater flows (Quinton and Baltzer, 2013; Connon et al., 2014; Haynes et al., 2018).

4.5.3. Opportunities for future research

Our modelling demonstrates that simple, affordable measurements of peat properties can be used to predict K_h in peatlands beyond the boreal and temperate regions to which many existing, pedotransfer functions are currently fitted (e.g., Liu and Lennartz, 2019; Morris et al., 2022). Generalisable models of peat K_{sat} have the potential to provide skilful estimations for the hydrological functioning of remote Arctic peatlands without the need for extensive field or laboratory measurements, although our findings indicate that permafrost peatlands firstly require greater representation in their training datasets. During our analysis, we found that changing the trophic type classification of Rensjön palsa mire from unspecified to raised bog reduced the predictive bias of the model by Morris et al. (2022) (Figure 4.3b–c). Developing additional categorical descriptors to account for permafrost-specific processes could

further improve model predictions of peat K_{sat} for Arctic regions, once suitable training data are available.

Further research is also required to explore spatial variability in peat hydraulic properties of permafrost peatlands in Fennoscandia and Siberia, because measurements remain sparse in these regions and other permafrost peatland types remain understudied, such as polygon mires (Helbig et al., 2013). The sparsity of previous research at Rensjön palsa mire means it is unknown when these palsas began to thaw, but spatial chronosequences of palsa mires with different ages of permafrost degradation could be analysed to assess whether the post-thaw stability of peat hydraulic properties changes with time. Limited aerial imagery of our study site indicates that thermokarst drainage and collapse scar formation occurred at some point between 1960 and 2013 (Sim et al., 2021b). For more intensively-studied sites, monthly observations of snow-cover, active-layer thickness, and disturbance (e.g., burning) may account for some unexplained variance in peat K_h (Ackley et al., 2021). Lastly, future studies could attempt to measure peat K_{sat} in newly terrestrialising areas of inundated fens, which represent the final stage of palsa degradation after collapse (Swindles et al., 2015) and are important for the longer-term hydrological functioning of the site following permafrost thaw.

4.6. Conclusions

We found that much of the variance in $\log_{10}(K_h)$ of degrading Arctic palsas can be explained using simple measurements of peat properties, in a similar manner to previous models of boreal and temperate peatlands. Our LMM showed that $\log_{10}$(depth) exerted the strongest, independent control on $\log_{10}(K_h)$, while the highly influential effects of von Post score and DBD were found to be highly collinear, meaning the latter was omitted from our final model. An existing pedotransfer function of peat K_{sat}, fitted primarily to boreal and temperate peatlands, was less skilful at predicting $\log_{10}(K_h)$ in degrading palsas than our site-specific LMM, with differences in predictive performance likely related to the high DBD of palsa peats, their floristic composition, or their

exposure to freeze-thaw processes. Near-surface peat K_h did not significantly differ between desiccating and collapsed palsas, indicating that any post-thaw changes to their hydrological functioning will be more likely driven by reduced hydraulic gradients than altered peat properties. Our study emphasises the need for permafrost peatlands to be better represented in large-scale models of peat K_{sat} before such models can be reliably extended to Arctic regions.

4.7. Acknowledgements

R.E.F. is in receipt of a UK Natural Environment Research Council (NERC) Training Grant (no. NE/S007458/1). The split cylinder permeameter was developed as part of grant NE/J007609/1 awarded by NERC. GTS acknowledges funding from the Dutch Foundation for the Conservation of Irish Bogs, Quaternary Research Association and Leverhulme Trust RPG-2021-354. We thank the Swedish Polar Research Secretariat and SITES for the support of the work done at the Abisko Scientific Research Station. SITES is supported by the Swedish Research Council's grant 4.3-2021-00164. We thank the County Administrative Board of Norrbotten for granting permission to sample within the Rautas fjällurskog nature reserve. David Ashley, Joshua Greenwood, Holly Armitage, Antony Windross, and Stephen Burgess provided technical and laboratory support, and Isaac Smith provided valuable logistic support (all University of Leeds, UK).

4.8. Supplementary material for Chapter 4

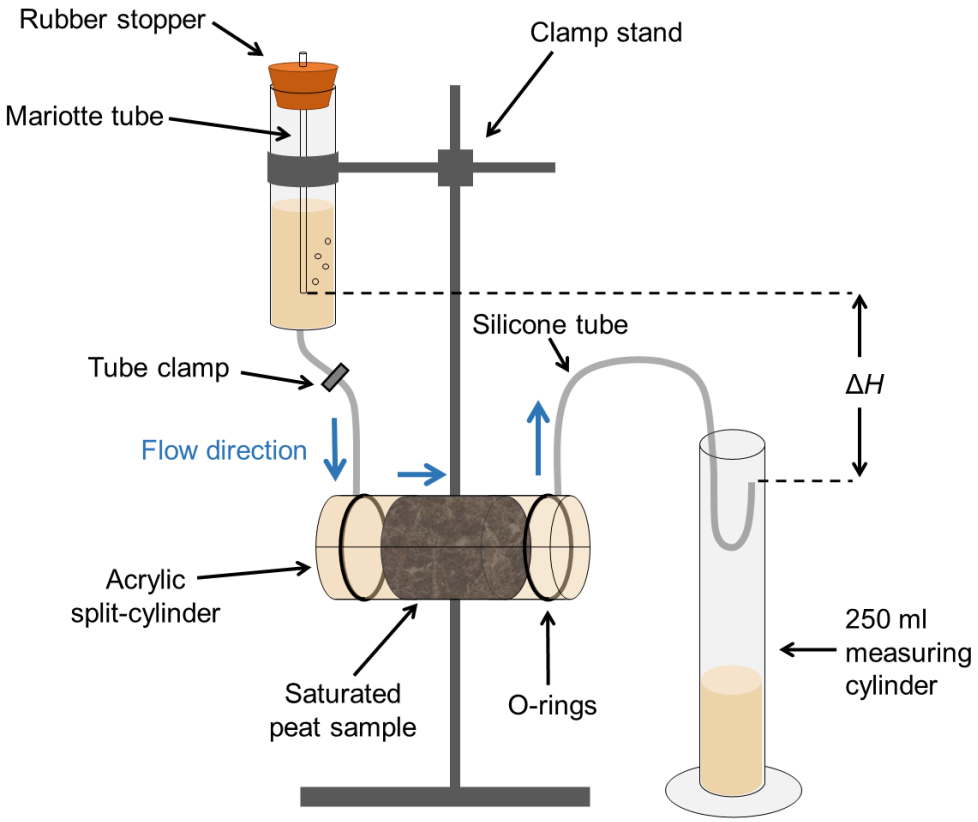

Figure S4.4. Diagram outlining the experimental setup for measuring horizontal saturated hydraulic conductivity of peat. The head difference across the sample (ΔH) is calculated from the end of the Mariotte bubble tube and the end of the outflow tube positioned in the measuring cylinder. We repositioned the Mariotte bubble tube to adjust ΔH for peats with different degrees of humification (e.g., a lower ΔH was required for highly permeable peats with open, interconnected pores).

4.9. Supplementary data for Chapter 4

The laboratory measurements used to produce this research are included in the supplementary dataset S4.1 (uploaded alongside this thesis).

Chapter 5
Extended discussion, priorities for future research, and conclusions

Each research chapter (Chapters 2, 3 and 4) includes its own discussion of the findings and a comparison to the wider literature. This chapter therefore aims to: summarise briefly the key findings for each research objective outlined in Chapter 1; discuss the potential wider applications of this research; provide an extended discussion for the timescale of peatland response; and identify priorities for future research.

5.1. Summary of key findings

This thesis has investigated the past, present and future development of circum-Arctic peatlands, through use of bioclimatic modelling, a meta-analysis of palaeoecological data, and laboratory analyses of peat hydraulic properties in degrading palsas. This section briefly summarises the key findings to demonstrate that each primary research objective has been achieved.

Thesis objective 1

Simulate the changing climate spaces of permafrost peatlands in Europe and Western Siberia under a range of 21st-century climate scenarios, and estimate the associated risk for present-day peatland SOC stocks.

In Chapter 2, I fitted climate envelope models for permafrost peatland landforms in Europe and Western Siberia, which demonstrated that cold, dry climates maintain palsas/peat plateaus and that polygon mires exist under colder extremes. Driving these models with future climate projections from the Coupled Model Intercomparison Project 6 (CMIP6) indicates that palsas/peat plateaus in Fennoscandia exist close to a climatic tipping point and are likely

to become climatically unsupported by the 2040s; indeed, some palsas/peat plateaus in this region may already exist beyond this climatic threshold. Under Shared Socioeconomic Pathway (SSP) scenarios of moderate- (SSP2-4.5) to no-mitigation (SSP5-8.5), my simulations indicate that a peat soil organic carbon (SOC) stock of 37.0 to 39.5 Gt could be vulnerable to climate-induced permafrost degradation by the 2090s, although the timescale and direction of peatland response remains uncertain. Only strong action to reduce emissions (SSP1-2.6) would retain a substantial area of suitable climate for permafrost peatlands by the 2090s (599,000 km^2), an area containing 14.9 Gt peat SOC. This analysis highlights the importance of socio-economic polices for determining the rate and extent of future permafrost peatland thaw.

The radiative forcing attributable to circum-Arctic peatlands following climate warming and permafrost degradation will be strongly determined by changes to peatland vegetation and water budgets. I therefore addressed research objectives 2 and 3 (Chapters 3 and 4, respectively) to resolve key knowledge gaps in scientific understanding of these ecohydrological controls.

Thesis objective 2

Determine the recent and long-term spatiotemporal dynamics of peatland vegetation succession, including shrubification, across the circum-Arctic (Chapter 3).

In Chapter 3, I constructed a palaeoecological dataset of 76 plant macrofossil records from circum-Arctic peatlands, including 35 records compiled into a meta-analysis catalogue for the first time. Peatland shrubification trends were often concealed when the plant macrofossil relative abundance data was averaged across large numbers of sites, so I normalised the data to magnify the direction of change in plant functional types (PFTs) in each core. Normalised trends showed a steady expansion of woody vegetation and *Sphagnum* in circum-Arctic peatlands from ~8,000 years BP to present, coinciding with widespread herbaceous decline. During the late-Holocene,

peatland shrubification was evident in the sporadic and discontinuous permafrost zones, while from ~600 years BP widespread increases in *Sphagnum* and non-*Sphagnum* mosses occurred in eastern Canada and the continuous permafrost zone, respectively. Past phases of peatland shrubification and moss expansion often coincided with peatland surface drying, resulting from shifting climate, permafrost aggradation, and peat accumulation. In recent centuries, peatland shrubification did not occur ubiquitously and some sites have evidenced notable declines in woody vegetation. These findings suggest that future peatland shrubification may be less widespread in degrading permafrost peatlands than in upland tundra and will primarily occur in sites with drying surfaces.

Thesis objective 3

Establish the controls on saturated hydraulic conductivity in a degrading permafrost peatland complex in northern Europe, and evaluate the predictive performance of an existing model trained on boreal and temperate peatlands.

In Chapter 4, I measured horizontal saturated hydraulic conductivity (K_h) and other peat properties in 82 near-surface samples from a degrading palsa complex near Rensjön, northern Sweden, in the laboratory. Peat K_h in degrading palsas ranged 4.85×10^{-7} to 3.61×10^{-4} m s^{-1} and declined with increasing depth, dry bulk density and humification (von Post score). My linear mixed-effects model (LMM), fitted to simple, low-cost measurements of peat properties, explained much of the variance in $\log_{10}$-transformed K_h ($r^2 = 0.605$), with $\log_{10}$(depth) found to exert the strongest control. Due to the high collinearity of von Post score and dry bulk density, only von Post score was retained in my final LMM. An existing, large-scale model by Morris et al. (2022) performed less well at predicting $\log_{10}(K_h)$ in degrading palsas ($r^2 = 0.528$), possibly because these palsa peats had higher levels of humification and compaction than many of the boreal and temperate peats to which that model was primarily fitted, although model bias was relatively low. The stage of palsa degradation (desiccating or collapsed) did not exert a significant control on

peat K_h, despite an apparently large collapse of the peat profile. It is possible that macroporosity, a property I did not measure in this analysis, may partly explain this similarity in peat K_h following palsa collapse. Freeze-thaw processes and woody roots of shrubs, which were prevalent on desiccating palsas, can create large pores even in highly humified, compacted peats. The findings of this chapter emphasise the need to improve the representation of permafrost peatlands in large-scale models of peat K_h before these models are applied to Arctic regions.

5.2. Broader applications of this research

Research throughout this thesis has demonstrated the complex, interrelated feedbacks between peatland permafrost, vegetation, hydrology, and climate, illustrating potential means to improve the representation of permafrost peatland ecosystems in large-scale model dynamics of the Earth's surface. Chapter 2 also illustrates that the need to do so is pressing, because permafrost peatlands in Europe and Western Siberia currently exist close to a climatic tipping point.

Chapter 2 of this thesis has presented a decadal time-series of projected 21st century changes to the suitable climate space for permafrost peatlands in Europe and Western Siberia, maps that could inform future modelling of these major peatland carbon stores. For example, my simulations provide a basis from which to target computationally-intensive, land-surface schemes on peatlands at risk of future climate-induced thaw, such as models of permafrost peatland microtopography (Smith et al., 2022). Process-based models, such as dynamic global vegetation models (DGVMs), contain representations of ecological, chemical, and hydrological peatland processes, which are not included in my climate envelope models. However, DGVMs do not currently differentiate between ice lenses or ice wedges and predict permafrost presence from simulations of active-layer thickness (Wania et al., 2009; Qiu et al., 2020). Furthermore, peatlands were not represented in CMIP6 Earth system models or their simulations of future permafrost degradation

(Chadburn et al., 2022). Existing projections of the peatland SOC stock at risk from future permafrost degradation are based on changes in mean annual air temperature under scenarios of global climate stabilisation at +0.5°C to +6°C above the preindustrial (Hugelius et al., 2020a). By comparison, my models also consider important changes in seasonality and precipitation and my projections account for spatiotemporal variability in 21st-century climate change under a range of possible anthropogenic emission scenarios. For those peatlands projected to be at risk from 21st century permafrost degradation (Figures 2.2 and S2.7–S2.10), scientific understanding for their future ecohydrological development and radiative forcing could now be refined using process-based models that account for site-specific characteristics (e.g., Treat et al., 2021, 2022).

My analyses of Holocene peatland vegetation change in Chapter 3 could enable new, large-scale spatiotemporal assessments of model simulations of permafrost peatland plant functional types (PFTs). For example, only a handful of core-based records were previously used to evaluate hindcast simulations of permafrost peatland vegetation change made by the Lund-Potsdam-Jena General Ecosystem Simulator (LPJ-GUESS) DGVM (Chaudhary et al., 2017), a model which has since projected widespread 21st-century shrub expansion in circum-Arctic peatlands (Chaudhary et al., 2022). Alternatively, my palaeoecological catalogue may be combined with existing datasets of peat properties (Loisel et al., 2014; Treat et al., 2016) and palaeohydrological reconstructions (Zhang et al., 2022) for calibrating ecohydrological models to permafrost peatlands, in a similar manner to the recent parameterisation of boreal processes in DigiBog_Boreal (Ramirez et al., 2023). My identification of recent spatial heterogeneity in peatland shrubification provides important context for field-based experiments (Limpens et al., 2021) and core-based reconstructions of 20th century shrub expansion in high latitude peatlands (Gałka et al., 2018; Sim et al., 2019).

From my laboratory measurements in Chapter 4, I have constructed the first model to predict peat K_h in Fennoscandian palsas, although its ability to predict K_h in palsas other than those in the study site remains to be tested. Both my site-specific LMM and an existing, large-scale model by Morris et al. (2022)

accounted for more than half of the variance in $\log_{10}(K_h)$ in degrading palsas near Rensjön, Sweden. It therefore appears reasonable that pedotransfer models based on simple, low-cost descriptors of peat properties may soon be used to predict saturated hydraulic conductivity (K_{sat}) in unstudied permafrost peatlands, avoiding the need for time-intensive field and laboratory experiments. However, I firstly recommend that permafrost peatlands are better represented in the training datasets of large-scale models, by combining my measurements from Chapter 4 with previous data from North America (e.g., Quinton et al., 2008; O'Connor et al., 2020; Ackley et al., 2021). Such an endeavour would be aided by some additional measurements of K_{sat} from permafrost peatlands in Fennoscandia and Siberia, where data remain sparse compared to western Canada and Alaska. The methods of Chapter 4 could be easily replicated for this purpose—a range of techniques exist to estimate peat K_{sat} in the field or laboratory (Morris et al., 2022), and I measured peat properties using simple, low-cost methods.

5.3. Timing of permafrost peatland response

Although permafrost peatlands can demonstrate abrupt responses to climatic perturbations, several internal mechanisms may enable these ecosystems to resist change for some time. For example, my research has suggested that some peatland permafrost in Fennoscandia may already persist under unsuitable climates (Chapter 2), while several of the palaeoecological records I have studied indicate non-linear trajectories of past peatland succession and signs of ecosystem resilience (Chapter 3). Additionally, peat hydraulic properties did not significantly differ between desiccated and collapsed areas of the degrading palsa complex near Rensjön, Sweden (Chapter 4). This section provides a deeper consideration of the factors controlling the timescale of permafrost peatland response.

Interactions between peatland permafrost and surface vegetation, hydrology, and microtopography can delay the onset of thaw and extend its duration under unsuitable climates (Halsey et al., 1995). So-called relict permafrost is known

to exist in some peatlands in continental western Canada (Halsey et al., 1995; Vitt et al., 2000) and northern Sweden (Sannel et al., 2016; Olvmo et al., 2020). However, there are no established methods for quantifying which permafrost peatlands presently exist in climatic equilibrium, or how long the temporal lag in permafrost degradation will be once climates become unsuitable. These uncertainties prevented me from estimating how much peatland permafrost will degrade during the 21st century (Chapter 2). Permafrost may be protected from warming climates by the low thermal conductivities of dry *Sphagnum* peats, and shading and reduced snow depths beneath shrubs and trees (Camill and Clark, 2000). Conversely, thaw may be accelerated by the cracking of desiccated peat surfaces (Swindles et al., 2015) or the combustion of peatland vegetation by wildfire (Ackley et al., 2021), both of which increase the thermal connectivity of permafrost to the atmosphere. Historical orthophotos have shown that some palsas in Fennoscandia have been laterally degrading for several decades (Olvmo et al., 2020; de la Barreda-Bautista et al., 2022; Verdonen et al., 2023), although the timing of aerial surveys is too sporadic to determine when thaw began. New remote-sensing methods that track vertical subsidence in palsas may be used to refine these estimates, but the temporal coverage of high-resolution satellite imagery also remains limited (de la Barreda-Bautista et al., 2022; Sjogersten et al., 2023).

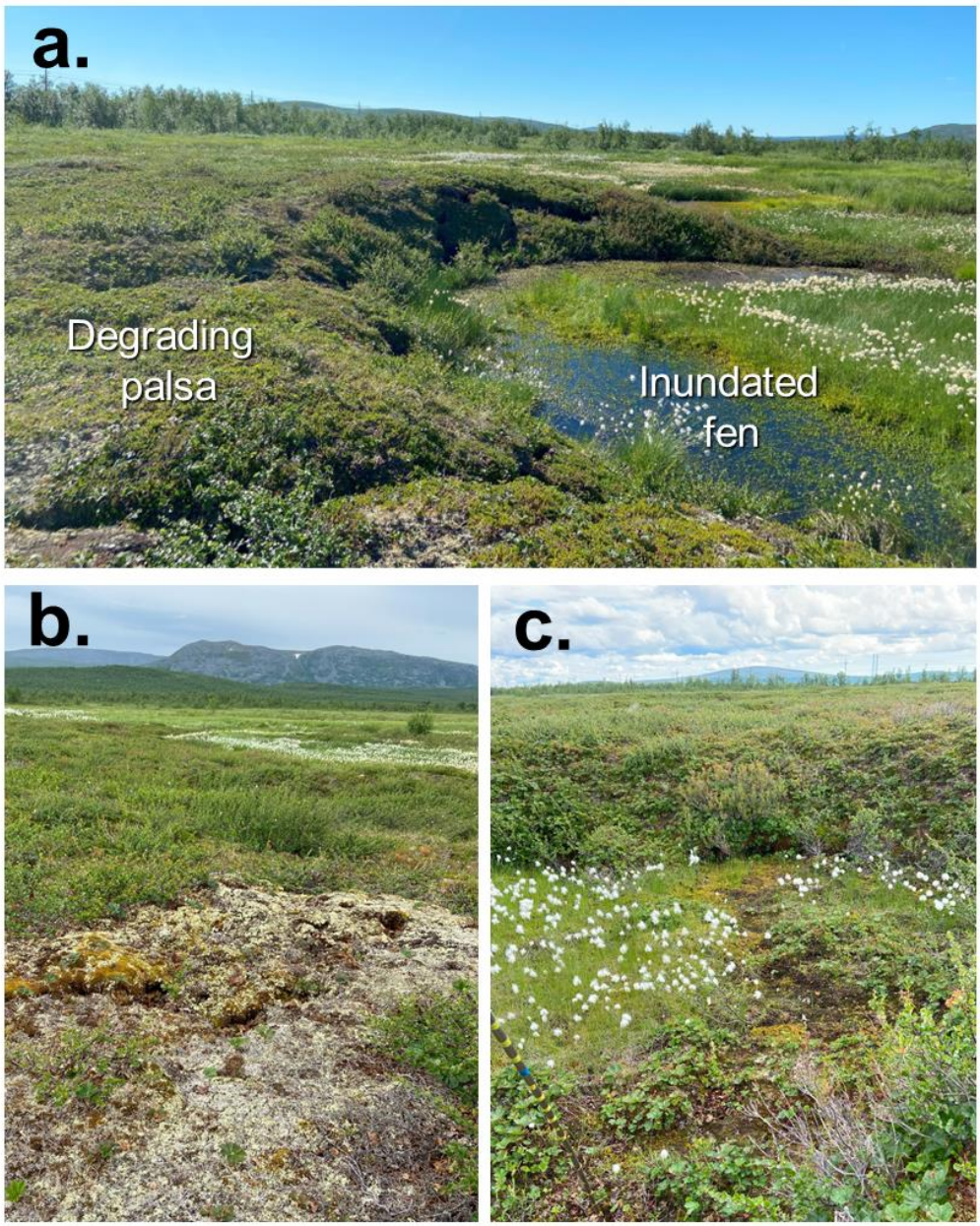

Figure 5.1. Site photographs of degrading palsas at Rensjön palsa mire, northern Sweden, (own images) showing: (a) the vegetation shift between degrading palsas and inundated thermokarst fens; and typical coring locations for (b) desiccating palsas with intact permafrost and (c) permafrost-free, collapsed palsas.

To somewhat account for this temporal lag, I fitted my climate envelope models in Chapter 2 using observational climate data from a period slightly before present (1961–1990), when the spatial coverage of meteorological stations was also greatest (Harris et al., 2020). However, it is possible that some

permafrost peatlands already existed under unsuitable climates at this time. Previous analyses by Fewster et al. (2020) found that climate envelope models of North American palsas/peat plateaus fitted to the same mid-20th century baseline (1961–1990) outperformed equivalent models fitted to preindustrial data from a global climate model (Valdes et al., 2017; Morris et al., 2018). Future studies could attempt to fit climate envelope models to earlier 20th century time periods (e.g., 1941–1970, 1951–1980, etc.) or proxy-based reconstructions of preindustrial climate (e.g., Emile-Geay et al., 2017) to investigate this further. Analysing multiple, baseline time periods would likely increase the range of model uncertainty, but may also improve predictive skill through increased model flexibility (Title and Bemmels, 2018).

Several of the plant macrofossil records I compiled for Chapter 3 evidenced ecological resistance or resilience (Belyea, 2009) of peatlands to Holocene environmental perturbations. Some *Sphagnum*-dominated peatlands may particularly resist succession under changing climate (Keuper et al., 2011), because *Sphagnum* mosses have broad hydrological tolerances (Rydin and Mcdonald, 1985), protect peat permafrost from warming climates (Zoltai, 1993), and engineer acidic, nutrient-poor conditions that can restrict shrubification (van Breemen, 1995). A previous palaeoecological analysis of Rensjön palsa mire, my study site for Chapter 4, identified *Sphagnum fuscum* resistance to 20th-century climate warming and surface drying (Sim et al., 2021b), which is similarly reflected in other Fennoscandian records (Piilo et al., 2023). Cores from western continental Canada have also demonstrated that *Sphagnum fuscum* can recover quickly following wildfire and associated permafrost thaw (e.g., Zoltai, 1993; Sannel and Kuhry, 2008). Resilience of peatland vegetation may ultimately be exceeded where long-term hydrological changes occur (Robitaille et al., 2021), for example surface inundation following permafrost collapse, which commonly drives succession towards sedge-dominated fens (Olefeldt et al., 2021). High-resolution drone photography may be used to study the recent responses of permafrost peatland vegetation to disturbance in more detail (e.g., Palace et al., 2018; Sjogersten et al., 2023).

In future decades, peatland resistance to change may be lessened if the magnitude of 21st-century climate change occurs to the same degree as projected by CMIP6 ESMs under no-mitigation scenarios (Chapter 2). High future warming could rapidly overcome the insulating effect that *Sphagnum* layers exert on peat permafrost, while increases to water stress and wildfire frequency may disrupt poleward shifts in peatland vegetation. The future stability of the permafrost peatland carbon store will therefore be closely tied to the trajectory of global anthropogenic emissions.

5.4. Research priorities

In this thesis, I have addressed three important knowledge gaps concerning past, present and future changes to permafrost peatlands under changing climate, at spatial scales ranging from the circum-Arctic (Chapter 3), to regional (Chapter 2 and 3), and site-level (Chapter 4). This section outlines persisting data gaps in peatland science at each of these scales that should be prioritised to build upon this work.

Across the circum-Arctic permafrost region, published data remains most spatially limited in central and eastern Siberia, where the past composition of peatland vegetation (Chapter 3), the modern distribution of permafrost peatland landforms and their carbon stocks (Chapter 2), and present-day peat hydraulic properties (Chapter 4) have been sparsely recorded. Other commonly understudied regions include parts of Alaska, Arctic Canada, the Kola Peninsula, Greenland and Svalbard. Spatial heterogeneity in peatland sampling restricted the spatial extent of my climate envelope modelling and palaeoecological comparisons (Chapters 2 and 3), while large-scale mapping of peat carbon stocks is still reliant on extensive spatial interpolation (e.g., Hugelius et al., 2020). Records of plant macrofossil relative abundance were largely unavailable for the Western Siberian lowlands (Chapter 3), where widespread future shrub expansion is projected to occur (Chaudhary et al., 2022). While lithological descriptions of peat-forming vegetation are available for some peatlands in this region (Treat et al., 2016; Treat and Jones, 2018),

such data were unsuitable for my study of compositional changes in peatland vegetation through time. Future permafrost peatland research should therefore focus on improving data availability in these understudied regions, although conducting fieldwork in remote, northerly locations is challenging. Any new data could be easily appended to the datasets I have constructed in this thesis, which are freely-available alongside the publications of Chapter 2 in *Nature Climate Change* (Fewster et al., 2022) and Chapter 3 in *Quaternary Science Reviews* (Fewster et al., 2023).

Since the publication of Chapter 2 (Fewster et al., 2022), Könönen et al. (2022) have attempted the first circum-Arctic simulations for the environmental spaces of palsas/peat plateaus, accounting for both climate and soil characteristics, and have made direct comparisons to my own published simulations. This study recorded a similar circum-Arctic distribution of observed palsas/peat plateaus to my own literature-based estimate (Figure S2.4) with minor additions, for example in European Russia and far eastern Siberia. Mapped distributions of permafrost peatland landforms have also recently been updated for the Labrador Sea coastline (Wang et al., 2023), but these data were not included in Könönen et al. (2022). Therefore, published maps still likely underestimate the true circum-Arctic distribution of permafrost peatland landforms, particularly in large parts of the Canadian and Alaskan interior and in central and eastern Siberia. Accordingly, the circum-Arctic simulations by Könönen et al. (2022) can be seen as an extrapolation of models fitted primarily to the well-constrained distribution of palsas/peat plateaus in Fennoscandia, Western Siberia, and parts of North America. However, there is currently insufficient observational data to validate circum-Arctic simulations, most notably in central and eastern Siberia, and it is unknown whether palsas/peat plateaus exhibit homogenous relationships with climate in these largely understudied regions. The importance of missing observations for bioclimatic model performance is illustrated by my climate envelope model for palsas/peat plateaus in Europe and Western Siberia demonstrating stronger predictive power (cross-validated informedness = 0.886; Chapter 2) than a previous model for North America, where landform observations were comparatively sparse (informedness = 0.624) (Fewster et

al., 2020). Furthermore, Könönen et al. (2022) only considered CMIP5 moderate- and high-warming scenarios (RCP4.5 and RCP8.5, respectively) for their future projections of suitable environmental space. For Europe and Western Siberia, these projections indicate similar widespread, 21st-century losses of suitable climates for palsas/peat plateaus to the updated versions of these scenarios that were considered by my own CMIP6 modelling (Figures 2.2, S2.8, and S2.10).

Large-scale analyses often group permafrost peatlands into broad classifications (e.g., palsa mire, polygon mire) that simplify the complex arrangement of permafrost landforms, permafrost-free collapse scars and inundated thermokarst features that exist within these sites (Figure 5.1). Climate envelope models somewhat describe this variability in their simulation of a continuous probability distribution for permafrost peatland presence, which is then converted to a binary prediction based on a defined cut-off threshold, and probabilistic maps could be analysed more explicitly by future studies. Non-climatic predictors, such as soil characteristics and geology, may also refine large-scale modelling of peatland permafrost, where appropriate datasets are available (O'Neill et al., 2019; Karjalainen et al., 2020; Könönen et al., 2022).

Existing core-based analyses of permafrost peatland complexes have predominately studied *Sphagnum*-dominated microhabitats, for example peat plateaus, while inundated fens and polygon mires have been less frequently sampled. It is currently unknown whether near-surface peat K_h will remain similarly consistent during the longer-term development of thermokarst fens, as I found it to during palsa desiccation and collapse at Rensjön palsa mire (Chapter 4), because inundated fens commonly exhibit an ecological transition towards sedge-dominated vegetation (Figure 5.1). I found these fen peats to be too wet and loose to retrieve useable samples from using Polyvinyl Chloride (PVC) cylinders and the scissor-cut method (Green and Baird, 2012), so it may be more appropriate to measure their hydraulic properties using alternative, field-based methods (e.g., Hogan et al., 2006). My core-based approach also restricted my laboratory determinations of peat K_{sat} to one direction (horizontal), so additional research is needed to quantify whether peat K_{sat} is

anisotropic (i.e., directionally-dependent) in degrading palsas. Ahead of my fieldwork in July 2022, transport of my sampling equipment to northern Sweden was delayed, and ultimately never completed, because of ongoing strikes by Scandinavian Airlines. This resulted in several days of lost time, while I sought alternative equipment from Kiruna and Abisko. These unforeseen logistical challenges and time constraints meant I was unable to sample more than one site for this first, detailed study of the peat hydraulic properties of Fennoscandian palsas. The spatiotemporal variability of peat K_{sat} in degrading palsas could now be explored further through peatland chronosequences, which have previously uncovered time-dependent changes in peat K_{sat} following agricultural disturbance (Hyväluoma et al., 2020). New measurements are also required for polygon mire peats (Helbig et al., 2013), but this is complicated by their remote location (Figure S2.4).

Encapsulating site-wide variability in permafrost peatlands is particularly challenging for core-based studies (Chapters 3 and 4), because peat cores are typically only a few centimetres wide and record changes in the immediate vicinity of the sampling location, forming point measurements within a heterogeneous landscape. By increasing the number of coring locations and by sampling a range of microhabitats, some interpretation of within-site heterogeneity can be made, for example for peat permeability (Baird et al., 2016) or past vegetation succession (Piilo et al., 2023). However, such detailed analyses are time-intensive to complete and representative sampling of some microhabitats (e.g., saturated fen peats) remains a challenge. Even where a representative number of cores are available, it is difficult to include these data in large-scale averages without introducing a spatial bias related to the varying number of cores between sites, although this bias may be reduced in certain cases through data normalisation (Treat and Jones, 2018).

Detailed, multiproxy reconstructions are useful for elucidating the drivers of past peatland developments, but many of the cores I studied in Chapter 3 only have published records of plant macrofossils and peat properties (e.g, dry bulk density), which limited my interpretations. Existing proxy reconstructions of permafrost peatland palaeohydrology, for example using testate amoebae, are spatially clustered and have only been synthesised for the past four centuries

(Zhang et al., 2022). Where plant macrofossils have been identified to a species-level, particularly *Sphagnum*, these data can provide some indication of palaeohydrological trends without the need for additional proxy evidence (e.g., Piilo et al., 2023), but this is only possible where macrofossils are sufficiently well-preserved. Additionally, palaeoecological records from permafrost peatlands often have low temporal resolutions, owing to slow peat accumulation under cold climates (e.g., Vardy et al., 1997, 2005; Oksanen et al., 2001), which restricted my analyses to coarse 200-year time steps. The precision of core chronologies has improved since the 1990s with the development of accelerator mass spectrometry techniques for radiocarbon (^{14}C) dating, which require smaller peat samples than older procedures (Holmquist et al., 2016), and refinements to lead-210 (^{210}Pb) dating (Aquino-López et al., 2018). These improvements have facilitated recent, decadal-scale reconstructions of late-Holocene vegetation change in some circum-Arctic peatlands, enabling regional-scale assessments of peatland responses to late 20th-century warming (e.g., Sim et al., 2021b; Magnan et al., 2022; Piilo et al., 2023). As more temporally-resolute, multiproxy records become available, changes to permafrost peatland ecohydrology during short-term Holocene climate events may be studied at broader spatial scales.

5.5. Thesis conclusions

This thesis provides an important advance in scientific understanding of the climatic controls, ecological responses and hydraulic characteristics of permafrost peatlands, research that should now be integrated into large-scale modelling of circum-Arctic peatlands. In Chapter 2, I developed the first climate envelope models of permafrost peatlands in Western Siberia, which have enabled new simulations for the loss of suitable climates under CMIP6 projections of 21st-century climate change, and some identification of the peat carbon stores at risk of permafrost degradation. In Chapter 3, I constructed a new dataset of previously-published plant macrofossil records and conducted a first, long-term analysis of the spatiotemporal extent of Holocene

shrubification in circum-Arctic peatlands. In Chapter 4, I performed the first laboratory measurements of peat K_h in degrading palsas in Fennoscandia and fitted a new model to predict K_h in palsas based on simple, low-cost measurements of peat properties. Throughout I have used methods that are easily replicable and compared my results to the wider published literature. Preferential sampling of *Sphagnum*-dominated microhabitats and remaining data gaps in North America and Siberia pose important barriers to permafrost peatland research and should be addressed by future studies. Lastly, in this chapter I have summarised the key findings, outlined the wider applications of my results and identified priorities for future research.

My research has highlighted that permafrost peatlands in Europe and Western Siberia exist close to their climatic threshold, particularly in Fennoscandia, and are projected to be widely exposed to unsuitable climates during the coming decades. Once climates become unsuitable and permafrost thaws, changes to the net carbon balance of circum-Arctic peatlands are difficult to predict and likely to be spatially heterogenous, driven by changes to peatland vegetation composition and hydrology. My palaeoecological analyses suggest that *Sphagnum* and woody vegetation have steadily increased in abundance in circum-Arctic peatlands since ~8,000 years BP, but during recent centuries peatland shrubification has been spatially heterogeneous, reflecting between-site variability in permafrost degradation and peatland surface drying. Hydrology appears to exert a primary control on ecological succession in permafrost peatlands, with ensuing implications for peatland carbon fluxes. However, my laboratory measurements of near-surface peat K_h in a degrading permafrost peatland in northern Sweden did not exhibit any significant difference between desiccating palsas and collapsed areas, suggesting that any post-thaw changes to peatland hydrology may be driven more by structural changes to peatland topography rather than alterations to peat properties. Taken together, these findings have important implications for understanding the radiative forcing potential of permafrost peatlands during the coming decades.

References

Aalto, J. and Luoto, M. 2014. Integrating climate and local factors for geomorphological distribution models. *Earth Surface Processes and Landforms*. **39**(13), pp.1729–1740.

Aalto, J., Venäläinen, A., Heikkinen, R.K. and Luoto, M. 2014. Potential for extreme loss in high-latitude Earth surface processes due to climate change. *Geophysical Research Letters*. **41**(11), pp.3914–3924.

Aalto, J., Harrison, S. and Luoto, M. 2017. Statistical modelling predicts almost complete loss of major periglacial processes in Northern Europe by 2100. *Nature Communications*. **8**(1), p.515.

Ackley, C., Tank, S.E., Haynes, K.M., Rezanezhad, F., McCarter, C. and Quinton, W.L. 2021. Coupled hydrological and geochemical impacts of wildfire in peatland-dominated regions of discontinuous permafrost. *Science of The Total Environment*. **782**, p.146841.

Åkerman, H.J. and Johansson, M. 2008. Thawing permafrost and thicker active layers in sub-arctic Sweden. *Permafrost and periglacial processes*. **19**(3), pp.279–292.

Anisimov, O.A. and Nelson, F.E. 1997. Permafrost zonation and climate change in the northern hemisphere: results from transient general circulation models. *Climatic Change*. **35**(2), pp.241–258.

Aquino-López, M.A., Blaauw, M., Christen, J.A. and Sanderson, N.K. 2018. Bayesian Analysis of 210Pb Dating. *Journal of Agricultural, Biological and Environmental Statistics*. **23**(3), pp.317–333.

Armstrong, R.A. 2014. When to use the B onferroni correction. *Ophthalmic and Physiological Optics*. **34**(5), pp.502–508.

Baird, A.J., Milner, A.M., Blundell, A., Swindles, G.T. and Morris, P.J. 2016. Microform-scale variations in peatland permeability and their ecohydrological implications. *Journal of Ecology*. **104**(2), pp.531–544.

Bates, D., Mächler, M., Bolker, B. and Walker, S. 2014. Fitting linear mixed-effects models using lme4. *arXiv preprint arXiv:1406.5823*.

Bauer, I.E. and Vitt, D.H. 2011. Peatland dynamics in a complex landscape: Development of a fen-bog complex in the Sporadic Discontinuous Permafrost zone of northern Alberta, Canada: Development of peatland in the Sporadic Discontinuous Permafrost zone, Canada. *Boreas*. **40**(4), pp.714–726.

Beaulieu-Audy, V., Garneau, M., Richard, P.J.H. and Asnong, H. 2009. Holocene palaeoecological reconstruction of three boreal peatlands in the La Grande Rivière region, Québec, Canada. *The Holocene*. **19**(3), pp.459–476.

Beckwith, C.W., Baird, A.J. and Heathwaite, A.L. 2003. Anisotropy and depth-related heterogeneity of hydraulic conductivity in a bog peat. I: laboratory measurements. *Hydrological Processes*. **17**(1), pp.89–101.

Belyea, L.R. 2009. Nonlinear Dynamics of Peatlands and Potential Feedbacks on the Climate System *In*: *Carbon Cycling in Northern Peatlands* [Online]. American Geophysical Union (AGU), pp.5–18. [Accessed 5 October 2022]. Available from: https://onlinelibrary.wiley.com/doi/abs/10.1029/2008GM000829.

Blaauw, M. 2010. Methods and code for 'classical' age-modelling of radiocarbon sequences. *Quaternary Geochronology*. **5**(5), pp.512–518.

Blaauw, M. and Christen, J.A. 2011. Flexible paleoclimate age-depth models using an autoregressive gamma process. *Bayesian Analysis*. **6**(3), pp.457–474.

Borge, A.F., Westermann, S., Solheim, I. and Etzelmüller, B. 2017. Strong degradation of palsas and peat plateaus in northern Norway during the last 60 years. *The Cryosphere*. **11**(1), pp.1–16.

Branham, J.E. and Strack, M. 2014. Saturated hydraulic conductivity in Sphagnum-dominated peatlands: do microforms matter? *Hydrological Processes*. **28**(14), pp.4352–4362.

Brown, J., Ferrians, O., Heginbottom, J. and Melnikov, E. 2002. Circum-Arctic map of permafrost and ground-ice conditions, version 2. *Boulder, Colorado USA, National Snow and Ice Data Center*.

Brown, R.J.E. 1960. The Distribution of Permafrost and Its Relation to Air Temperature in Canada and the U. S. S. R. *Arctic*. **13**(3), pp.163–177.

Brownrigg, O.S. code by R.A.B. and A.R.W.R. version by R. 2022. mapdata: Extra Map Databases. [Accessed 2 May 2023]. Available from: https://cran.r-project.org/web/packages/mapdata/index.html.

Brunner, L., Pendergrass, A.G., Lehner, F., Merrifield, A.L., Lorenz, R. and Knutti, R. 2020. Reduced global warming from CMIP6 projections when weighting models by performance and independence. *Earth System Dynamics*. **11**(4), pp.995–1012.

Burd, K., Estop-Aragonés, C., Tank, S.E. and Olefeldt, D. 2020. Lability of dissolved organic carbon from boreal peatlands: interactions between permafrost thaw, wildfire, and season M. A. Naeth, ed. *Canadian Journal of Soil Science*. **100**(4), pp.503–515.

Burke, E.J., Zhang, Y. and Krinner, G. 2020. Evaluating permafrost physics in the Coupled Model Intercomparison Project 6 (CMIP6) models and their sensitivity to climate change. *The Cryosphere*. **14**(9), pp.3155–3174.

Camill, P. and Clark, J.S. 1998. Climate Change Disequilibrium of Boreal Permafrost Peatlands Caused by Local Processes. *The American Naturalist*. **151**(3), pp.207–222.

Camill, P. 1999. Peat accumulation and succession following permafrost thaw in the boreal peatlands of Manitoba, Canada. *Écoscience*. **6**(4), pp.592–602.

Camill, P. and Clark, J.S. 2000. Long-term Perspectives on Lagged Ecosystem Responses to Climate Change: Permafrost in Boreal Peatlands and the Grassland/Woodland Boundary. *Ecosystems*. **3**(6), pp.534–544.

Camill, P., Lynch, J.A., Clark, J.S., Adams, J.B. and Jordan, B. 2001. Changes in Biomass, Aboveground Net Primary Production, and Peat Accumulation

following Permafrost Thaw in the Boreal Peatlands of Manitoba, Canada. *Ecosystems*. **4**(5), pp.461–478.

Camill, P. 2005. Permafrost Thaw Accelerates in Boreal Peatlands During Late-20th Century Climate Warming. *Climatic Change*. **68**(1–2), pp.135–152.

Camill, P., Barry, A., Williams, E., Andreassi, C., Limmer, J. and Solick, D. 2009. Climate-vegetation-fire interactions and their impact on long-term carbon dynamics in a boreal peatland landscape in northern Manitoba, Canada. *Journal of Geophysical Research: Biogeosciences*. **114**(G4).

Chadburn, S.E., Burke, E.J., Gallego-Sala, A.V., Smith, N.D., Bret-Harte, M.S., Charman, D.J., Drewer, J., Edgar, C.W., Euskirchen, E.S., Fortuniak, K., Gao, Y., Nakhavali, M., Pawlak, W., Schuur, E.A.G. and Westermann, S. 2022. A new approach to simulate peat accumulation, degradation and stability in a global land surface scheme (JULES vn5.8_accumulate_soil) for northern and temperate peatlands. *Geoscientific Model Development*. **15**(4), pp.1633–1657.

Chambers, F.M., Beilman, D.W. and Yu, Z. 2011. Methods for determining peat humification and for quantifying peat bulk density, organic matter and carbon content for palaeostudies of climate and peatland carbon dynamics. **7**(2010/11), p.1-10.

Chaudhary, N., Miller, P.A. and Smith, B. 2017. Modelling Holocene peatland dynamics with an individual-based dynamic vegetation model. *Biogeosciences*. **14**(10), pp.2571–2596.

Chaudhary, N., Westermann, S., Lamba, S., Shurpali, N., Sannel, A.B.K., Schurgers, G., Miller, P.A. and Smith, B. 2020. Modelling past and future peatland carbon dynamics across the pan-Arctic. *Global Change Biology*. **26**(7), pp.4119–4133.

Chaudhary, N., Zhang, W., Lamba, S. and Westermann, S. 2022. Modeling Pan-Arctic Peatland Carbon Dynamics Under Alternative Warming Scenarios. *Geophysical Research Letters*. **49**(10), e2021GL095276.

Chen, Y., Hu, F.S. and Lara, M.J. 2021. Divergent shrub-cover responses driven by climate, wildfire, and permafrost interactions in Arctic tundra ecosystems. *Global Change Biology*. **27**(3), pp.652–663.

Clarke, K.R. 1993. Non-parametric multivariate analyses of changes in community structure. *Austral Ecology*. **18**(1), pp.117–143.

Clymo, R. 1984. The limits to peat bog growth. *Philosophical Transactions of the Royal Society of London. B, Biological Sciences*. **303**(1117), pp.605–654.

Connon, R.F., Quinton, W.L., Craig, J.R. and Hayashi, M. 2014. Changing hydrologic connectivity due to permafrost thaw in the lower Liard River valley, NWT, Canada. *Hydrological Processes*. **28**(14), pp.4163–4178.

Crichton, K.A., Anderson, K., Charman, D.J. and Gallego-Sala, A. 2022. Seasonal climate drivers of peak NDVI in a series of Arctic peatlands. *Science of The Total Environment*. **838**, p.156419.

Davies, M.A., Mclaughlin, J.W., Packalen, M.S. and Finkelstein, S.A. 2022. Holocene carbon storage and testate amoeba community structure in treed peatlands of the western Hudson Bay Lowlands margin, Canada. *Journal of Quaternary Science*. **38**(1).

Davy, R. and Outten, S. 2020. The Arctic Surface Climate in CMIP6: Status and Developments since CMIP5. *Journal of Climate*. **33**(18), pp.8047–8068.

de Klerk, P., Donner, N., Karpov, N.S., Minke, M. and Joosten, H. 2011. Short-term dynamics of a low-centred ice-wedge polygon near Chokurdakh (NE Yakutia, NE Siberia) and climate change during the last ca 1250 years. *Quaternary Science Reviews*. **30**(21–22), pp.3013–3031.

de la Barreda-Bautista, B., Boyd, D.S., Ledger, M., Siewert, M.B., Chandler, C., Bradley, A.V., Gee, D., Large, D.J., Olofsson, J., Sowter, A. and Sjögersten, S. 2022. Towards a Monitoring Approach for Understanding Permafrost Degradation and Linked Subsidence in Arctic Peatlands. *Remote Sensing*. **14**(3), p.444.

Dearborn, K.D., Wallace, C.A., Patankar, R. and Baltzer, J.L. 2021. Permafrost thaw in boreal peatlands is rapidly altering forest community composition. *Journal of Ecology*. **109**(3), pp.1452–1467.

Disher, B.S., Connon, R.F., Haynes, K.M., Hopkinson, C. and Quinton, W.L. 2021. The hydrology of treed wetlands in thawing discontinuous permafrost regions. *Ecohydrology*. **14**(5), p.e2296.

Dormann, C.F., Elith, J., Bacher, S., Buchmann, C., Carl, G., Carré, G., Marquéz, J.R.G., Gruber, B., Lafourcade, B., Leitão, P.J., Münkemüller, T., McClean, C., Osborne, P.E., Reineking, B., Schröder, B., Skidmore, A.K., Zurell, D. and Lautenbach, S. 2013. Collinearity: a review of methods to deal with it and a simulation study evaluating their performance. *Ecography*. **36**(1), pp.27–46.

Du, R., Peng, X., Frauenfeld, O.W., Sun, W., Liang, B., Chen, C., Jin, H. and Zhao, Y. 2022. The role of peat on permafrost thaw based on field observations. *CATENA*. **208**, p.105772.

Edvardsson, J., Stoffel, M., Corona, C., Bragazza, L., Leuschner, H.H., Charman, D.J. and Helama, S. 2016. Subfossil peatland trees as proxies for Holocene palaeohydrology and palaeoclimate. *Earth-Science Reviews*. **163**, pp.118–140.

Ekono, I. 1981. Report on energy use of peat. Contribution to U.N. Conference on New and Renewable Sources of Energy, Nairobi.

Elliott, S.M., Roe, H.M. and Patterson, R.T. 2012. Testate amoebae as indicators of hydroseral change: An 8500 year record from Mer Bleue Bog, eastern Ontario, Canada. *Quaternary International*. **268**, pp.128–144.

Ellis, C.J. and Rochefort, L. 2004. CENTURY-SCALE DEVELOPMENT OF POLYGON-PATTERNED TUNDRA WETLAND, BYLOT ISLAND (73° N, 80° W). *Ecology*. **85**(4), pp.963–978.

Elmendorf, S.C., Henry, G.H.R., Hollister, R.D., Björk, R.G., Boulanger-Lapointe, N., Cooper, E.J., Cornelissen, J.H.C., Day, T.A., Dorrepaal, E., Elumeeva, T.G., Gill, M., Gould, W.A., Harte, J., Hik, D.S., Hofgaard, A., Johnson, D.R., Johnstone, J.F., Jónsdóttir, I.S., Jorgenson, J.C., Klanderud,

K., Klein, J.A., Koh, S., Kudo, G., Lara, M., Lévesque, E., Magnússon, B., May, J.L., Mercado-Dı´az, J.A., Michelsen, A., Molau, U., Myers-Smith, I.H., Oberbauer, S.F., Onipchenko, V.G., Rixen, C., Martin Schmidt, N., Shaver, G.R., Spasojevic, M.J., Þórhallsdóttir, Þ.E., Tolvanen, A., Troxler, T., Tweedie, C.E., Villareal, S., Wahren, C.-H., Walker, X., Webber, P.J., Welker, J.M. and Wipf, S. 2012. Plot-scale evidence of tundra vegetation change and links to recent summer warming. *Nature Climate Change*. **2**(6), pp.453–457.

Emile-Geay, J., McKay, N.P., Kaufman, D.S., von Gunten, L., Wang, J., Anchukaitis, K.J., Abram, N.J., Addison, J.A., Curran, M.A.J., Evans, M.N., Henley, B.J., Hao, Z., Martrat, B., McGregor, H.V., Neukom, R., Pederson, G.T., Stenni, B., Thirumalai, K., Werner, J.P., Xu, C., Divine, D.V., Dixon, B.C., Gergis, J., Mundo, I.A., Nakatsuka, T., Phipps, S.J., Routson, C.C., Steig, E.J., Tierney, J.E., Tyler, J.J., Allen, K.J., Bertler, N.A.N., Björklund, J., Chase, B.M., Chen, M.-T., Cook, E., de Jong, R., DeLong, K.L., Dixon, D.A., Ekaykin, A.A., Ersek, V., Filipsson, H.L., Francus, P., Freund, M.B., Frezzotti, M., Gaire, N.P., Gajewski, K., Ge, Q., Goosse, H., Gornostaeva, A., Grosjean, M., Horiuchi, K., Hormes, A., Husum, K., Isaksson, E., Kandasamy, S., Kawamura, K., Kilbourne, K.H., Koç, N., Leduc, G., Linderholm, H.W., Lorrey, A.M., Mikhalenko, V., Mortyn, P.G., Motoyama, H., Moy, A.D., Mulvaney, R., Munz, P.M., Nash, D.J., Oerter, H., Opel, T., Orsi, A.J., Ovchinnikov, D.V., Porter, T.J., Roop, H.A., Saenger, C., Sano, M., Sauchyn, D., Saunders, K.M., Seidenkrantz, M.-S., Severi, M., Shao, X., Sicre, M.-A., Sigl, M., Sinclair, K., St. George, S., St. Jacques, J.-M., Thamban, M., Kuwar Thapa, U., Thomas, E.R., Turney, C., Uemura, R., Viau, A.E., Vladimirova, D.O., Wahl, E.R., White, J.W.C., Yu, Z., Zinke, J., and PAGES2k Consortium 2017. A global multiproxy database for temperature reconstructions of the Common Era. *Scientific Data*. **4**(1), p.170088.

ESRI 2018. *ArcMap* (v.10.6.1). [Software].

ESRI 2023. World Imagery - Overview. [Accessed 22 April 2023]. Available from: https://www.arcgis.com/home/item.html?id=10df2279f9684e4a9f6a7f08febac2a9.

Estop-Aragonés, C., Czimczik, C.I., Heffernan, L., Gibson, C., Walker, J.C., Xu, X. and Olefeldt, D. 2018. Respiration of aged soil carbon during fall in permafrost peatlands enhanced by active layer deepening following wildfire but limited following thermokarst. *Environmental Research Letters*. **13**(8), p.085002.

Everett, K.R. 1983. Histosols *In*: *Developments in Soil Science*. Elsevier, pp.1–53.

Eyring, V., Bony, S., Meehl, G.A., Senior, C.A., Stevens, B., Stouffer, R.J. and Taylor, K.E. 2016. Overview of the Coupled Model Intercomparison Project Phase 6 (CMIP6) experimental design and organization. *Geoscientific Model Development*. **9**(5), pp.1937–1958.

Fan, X., Duan, Q., Shen, C., Wu, Y. and Xing, C. 2020. Global surface air temperatures in CMIP6: historical performance and future changes. *Environmental Research Letters*. **15**(10), p.104056.

Fang, K., Morris, J.L., Salonen, J.S., Miller, P.A., Renssen, H., Sykes, M.T. and Seppä, H. 2013. How robust are Holocene treeline simulations? A model–data comparison in the European Arctic treeline region. *Journal of Quaternary Science*. **28**(6), pp.595–604.

Fewster, R.E., Morris, P.J., Swindles, G.T., Gregoire, L.J., Ivanovic, R.F., Valdes, P.J. and Mullan, D. 2020. Drivers of Holocene palsa distribution in North America. *Quaternary Science Reviews*. **240**, p.106337.

Fewster, R.E., Morris, P.J., Ivanovic, R.F., Swindles, G.T., Peregon, A.M. and Smith, C.J. 2022. Imminent loss of climate space for permafrost peatlands in Europe and Western Siberia. *Nature Climate Change*. **12**(4), pp.373–379.

Fewster, R.E., Morris, P.J., Swindles, G.T., Ivanovic, R.F., Treat, C.C. and Jones, M.C. 2023. Holocene vegetation dynamics of circum-Arctic permafrost peatlands. *Quaternary Science Reviews*. **307**, p.108055.

Flynn, C.M. and Mauritsen, T. 2020. On the climate sensitivity and historical warming evolution in recent coupled model ensembles. *Atmospheric Chemistry and Physics*. **20**(13), pp.7829–7842.

Forster, P., Storelvmo, T., Armour, K., Collins, W., Dufresne, J., Frame, D., Lunt, D., Mauritsen, T., Palmer, M., Watanabe, M., Wild, M. and Zhang, H. 2021. The Earth's Energy Budget, Climate Feedbacks, and Climate Sensitivity *In*: *Climate Change 2021: The Physical Science Basis. Contribution of Working Group I to the Sixth Assessment Report of the Intergovernmental Panel on Climate Change*. Cambridge: Cambridge University Press.

Fox, J. and Weisberg, S. 2018. *An R companion to applied regression*. Sage publications.

Fritz, M., Wolter, J., Rudaya, N., Palagushkina, O., Nazarova, L., Obu, J., Rethemeyer, J., Lantuit, H. and Wetterich, S. 2016. Holocene ice-wedge polygon development in northern Yukon permafrost peatlands (Canada). *Quaternary Science Reviews*. **147**, pp.279–297.

Fronzek, S., Luoto, M. and Carter, T. 2006. Potential effect of climate change on the distribution of palsa mires in subarctic Fennoscandia. *Climate Research*. **32**, pp.1–12.

Fronzek, S., Carter, T.R., Luoto, M., Olesen, J., Semenov, M. and Berry, P. 2011. Evaluating sources of uncertainty in modelling the impact of probabilistic climate change on sub-arctic palsa mires. *Natural Hazards & Earth System Sciences*. **11**(11).

Gajewski, K. 2015. Quantitative reconstruction of Holocene temperatures across the Canadian Arctic and Greenland. *Global and Planetary Change*. **128**, pp.14–23.

Gajewski, K., Viau, A., Sawada, M., Atkinson, D. and Wilson, S. 2001. Sphagnum peatland distribution in North America and Eurasia during the past 21,000 years. *Global Biogeochemical Cycles*. **15**(2), pp.297–310.

Galar, M., Fernández, A., Barrenechea, E., Bustince, H. and Herrera, F. 2011. An overview of ensemble methods for binary classifiers in multi-class problems: Experimental study on one-vs-one and one-vs-all schemes. *Pattern Recognition*. **44**(8), pp.1761–1776.

Gałka, M., Swindles, G.T., Szal, M., Fulweber, R. and Feurdean, A. 2018. Response of plant communities to climate change during the late Holocene:

Palaeoecological insights from peatlands in the Alaskan Arctic. *Ecological Indicators*. **85**, pp.525–536.

Gallego-Sala, A.V., Charman, D.J., Brewer, S., Page, S.E., Prentice, I.C., Friedlingstein, P., Moreton, S., Amesbury, M.J., Beilman, D.W., Björck, S., Blyakharchuk, T., Bochicchio, C., Booth, R.K., Bunbury, J., Camill, P., Carless, D., Chimner, R.A., Clifford, M., Cressey, E., Courtney-Mustaphi, C., De Vleeschouwer, F., de Jong, R., Fialkiewicz-Koziel, B., Finkelstein, S.A., Garneau, M., Githumbi, E., Hribjlan, J., Holmquist, J., Hughes, P.D.M., Jones, C., Jones, M.C., Karofeld, E., Klein, E.S., Kokfelt, U., Korhola, A., Lacourse, T., Le Roux, G., Lamentowicz, M., Large, D., Lavoie, M., Loisel, J., Mackay, H., MacDonald, G.M., Makila, M., Magnan, G., Marchant, R., Marcisz, K., Martínez Cortizas, A., Massa, C., Mathijssen, P., Mauquoy, D., Mighall, T., Mitchell, F.J.G., Moss, P., Nichols, J., Oksanen, P.O., Orme, L., Packalen, M.S., Robinson, S., Roland, T.P., Sanderson, N.K., Sannel, A.B.K., Silva-Sánchez, N., Steinberg, N., Swindles, G.T., Turner, T.E., Uglow, J., Väliranta, M., van Bellen, S., van der Linden, M., van Geel, B., Wang, G., Yu, Z., Zaragoza-Castells, J. and Zhao, Y. 2018. Latitudinal limits to the predicted increase of the peatland carbon sink with warming. *Nature Climate Change*. **8**(10), pp.907–913.

Gharedaghloo, B., Price, J.S., Rezanezhad, F. and Quinton, W.L. 2018. Evaluating the hydraulic and transport properties of peat soil using pore network modeling and X-ray micro computed tomography. *Journal of Hydrology*. **561**, pp.494–508.

Gibson, C.M., Chasmer, L.E., Thompson, D.K., Quinton, W.L., Flannigan, M.D. and Olefeldt, D. 2018. Wildfire as a major driver of recent permafrost thaw in boreal peatlands. *Nature Communications*. **9**(1), p.3041.

Gibson, C.M., Estop-Aragonés, C., Flannigan, M., Thompson, D.K. and Olefeldt, D. 2019. Increased deep soil respiration detected despite reduced overall respiration in permafrost peat plateaus following wildfire. *Environmental Research Letters*. **14**(12), p.125001.

Goslar, T., van der Knaap, W.O., Hicks, S., Andrič, M., Czernik, J., Goslar, E., Räsänen, S. and Hyötylä, H. 2005. Radiocarbon Dating of Modern Peat

Profiles: Pre- and Post-Bomb ^{14}C Variations in the Construction of Age-Depth Models. *Radiocarbon*. **47**(1), pp.115–134.

Graham, M.H. 2003. Confronting multicollinearity in ecological multiple regression. *Ecology*. **84**(11), pp.2809–2815.

Green, S.M. and Baird, A.J. 2012. A mesocosm study of the role of the sedge Eriophorum angustifolium in the efflux of methane—including that due to episodic ebullition—from peatlands. *Plant and Soil*. **351**(1), pp.207–218.

Grosse, G., Harden, J., Turetsky, M., McGuire, A.D., Camill, P., Tarnocai, C., Frolking, S., Schuur, E.A.G., Jorgenson, T., Marchenko, S., Romanovsky, V., Wickland, K.P., French, N., Waldrop, M., Bourgeau-Chavez, L. and Striegl, R.G. 2011. Vulnerability of high-latitude soil organic carbon in North America to disturbance. *Journal of Geophysical Research: Biogeosciences*. **116**(G4).

Gupta, S., Hengl, T., Lehmann, P., Bonetti, S. and Or, D. 2021. SoilKsatDB: global database of soil saturated hydraulic conductivity measurements for geoscience applications. *Earth System Science Data*. **13**(4), pp.1593–1612.

Halsey, L.A., Vitt, D.H. and Zoltai, S.C. 1995. Disequilibrium response of permafrost in boreal continental western Canada to climate change. *Climatic Change*. **30**(1), pp.57–73.

Harris, I., Osborn, T.J., Jones, P. and Lister, D. 2020. Version 4 of the CRU TS monthly high-resolution gridded multivariate climate dataset. *Scientific data*. **7**(1), pp.1–18.

Haynes, K.M., Connon, R.F. and Quinton, W.L. 2018. Permafrost thaw induced drying of wetlands at Scotty Creek, NWT, Canada. *Environmental Research Letters*. **13**(11), p.114001.

Heffernan, L., Estop-Aragonés, C., Knorr, K.-H., Talbot, J. and Olefeldt, D. 2020. Long-term Impacts of Permafrost Thaw on Carbon Storage in Peatlands: Deep Losses Offset by Surficial Accumulation. *Journal of Geophysical Research: Biogeosciences*. **125**(3), e2019JG005501.

Heffernan, L., Cavaco, M.A., Bhatia, M.P., Estop-Aragonés, C., Knorr, K.-H. and Olefeldt, D. 2022. High peatland methane emissions following permafrost

thaw: enhanced acetoclastic methanogenesis during early successional stages. *Biogeosciences*. **19**(12), pp.3051–3071.

Heijmans, M.M.P.D., van der Knaap, Y.A.M., Holmgren, M. and Limpens, J. 2013. Persistent versus transient tree encroachment of temperate peat bogs: effects of climate warming and drought events. *Global Change Biology*. **19**(7), pp.2240–2250.

Heijmans, M.M.P.D., Magnússon, R., Lara, M., Frost, G., Myers-Smith, I., Van Huissteden, K., Jorgenson, M., Fedorov, A., Epstein, H., Lawrence, D. and Limpens, J. 2022. Tundra vegetation change and impacts on permafrost. *Nature Reviews Earth & Environment*. **3**, pp.68–84.

Heikkinen, J.E.P., Maljanen, M., Aurela, M., Hargreaves, K.J. and Martikainen, P.J. 2002. Carbon dioxide and methane dynamics in a sub-Arctic peatland in northern Finland. *Polar Research*. **21**(1), pp.49–62.

Helbig, M., Boike, J., Langer, M., Schreiber, P., Runkle, B.R.K. and Kutzbach, L. 2013. Spatial and seasonal variability of polygonal tundra water balance: Lena River Delta, northern Siberia (Russia). *Hydrogeology Journal*. **21**(1), pp.133–147.

Hiller, A., Boettger, T. and Kremenetski, C. 2001. Mediaeval climatic warming recorded by radiocarbon dated alpine tree-line shift on the Kola Peninsula, Russia. *The Holocene*. **11**(4), pp.491–497.

Hobbs, N.B. 1986. Mire morphology and the properties and behaviour of some British and foreign peats. *Quarterly Journal of Engineering Geology*. **19**(1), pp.7–80.

Hogan, J.M., van der Kamp, G., Barbour, S.L. and Schmidt, R. 2006. Field methods for measuring hydraulic properties of peat deposits. *Hydrological Processes*. **20**(17), pp.3635–3649.

Holden, J., Burt, T.P. and Cox, N.J. 2001. Macroporosity and infiltration in blanket peat: the implications of tension disc infiltrometer measurements. *Hydrological Processes*. **15**(2), pp.289–303.

Holden, J. 2006. Chapter 14 Peatland hydrology *In*: I. P. Martini, A. Martínez Cortizas and W. Chesworth, eds. *Developments in Earth Surface Processes* [Online]. Peatlands. Elsevier, pp.319–346. [Accessed 31 March 2023]. Available from: https://www.sciencedirect.com/science/article/pii/S0928202506090146.

Holden, J. 2009. Flow through macropores of different size classes in blanket peat. *Journal of Hydrology*. **364**(3), pp.342–348.

Holmes, M.E., Crill, P.M., Burnett, W.C., McCalley, C.K., Wilson, R.M., Frolking, S., Chang, K.-Y., Riley, W.J., Varner, R.K., Hodgkins, S.B., Coordinators, I.P., Team, I.F., McNichol, A.P., Saleska, S.R., Rich, V.I. and Chanton, J.P. 2022. Carbon Accumulation, Flux, and Fate in Stordalen Mire, a Permafrost Peatland in Transition. *Global Biogeochemical Cycles*. **36**(1), e2021GB007113.

Holmgren, M., Lin, C.-Y., Murillo, J.E., Nieuwenhuis, A., Penninkhof, J., Sanders, N., van Bart, T., van Veen, H., Vasander, H., Vollebregt, M.E. and Limpens, J. 2015. Positive shrub–tree interactions facilitate woody encroachment in boreal peatlands. *Journal of Ecology*. **103**(1), pp.58–66.

Holmquist, J.R., Finkelstein, S.A., Garneau, M., Massa, C., Yu, Z. and MacDonald, G.M. 2016. A comparison of radiocarbon ages derived from bulk peat and selected plant macrofossils in basal peat cores from circum-arctic peatlands. *Quaternary Geochronology*. **31**, pp.53–61.

Hough, M., McCabe, S., Vining, S.R., Pickering Pedersen, E., Wilson, R.M., Lawrence, R., Chang, K.-Y., Bohrer, G., Coordinators, T.I., Riley, W.J., Crill, P.M., Varner, R.K., Blazewicz, S.J., Dorrepaal, E., Tfaily, M.M., Saleska, S.R. and Rich, V.I. 2022. Coupling plant litter quantity to a novel metric for litter quality explains C storage changes in a thawing permafrost peatland. *Global Change Biology*. **28**(3), pp.950–968.

Hugelius, G., Tarnocai, C., Broll, G., Canadell, J., Kuhry, P. and Swanson, D. 2013. The Northern Circumpolar Soil Carbon Database: spatially distributed datasets of soil coverage and soil carbon storage in the northern permafrost regions. *Earth System Science Data*. **5**(1), p.3.

Hugelius, G., Loisel, J., Chadburn, S., Jackson, R.B., Jones, M., MacDonald, G., Marushchak, M., Olefeldt, D., Packalen, M., Siewert, M.B., Treat, C., Turetsky, M., Voigt, C. and Yu, Z. 2020a. Large stocks of peatland carbon and nitrogen are vulnerable to permafrost thaw. *Proceedings of the National Academy of Sciences*. **117**(34), pp.20438–20446.

Hugelius, G., Loisel, J., Chadburn, S.E., Jackson, R.B., Jones, M., MacDonald, G., Marushchak, M., Olefeldt, D., Packalen, M., Siewert, M., Treat, C., Turetsky, M., Voigt, C. and Yu, Z. 2020b. Maps of northern peatland extent, depth, carbon storage and nitrogen storage | Bolin Centre Database. [Accessed 2 May 2023]. Available from: https://bolin.su.se/data/hugelius-2020-peatland-1.

Hughes, P.D.M. 2000. A reappraisal of the mechanisms leading to ombrotrophy in British raised mires. *Ecology Letters*. **3**(1), pp.7–9.

Hughes, P.D.M. and Barber, K.E. 2003. Mire Development across the Fen-Bog Transition on the Teifi Floodplain at Tregaron Bog, Ceredigion, Wales, and a Comparison with 13 Other Raised Bogs. *Journal of Ecology*. **91**(2), pp.253–264.

Hunt, S., Yu, Z. and Jones, M. 2013. Lateglacial and Holocene climate, disturbance and permafrost peatland dynamics on the Seward Peninsula, western Alaska. *Quaternary Science Reviews*. **63**, pp.42–58.

Hurvich, C.M. and Tsai, C.-L. 1989. Regression and time series model selection in small samples. *Biometrika*. **76**(2), pp.297–307.

Hyväluoma, J., Räty, M., Kaseva, J. and Keskinen, R. 2020. Changes over time in near-saturated hydraulic conductivity of peat soil following reclamation for agriculture. *Hydrological Processes*. **34**(2), pp.237–243.

Ingram, H. a. P. 1982. Size and shape in raised mire ecosystems: a geophysical model. *Nature*. **297**(5864), pp.300–303.

Johansson, T., Malmer, N., Crill, P.M., Friborg, T., Åkerman, J.H., Mastepanov, M. and Christensen, T.R. 2006. Decadal vegetation changes in a northern peatland, greenhouse gas fluxes and net radiative forcing. *Global Change Biology*. **12**(12), pp.2352–2369.

Jones, M.C. and Yu, Z. 2010. Rapid deglacial and early Holocene expansion of peatlands in Alaska. *Proceedings of the National Academy of Sciences*. **107**(16), pp.7347–7352.

Jones, M.C., Booth, R.K., Yu, Z. and Ferry, P. 2013. A 2200-Year Record of Permafrost Dynamics and Carbon Cycling in a Collapse-Scar Bog, Interior Alaska. *Ecosystems*. **16**(1), pp.1–19.

Jones, M.C., Harden, J., O'Donnell, J., Manies, K., Jorgenson, T., Treat, C. and Ewing, S. 2017. Rapid carbon loss and slow recovery following permafrost thaw in boreal peatlands. *Global Change Biology*. **23**(3), pp.1109–1127.

Jorgenson, M.T., Romanovsky, V., Harden, J., Shur, Y., O'Donnell, J., Schuur, E.A.G., Kanevskiy, M. and Marchenko, S. 2010. Resilience and vulnerability of permafrost to climate changeThis article is one of a selection of papers from The Dynamics of Change in Alaska's Boreal Forests: Resilience and Vulnerability in Response to Climate Warming. *Canadian Journal of Forest Research*. **40**(7), pp.1219–1236.

Jorgenson, M.T. and Grunblatt, J. 2013. *Landscape-level ecological mapping of northern alaska and field site photography.* Fairbanks, Alaska: Arctic Landscape Conservation Cooperative, U.S. Fish & Wildlife Service.

Karjalainen, O., Luoto, M., Aalto, J., Etzelmüller, B., Grosse, G., Jones, B.M., Lilleøren, K.S. and Hjort, J. 2020. High potential for loss of permafrost landforms in a changing climate. *Environmental Research Letters*. **15**(10), p.104065.

Kaufman, D.S., Ager, T.A., Anderson, N.J., Anderson, P.M., Andrews, J.T., Bartlein, P.J., Brubaker, L.B., Coats, L.L., Cwynar, L.C., Duvall, M.L., Dyke, A.S., Edwards, M.E., Eisner, W.R., Gajewski, K., Geirsdóttir, A., Hu, F.S., Jennings, A.E., Kaplan, M.R., Kerwin, M.W., Lozhkin, A.V., MacDonald, G.M., Miller, G.H., Mock, C.J., Oswald, W.W., Otto-Bliesner, B.L., Porinchu, D.F., Rühland, K., Smol, J.P., Steig, E.J. and Wolfe, B.B. 2004. Holocene thermal maximum in the western Arctic (0–180°W). *Quaternary Science Reviews*. **23**(5), pp.529–560.

Kaufman, D.S., Axford, Y.L., Henderson, A.C.G., McKay, N.P., Oswald, W.W., Saenger, C., Anderson, R.S., Bailey, H.L., Clegg, B., Gajewski, K., Hu, F.S., Jones, M.C., Massa, C., Routson, C.C., Werner, A., Wooller, M.J. and Yu, Z. 2016. Holocene climate changes in eastern Beringia (NW North America) – A systematic review of multi-proxy evidence. *Quaternary Science Reviews*. **147**, pp.312–339.

Kettles, I.M., Robinson, S.D., Bastien, D.F., Garneau, M. and Hall, G.E.M. 2003. *PHYSICAL, GEOCHEMICAL, MACROFOSSIL AND GROUND PENETRATING RADAR INFORMATION ON FOURTEEN PERMAFROST-AFFECTED PEATLANDS IN THE MACKENZIE VALLEY, NORTHWEST TERRITORIES*. Geological Sruvey of Canada.

Keuper, F., Dorrepaal, E., Van Bodegom, P.M., Aerts, R., Van Logtestijn, R.S.P., Callaghan, T.V. and Cornelissen, J.H.C. 2011. A Race for Space? How Sphagnum fuscum stabilizes vegetation composition during long-term climate manipulations. *Global Change Biology*. **17**(6), pp.2162–2171.

Kirpotin, S., Polishchuk, Y., Bryksina, N., Sugaipova, A., Kouraev, A., Zakharova, E., Pokrovsky, O.S., Shirokova, L., Kolmakova, M., Manassypov, R. and Dupre, B. 2011. West Siberian palsa peatlands: distribution, typology, cyclic development, present day climate-driven changes, seasonal hydrology and impact on CO2 cycle. *International Journal of Environmental Studies*. **68**(5), pp.603–623.

Kjellman, S.E., Axelsson, P.E., Etzelmüller, B., Westermann, S. and Sannel, A.B.K. 2018. Holocene development of subarctic permafrost peatlands in Finnmark, northern Norway. *The Holocene*. **28**(12), pp.1855–1869.

Klaminder, J., Yoo, K., Rydberg, J. and Giesler, R. 2008. An explorative study of mercury export from a thawing palsa mire. *Journal of Geophysical Research: Biogeosciences*. **113**(G4).

Könönen, O.H., Karjalainen, O., Aalto, J., Luoto, M. and Hjort, J. 2022. Environmental spaces for palsas and peat plateaus are disappearing at a circumpolar scale. *The Cryosphere Discussions*. pp.1–37.

Korhola, A., Vasko, K., Toivonen, H. and Olander, H. 2002. Holocene temperature changes in northern Fennoscandia reconstructed from chironomids using Bayesian modelling. *Quaternary Science Reviews*. **21**(16–17), pp.1841–1860.

Kuhry, P. 2008. Palsa and peat plateau development in the Hudson Bay Lowlands, Canada: timing, pathways and causes. *Boreas*. **37**(2), pp.316–327.

Kullman, L. 2015. Higher-than-present Medieval pine (Pinus sylvestris) treeline along the Swedish Scandes. *Landscape Online*. **42**, pp.1–14.

Langlais, K., Bhiry, N. and Lavoie, M. 2021. Holocene dynamics of an inland palsa peatland at Wiyâshâkimî Lake (Nunavik, Canada). *Écoscience*. **28**(3–4), pp.269–282.

Lara, M.J., Nitze, I., Grosse, G. and McGuire, A.D. 2018. Tundra landform and vegetation productivity trend maps for the Arctic Coastal Plain of northern Alaska. *Scientific data*. **5**, p.180058.

Latombe, G., Burke, A., Vrac, M., Levavasseur, G., Dumas, C., Kageyama, M. and Ramstein, G. 2018. Comparison of spatial downscaling methods of general circulation model results to study climate variability during the Last Glacial Maximum. *Geoscientific Model Development*. **11**(7), pp.2563–2579.

Lennartz, B. and Liu, H. 2019. Hydraulic Functions of Peat Soils and Ecosystem Service. *Frontiers in Environmental Science*. **7**.

Leuschner, H.H., Sass-Klaassen, U., Jansma, E., Baillie, M.G.L. and Spurk, M. 2002. Subfossil European bog oaks: population dynamics and long-term growth depressions as indicators of changes in the Holocene hydro-regime and climate. *The Holocene*. **12**(6), pp.695–706.

Limpens, J., Berendse, F., Blodau, C., Canadell, J.G., Freeman, C., Holden, J., Roulet, N., Rydin, H. and Schaepman-Strub, G. 2008. Peatlands and the carbon cycle: from local processes to global implications – a synthesis. *Biogeosciences*. **5**(5), pp.1475–1491.

Limpens, J., Holmgren, M., Jacobs, C.M.J., Zee, S.E.A.T.M.V. der, Karofeld, E. and Berendse, F. 2014a. How Does Tree Density Affect Water Loss of Peatlands? A Mesocosm Experiment. *PLOS ONE*. **9**(3), p.e91748.

Limpens, J., van Egmond, E., Li, B. and Holmgren, M. 2014b. Do plant traits explain tree seedling survival in bogs? *Functional Ecology*. **28**(1), pp.283–290.

Limpens, J., Fijen, T.P.M., Keizer, I., Meijer, J., Olsthoorn, F., Pereira, A., Postma, R., Suyker, M., Vasander, H. and Holmgren, M. 2021. Shrubs and Degraded Permafrost Pave the Way for Tree Establishment in Subarctic Peatlands. *Ecosystems*. **24**(2), pp.370–383.

Lin, L.K.-I. 1989. A concordance correlation coefficient to evaluate reproducibility. *Biometrics*. **45**(1), pp.255–268.

Liu, H. and Lennartz, B. 2019. Hydraulic properties of peat soils along a bulk density gradient—A meta study. *Hydrological Processes*. **33**(1), pp.101–114.

Liu, H., Rezanezhad, F., Zak, D., Li, X. and Lennartz, B. 2022. Freeze-thaw cycles alter soil hydro-physical properties and dissolved organic carbon release from peat. *Frontiers in Environmental Science*. **10**.

Loisel, J. and Garneau, M. 2010. Late Holocene paleoecohydrology and carbon accumulation estimates from two boreal peat bogs in eastern Canada: Potential and limits of multi-proxy archives. *Palaeogeography, Palaeoclimatology, Palaeoecology*. **291**(3–4), pp.493–533.

Loisel, J., Gallego-Sala, A.V. and Yu, Z. 2012. Global-scale pattern of peatland *Sphagnum* growth driven by photosynthetically active radiation and growing season length. *Biogeosciences*. **9**(7), pp.2737–2746.

Loisel, J., Yu, Z., Beilman, D.W., Camill, P., Alm, J., Amesbury, M.J., Anderson, D., Andersson, S., Bochicchio, C., Barber, K., Belyea, L.R., Bunbury, J., Chambers, F.M., Charman, D.J., De Vleeschouwer, F., Fiałkiewicz-Kozieł, B., Finkelstein, S.A., Gałka, M., Garneau, M., Hammarlund, D., Hinchcliffe, W., Holmquist, J., Hughes, P., Jones, M.C., Klein, E.S., Kokfelt, U., Korhola, A., Kuhry, P., Lamarre, A., Lamentowicz, M., Large, D., Lavoie, M., MacDonald, G., Magnan, G., Mäkilä, M., Mallon, G., Mathijssen, P., Mauquoy, D., McCarroll, J., Moore, T.R., Nichols, J., O'Reilly, B., Oksanen, P.,

Packalen, M., Peteet, D., Richard, P.J., Robinson, S., Ronkainen, T., Rundgren, M., Sannel, A.B.K., Tarnocai, C., Thom, T., Tuittila, E.-S., Turetsky, M., Väliranta, M., van der Linden, M., van Geel, B., van Bellen, S., Vitt, D., Zhao, Y. and Zhou, W. 2014. A database and synthesis of northern peatland soil properties and Holocene carbon and nitrogen accumulation. *The Holocene*. **24**(9), pp.1028–1042.

Loisel, J. and Bunsen, M. 2020. Abrupt Fen-Bog Transition Across Southern Patagonia: Timing, Causes, and Impacts on Carbon Sequestration. *Frontiers in Ecology and Evolution*. **8**.

Lourenco, M., Fitchett, J.M. and Woodborne, S. 2022. Peat definitions: A critical review. *Progress in Physical Geography: Earth and Environment*. **0**(0), pp.1-15.

Lüdecke, D. 2018. sjmisc: Data and variable transformation functions. *Journal of Open Source Software*. **3**(26), p.754.

Luoto, M. and Seppälä, M. 2002. Modelling the distribution of palsas in Finnish Lapland with logistic regression and GIS. *Permafrost and Periglacial Processes*. **13**(1), pp.17–28.

Luoto, M. and Seppälä, M. 2003. Thermokarst ponds as indicators of the former distribution of palsas in Finnish Lapland. *Permafrost and Periglacial Processes*. **14**(1), pp.19–27.

Luoto, M., Fronzek, S. and Zuidhoff, F.S. 2004. Spatial modelling of palsa mires in relation to climate in northern Europe. *Earth Surface Processes and Landforms*. **29**(11), pp.1373–1387.

MacDonald, G.M., Velichko, A.A., Kremenetski, C.V., Borisova, O.K., Goleva, A.A., Andreev, A.A., Cwynar, L.C., Riding, R.T., Forman, S.L., Edwards, T.W.D., Aravena, R., Hammarlund, D., Szeicz, J.M. and Gattaulin, V.N. 2000. Holocene Treeline History and Climate Change Across Northern Eurasia. *Quaternary Research*. **53**(3), pp.302–311.

MacDonald, G.M., Beilman, D.W., Kremenetski, K.V., Sheng, Y., Smith, L.C. and Velichko, A.A. 2006. Rapid Early Development of Circumarctic Peatlands and Atmospheric CH_4 and CO_2 Variations. *Science*. **314**(5797), pp.285–288.

Magnan, G. and Garneau, M. 2014. Evaluating long-term regional climate variability in the maritime region of the St. Lawrence North Shore (eastern Canada) using a multi-site comparison of peat-based paleohydrological records. *Journal of Quaternary Science*. **29**(3), pp.209–220.

Magnan, G., van Bellen, S., Davies, L., Froese, D., Garneau, M., Mullan-Boudreau, G., Zaccone, C. and Shotyk, W. 2018. Impact of the Little Ice Age cooling and 20th century climate change on peatland vegetation dynamics in central and northern Alberta using a multi-proxy approach and high-resolution peat chronologies. *Quaternary Science Reviews*. **185**, pp.230–243.

Magnan, G., Sanderson, N.K., Piilo, S., Pratte, S., Väliranta, M., van Bellen, S., Zhang, H. and Garneau, M. 2022. Widespread recent ecosystem state shifts in high-latitude peatlands of northeastern Canada and implications for carbon sequestration. *Global Change Biology*. **28**(5), pp.1919–1934.

Magnússon, R.Í., Limpens, J., van Huissteden, J., Kleijn, D., Maximov, T.C., Rotbarth, R., Sass-Klaassen, U. and Heijmans, M.M.P.D. 2020. Rapid Vegetation Succession and Coupled Permafrost Dynamics in Arctic Thaw Ponds in the Siberian Lowland Tundra. *Journal of Geophysical Research: Biogeosciences*. **125**(7), e2019JG005618.

Magnússon, R.Í., Limpens, J., Kleijn, D., van Huissteden, K., Maximov, T.C., Lobry, S. and Heijmans, M.M.P.D. 2021. Shrub decline and expansion of wetland vegetation revealed by very high resolution land cover change detection in the Siberian lowland tundra. *Science of The Total Environment*. **782**, p.146877.

Mamet, S.D., Chun, K.P., Kershaw, G.G., Loranty, M.M. and Peter Kershaw, G. 2017. Recent increases in permafrost thaw rates and areal loss of palsas in the Western Northwest Territories, Canada. *Permafrost and periglacial processes*. **28**(4), pp.619–633.

Mann, M.E., Zhang, Z., Rutherford, S., Bradley, R.S., Hughes, M.K., Shindell, D., Ammann, C., Faluvegi, G. and Ni, F. 2009. Global Signatures and Dynamical Origins of the Little Ice Age and Medieval Climate Anomaly. *Science*. **326**(5957), pp.1256–1260.

Masson-Delmotte, V., Zhai, P., Pirani, A., Connors, S.L., Péan, C., Berger, S., Caud, N., Chen, Y., Goldfarb, L. and Gomis, M. 2021. Climate change 2021: the physical science basis. *Contribution of working group I to the sixth assessment report of the intergovernmental panel on climate change*. **2**.

Mauquoy, D., Hughes, P.D.M. and van Geel, B. 2010. A protocol for plant macrofossil analysis of peat deposits. , p.6.

McCarter, C.P.R., Rezanezhad, F., Quinton, W.L., Gharedaghloo, B., Lennartz, B., Price, J., Connon, R. and Van Cappellen, P. 2020. Pore-scale controls on hydrological and geochemical processes in peat: Implications on interacting processes. *Earth-Science Reviews*. **207**, p.103227.

McCrystall, M.R., Stroeve, J., Serreze, M., Forbes, B.C. and Screen, J.A. 2021. New climate models reveal faster and larger increases in Arctic precipitation than previously projected. *Nature Communications*. **12**(1), p.6765.

McKay, N.P., Kaufman, D.S., Routson, C.C., Erb, M.P. and Zander, P.D. 2018. The Onset and Rate of Holocene Neoglacial Cooling in the Arctic. *Geophysical Research Letters*. **45**(22), 12,487-12,496.

Meehl, G.A., Senior, C.A., Eyring, V., Flato, G., Lamarque, J.-F., Stouffer, R.J., Taylor, K.E. and Schlund, M. 2020. Context for interpreting equilibrium climate sensitivity and transient climate response from the CMIP6 Earth system models. *Science Advances*. **6**(26), p.eaba1981.

Mekonnen, Z.A., Riley, W.J., Berner, L.T., Bouskill, N.J., Torn, M.S., Iwahana, G., Breen, A.L., Myers-Smith, I.H., Criado, M.G., Liu, Y., Euskirchen, E.S., Goetz, S.J., Mack, M.C. and Grant, R.F. 2021. Arctic tundra shrubification: a review of mechanisms and impacts on ecosystem carbon balance. *Environmental Research Letters*. **16**(5), p.053001.

Menard, S. 2011. Standards for Standardized Logistic Regression Coefficients. *Social Forces*. **89**(4), pp.1409–1428.

Minayeva, T., Sirin, A., Kershaw, P. and Bragg, O. 2016. Arctic Peatlands *In*:, pp.275–288.

Miner, K.R., Turetsky, M.R., Malina, E., Bartsch, A., Tamminen, J., McGuire, A.D., Fix, A., Sweeney, C., Elder, C.D. and Miller, C.E. 2022. Permafrost carbon emissions in a changing Arctic. *Nature Reviews Earth & Environment*. **3**(1), pp.55–67.

Minke, M., Donner, N., Karpov, N., de Klerk, P. and Joosten, H. 2007. Distribution, diversity, development and dynamics of polygon mires: Examples from NE Yakutia (NE Siberia). *Peatlands International*. **2007**, pp.36–40.

Minke, M., Donner, N., Karpov, N., de Klerk, P. and Joosten, H. 2009. Patterns in vegetation composition, surface height and thaw depth in polygon mires in the Yakutian Arctic (NE Siberia): a microtopographical characterisation of the active layer. *Permafrost and Periglacial Processes*. **20**(4), pp.357–368.

Moore, T.R., Bubier, J.L. and Bledzki, L. 2007. Litter decomposition in temperate peatland ecosystems: the effect of substrate and site. *Ecosystems*. **10**(6), pp.949–963.

Morison, M.Q., Macrae, M.L., Petrone, R.M. and Fishback, L. 2017. Seasonal dynamics in shallow freshwater pond-peatland hydrochemical interactions in a subarctic permafrost environment. *Hydrological Processes*. **31**(2), pp.462–475.

Morris, P.J., Swindles, G.T., Valdes, P.J., Ivanovic, R.F., Gregoire, L.J., Smith, M.W., Tarasov, L., Haywood, A.M. and Bacon, K.L. 2018. Global peatland initiation driven by regionally asynchronous warming. *Proceedings of the National Academy of Sciences*. **115**(19), pp.4851–4856.

Morris, P.J., Baird, A.J., Eades, P.A. and Surridge, B.W.J. 2019. Controls on Near-Surface Hydraulic Conductivity in a Raised Bog. *Water Resources Research*. **55**(2), pp.1531–1543.

Morris, P.J., Davies, M.L., Baird, A.J., Balliston, N., Bourgault, M.-A., Clymo, R.S., Fewster, R.E., Furukawa, A.K., Holden, J., Kessel, E., Ketcheson, S.J., Kløve, B., Larocque, M., Marttila, H., Menberu, M.W., Moore, P.A., Price, J.S., Ronkanen, A.-K., Rosa, E., Strack, M., Surridge, B.W.J., Waddington, J.M., Whittington, P. and Wilkinson, S.L. 2022. Saturated Hydraulic Conductivity in

Northern Peats Inferred From Other Measurements. *Water Resources Research*. **58**(11), e2022WR033181.

Müller, J. and Joos, F. 2021. Committed and projected future changes in global peatlands – continued transient model simulations since the Last Glacial Maximum. *Biogeosciences*. **18**(12), pp.3657–3687.

Muller, S.W. 1945. ... *Permafrost, Or Permanently Frozen Ground: And Related Engineering Problems*. Army map service, US Army.

Myers-Smith, I.H., Elmendorf, S.C., Beck, P.S.A., Wilmking, M., Hallinger, M., Blok, D., Tape, K.D., Rayback, S.A., Macias-Fauria, M., Forbes, B.C., Speed, J.D.M., Boulanger-Lapointe, N., Rixen, C., Lévesque, E., Schmidt, N.M., Baittinger, C., Trant, A.J., Hermanutz, L., Collier, L.S., Dawes, M.A., Lantz, T.C., Weijers, S., Jørgensen, R.H., Buchwal, A., Buras, A., Naito, A.T., Ravolainen, V., Schaepman-Strub, G., Wheeler, J.A., Wipf, S., Guay, K.C., Hik, D.S. and Vellend, M. 2015. Climate sensitivity of shrub growth across the tundra biome. *Nature Climate Change*. **5**(9), pp.887–891.

Myers-Smith, I.H. and Hik, D.S. 2018. Climate warming as a driver of tundra shrubline advance. *Journal of Ecology*. **106**(2), pp.547–560.

Myers-Smith, I.H., Kerby, J.T., Phoenix, G.K., Bjerke, J.W., Epstein, H.E., Assmann, J.J., John, C., Andreu-Hayles, L., Angers-Blondin, S., Beck, P.S.A., Berner, L.T., Bhatt, U.S., Bjorkman, A.D., Blok, D., Bryn, A., Christiansen, C.T., Cornelissen, J.H.C., Cunliffe, A.M., Elmendorf, S.C., Forbes, B.C., Goetz, S.J., Hollister, R.D., de Jong, R., Loranty, M.M., Macias-Fauria, M., Maseyk, K., Normand, S., Olofsson, J., Parker, T.C., Parmentier, F.-J.W., Post, E., Schaepman-Strub, G., Stordal, F., Sullivan, P.F., Thomas, H.J.D., Tømmervik, H., Treharne, R., Tweedie, C.E., Walker, D.A., Wilmking, M. and Wipf, S. 2020. Complexity revealed in the greening of the Arctic. *Nature Climate Change*. **10**(2), pp.106–117.

Nagare, R.M., Schincariol, R.A., Quinton, W.L. and Hayashi, M. 2012. Effects of freezing on soil temperature, freezing front propagation and moisture redistribution in peat: laboratory investigations. *Hydrology and Earth System Sciences*. **16**(2), pp.501–515.

Nagare, R.M., Schincariol, R.A., Mohammed, A.A., Quinton, W.L. and Hayashi, M. 2013. Measuring saturated hydraulic conductivity and anisotropy of peat by a modified split-container method. *Hydrogeology Journal*. **21**(2), pp.515–520.

Nakatsubo, T., Uchida, M., Sasaki, A., Kondo, M., Yoshitake, S. and Kanda, H. 2015. Carbon accumulation rate of peatland in the High Arctic, Svalbard: Implications for carbon sequestration. *Polar Science*. **9**(2), pp.267–275.

National Wetlands Working Group 1998. Wetlands of Canda. *Sustanable Development Branch Environment Canada, Ottawa*. **452**.

O'Connor, M.T., Cardenas, M.B., Neilson, B.T., Nicholaides, K.D. and Kling, G.W. 2019. Active Layer Groundwater Flow: The Interrelated Effects of Stratigraphy, Thaw, and Topography. *Water Resources Research*. **55**(8), pp.6555–6576.

O'Connor, M.T., Cardenas, M.B., Ferencz, S.B., Wu, Y., Neilson, B.T., Chen, J. and Kling, G.W. 2020. Empirical Models for Predicting Water and Heat Flow Properties of Permafrost Soils. *Geophysical Research Letters*. **47**(11), e2020GL087646.

O'Donnell, J.A., Romanovsky, V.E., Harden, J.W. and McGuire, A.D. 2009. The Effect of Moisture Content on the Thermal Conductivity of Moss and Organic Soil Horizons From Black Spruce Ecosystems in Interior Alaska. *Soil Science*. **174**(12), pp.646–651.

O'Neill, B.C., Tebaldi, C., van Vuuren, D.P., Eyring, V., Friedlingstein, P., Hurtt, G., Knutti, R., Kriegler, E., Lamarque, J.-F., Lowe, J., Meehl, G.A., Moss, R., Riahi, K. and Sanderson, B.M. 2016. The Scenario Model Intercomparison Project (ScenarioMIP) for CMIP6. *Geoscientific Model Development*. **9**(9), pp.3461–3482.

O'Neill, B.C., Kriegler, E., Ebi, K.L., Kemp-Benedict, E., Riahi, K., Rothman, D.S., van Ruijven, B.J., van Vuuren, D.P., Birkmann, J., Kok, K., Levy, M. and Solecki, W. 2017. The roads ahead: Narratives for shared socioeconomic pathways describing world futures in the 21st century. *Global Environmental Change*. **42**, pp.169–180.

O'Neill, H.B., Wolfe, S.A. and Duchesne, C. 2019. New ground ice maps for Canada using a paleogeographic modelling approach. *The Cryosphere*. **13**(3), pp.753–773.

Ohlson, M. 1998. Age-depth relationships in Scandinavian surface peat: a quantitative analysis. *Oikos*. **82**(1), pp.29-36.

Ohlson, M., Økland, R.H., Nordbakken, J.-F. and Dahlberg, B. 2001. Fatal interactions between Scots pine and Sphagnum mosses in bog ecosystems. *Oikos*. **94**(3), pp.425–432.

Oksanen, P.O., Kuhry, P. and Alekseeva, R.N. 2001. Holocene development of the Rogovaya River peat plateau, European Russian Arctic. *The Holocene*. **11**(1), pp.25–40.

Oksanen, P.O., Kuhry, P. and Alekseeva, R.N. 2003. Holocene Development and Permafrost History of the Usinsk Mire, Northeast European Russia. *Géographie physique et Quaternaire*. **57**(2–3), pp.169–187.

Oksanen, J., Simpson, G.L., Blanchet, F.G., Kindt, R., Legendre, P., Minchin, P.R., O'Hara, R.B., Solymos, P., Stevens, M.H.H., Szoecs, E., Wagner, H., Barbour, M., Bedward, M., Bolker, B., Borcard, D., Carvalho, G., Chirico, M., Caceres, M.D., Durand, S., Evangelista, H.B.A., FitzJohn, R., Friendly, M., Furneaux, B., Hannigan, G., Hill, M.O., Lahti, L., McGlinn, D., Ouellette, M.-H., Cunha, E.R., Smith, T., Stier, A., Braak, C.J.F.T. and Weedon, J. 2022. vegan: Community Ecology Package. [Accessed 21 September 2022]. Available from: https://CRAN.R-project.org/package=vegan.

Olefeldt, D. and Roulet, N.T. 2012. Effects of permafrost and hydrology on the composition and transport of dissolved organic carbon in a subarctic peatland complex. *Journal of Geophysical Research: Biogeosciences*. **117**(G1).

Olefeldt, D., Turetsky, M.R., Crill, P.M. and McGuire, A.D. 2013. Environmental and physical controls on northern terrestrial methane emissions across permafrost zones. *Global Change Biology*. **19**(2), pp.589–603.

Olefeldt, D. and Roulet, N.T. 2014. Permafrost conditions in peatlands regulate magnitude, timing, and chemical composition of catchment dissolved organic carbon export. *Global Change Biology*. **20**(10), pp.3122–3136.

Olefeldt, D., Goswami, S., Grosse, G., Hayes, D., Hugelius, G., Kuhry, P., McGuire, A.D., Romanovsky, V.E., Sannel, A.B.K., Schuur, E. a. G. and Turetsky, M.R. 2016. Circumpolar distribution and carbon storage of thermokarst landscapes. *Nature Communications*. **7**(1), p.13043.

Olefeldt, D., Heffernan, L., Jones, M.C., Sannel, A.B.K., Treat, C.C. and Turetsky, M.R. 2021. Permafrost Thaw in Northern Peatlands: Rapid Changes in Ecosystem and Landscape Functions *In*: J. G. Canadell and R. B. Jackson, eds. *Ecosystem Collapse and Climate Change* [Online]. Ecological Studies. Cham: Springer International Publishing, pp.27–67. [Accessed 30 August 2022]. Available from: https://doi.org/10.1007/978-3-030-71330-0_3.

Olvmo, M., Holmer, B., Thorsson, S., Reese, H. and Lindberg, F. 2020. Sub-arctic palsa degradation and the role of climatic drivers in the largest coherent palsa mire complex in Sweden (Vissátvuopmi), 1955–2016. *Scientific Reports*. **10**(1), p.8937.

Ouzilleau Samson, D., Bhiry, N. and Lavoie, M. 2010. Late-Holocene palaeoecology of a polygonal peatland on the south shore of Hudson Strait, northern Québec, Canada. *The Holocene*. **20**(4), pp.525–536.

Päivänen, J. 1973. *Hydraulic conductivity and water retention in peat soils.* Suomen metsätieteellinen seura.

Palace, M., Herrick, C., DelGreco, J., Finnell, D., Garnello, A.J., McCalley, C., McArthur, K., Sullivan, F. and Varner, R.K. 2018. Determining Subarctic Peatland Vegetation Using an Unmanned Aerial System (UAS). *Remote Sensing*. **10**(9), p.1498.

Parviainen, M. and Luoto, M. 2007. Climate envelopes of mire complex types in fennoscandia. *Geografiska Annaler: Series A, Physical Geography*. **89**(2), pp.137–151.

Payette, S. 1984. Peat Inception and Climatic Change in Northern Quebec *In*: N.-A. Mörner and W. Karlén, eds. *Climatic Changes on a Yearly to Millennial Basis: Geological, Historical and Instrumental Records* [Online]. Dordrecht: Springer Netherlands, pp.173–179. [Accessed 12 August 2022]. Available from: https://doi.org/10.1007/978-94-015-7692-5_17.

Payette, S. and Lavoie, C. 1994. The arctic tree line as a record of past and recent climatic changes. *Environmental Reviews*. **2**(1), pp.78–90.

Payette, S., Delwaide, A., Caccianiga, M. and Beauchemin, M. 2004. Accelerated thawing of subarctic peatland permafrost over the last 50 years. *Geophysical Research Letters*. **31**(18).

Pearce, J. and Ferrier, S. 2000. Evaluating the predictive performance of habitat models developed using logistic regression. *Ecological modelling*. **133**(3), pp.225–245.

Pelletier, N., Talbot, J., Olefeldt, D., Turetsky, M., Blodau, C., Sonnentag, O. and Quinton, W.L. 2017. Influence of Holocene permafrost aggradation and thaw on the paleoecology and carbon storage of a peatland complex in northwestern Canada. *The Holocene*. **27**(9), pp.1391–1405.

Peregon, A., Maksyutov, S., Kosykh, N.P. and Mironycheva-Tokareva, N.P. 2008. Map-based inventory of wetland biomass and net primary production in western Siberia. *Journal of Geophysical Research: Biogeosciences*. **113**(G1).

Petrucci, C.J. 2009. A primer for social worker researchers on how to conduct a multinomial logistic regression. *Journal of social service research*. **35**(2), pp.193–205.

Pichan, S. and O'Kelly, B.C. 2012. Effect of Decomposition on the Compressibility of Fibrous Peat *In*: *GeoCongress 2012* [Online]. Oakland, California, United States: American Society of Civil Engineers, pp.4329–4338. [Accessed 6 April 2023]. Available from: http://ascelibrary.org/doi/10.1061/9780784412121.445.

Piilo, S.R., Väliranta, M.M., Amesbury, M.J., Aquino-López, M.A., Charman, D.J., Gallego-Sala, A., Garneau, M., Koroleva, N., Kärppä, M., Laine, A.M., Sannel, A.B.K., Tuittila, E.-S. and Zhang, H. 2023. Consistent centennial-scale change in European sub-Arctic peatland vegetation toward Sphagnum dominance—Implications for carbon sink capacity. *Global Change Biology*. **29**(6), pp.1530–1544.

Pissart, A. 2002. Palsas, lithalsas and remnants of these periglacial mounds. A progress report. *Progress in Physical Geography*. **26**(4), pp.605–621.

Pouliot, R., Rochefort, L., Karofeld, E. and Mercier, C. 2011. Initiation of Sphagnum moss hummocks in bogs and the presence of vascular plants: Is there a link? *Acta Oecologica*. **37**(4), pp.346–354.

Powers, D.M. 2011. Evaluation: from precision, recall and F-measure to ROC, informedness, markedness and correlation. *International Journal of Machine Learning Technology*. **2**(1), pp.37–63.

Primeau, G. and Garneau, M. 2021. Carbon accumulation in peatlands along a boreal to subarctic transect in eastern Canada. *The Holocene*. **31**(5), pp.858–869.

QGIS.org 2020. QGIS.

Qiu, C., Zhu, D., Ciais, P., Guenet, B. and Peng, S. 2020. The role of northern peatlands in the global carbon cycle for the 21st century. *Global Ecology and Biogeography*. **29**(5), pp.956–973.

Quinton, W.L., Gray, D. and Marsh, P. 2000. Subsurface drainage from hummock-covered hillslopes in the Arctic tundra. *Journal of Hydrology*. **237**(1–2), pp.113–125.

Quinton, W.L., Carey, S.K. and Goeller, N.T. 2004. Snowmelt runoff from northern alpine tundra hillslopes: major processes and methods of simulation. *Hydrology and Earth System Sciences*. **8**(5), pp.877–890.

Quinton, W.L., Hayashi, M. and Carey, S.K. 2008. Peat hydraulic conductivity in cold regions and its relation to pore size and geometry. *Hydrological Processes*. **22**(15), pp.2829–2837.

Quinton, W.L. and Baltzer, J.L. 2013. The active-layer hydrology of a peat plateau with thawing permafrost (Scotty Creek, Canada). *Hydrogeology Journal*. **21**(1), pp.201–220.

Quinton, W.L., Berg, A., Braverman, M., Carpino, O., Chasmer, L., Connon, R., Craig, J., Devoie, É., Hayashi, M., Haynes, K., Olefeldt, D., Pietroniro, A., Rezanezhad, F., Schincariol, R. and Sonnentag, O. 2019. A synthesis of three decades of hydrological research at Scotty Creek, NWT, Canada. *Hydrology and Earth System Sciences*. **23**(4), pp.2015–2039.

R Core Team 2022. R: The R Project for Statistical Computing. [Accessed 26 July 2022]. Available from: https://www.r-project.org/.

Railton, J. and Sparling, J. 1973. Preliminary studies on the ecology of palsa mounds in northern Ontario. *Canadian Journal of Botany*. **51**, pp.1037–1044.

Ramirez, J.A., Peleg, N., Baird, A.J., Young, D.M., Morris, P.J., Larocque, M. and Garneau, M. 2023. Modelling peatland development in high-boreal Quebec, Canada, with DigiBog_Boreal. *Ecological Modelling*. **478**, p.110298.

Reimer, P.J., Austin, W.E.N., Bard, E., Bayliss, A., Blackwell, P.G., Ramsey, C.B., Butzin, M., Cheng, H., Edwards, R.L., Friedrich, M., Grootes, P.M., Guilderson, T.P., Hajdas, I., Heaton, T.J., Hogg, A.G., Hughen, K.A., Kromer, B., Manning, S.W., Muscheler, R., Palmer, J.G., Pearson, C., Plicht, J. van der, Reimer, R.W., Richards, D.A., Scott, E.M., Southon, J.R., Turney, C.S.M., Wacker, L., Adolphi, F., Büntgen, U., Capano, M., Fahrni, S.M., Fogtmann-Schulz, A., Friedrich, R., Köhler, P., Kudsk, S., Miyake, F., Olsen, J., Reinig, F., Sakamoto, M., Sookdeo, A. and Talamo, S. 2020. The IntCal20 Northern Hemisphere Radiocarbon Age Calibration Curve (0–55 cal kBP). *Radiocarbon*. **62**(4), pp.725–757.

Rezanezhad, F., Price, J.S., Quinton, W.L., Lennartz, B., Milojevic, T. and Van Cappellen, P. 2016. Structure of peat soils and implications for water storage, flow and solute transport: A review update for geochemists. *Chemical Geology*. **429**, pp.75–84.

Robinson, C., Roy-Léveillée, P., Turner, K. and Basiliko, N. 2021. Impacts of Shrubification on Ground Temperatures and Carbon Cycling in a Sub-Arctic Fen near Churchill, MB *In*: *Permafrost 2021: Merging Permafrost Science and Cold Regions Engineering*. American Society of Civil Engineers Reston, VA, pp.60–70.

Robitaille, M., Garneau, M., van Bellen, S. and Sanderson, N.K. 2021. Long-term and recent ecohydrological dynamics of patterned peatlands in north-central Quebec (Canada). *The Holocene*. **31**(5), pp.844–857.

Rodysill, J.R., Anderson, Lesleigh, Cronin, T.M., Jones, M.C., Thompson, R.S., Wahl, D.B., Willard, D.A., Addison, J.A., Alder, J.R., Anderson, K.H.,

Anderson, Lysanna, Barron, J.A., Bernhardt, C.E., Hostetler, S.W., Kehrwald, N.M., Khan, N.S., Richey, J.N., Starratt, S.W., Strickland, L.E., Toomey, M.R., Treat, C.C. and Wingard, G.L. 2018. A North American Hydroclimate Synthesis (NAHS) of the Common Era. *Global and Planetary Change*. **162**, pp.175–198.

Rohatgi, A. 2021. WebPlotDigitzer. Available from: https://automeris.io/WebPlotDigitizer.

Rycroft, D.W., Williams, D.J.A. and Ingram, H.A.P. 1975. The Transmission of Water Through Peat: I. Review. *Journal of Ecology*. **63**(2), pp.535–556.

Rydin, H. and Mcdonald, A.J.S. 1985. Tolerance of Sphagnum to water level. *Journal of Bryology*. **13**(4), pp.571–578.

Salonen, J.S., Seppä, H., Väliranta, M., Jones, V.J., Self, A., Heikkilä, M., Kultti, S. and Yang, H. 2011. The Holocene thermal maximum and late-Holocene cooling in the tundra of NE European Russia. *Quaternary Research*. **75**(3), pp.501–511.

Sannel, A.B.K. and Kuhry, P. 2008. Long-term stability of permafrost in subarctic peat plateaus, west-central Canada. *The Holocene*. **18**(4), pp.589–601.

Sannel, A.B.K., Hugelius, G., Jansson, P. and Kuhry, P. 2016. Permafrost Warming in a Subarctic Peatland – Which Meteorological Controls are Most Important? *Permafrost and Periglacial Processes*. **27**(2), pp.177–188.

Sannel, A.B.K., Hempel, L., Kessler, A. and Pr≐skienis, V. 2018. Holocene development and permafrost history in sub-arctic peatlands in Tavvavuoma, northern Sweden. *Boreas*. **47**(2), pp.454–468.

Schädel, C., Bader, M.K.-F., Schuur, E.A.G., Biasi, C., Bracho, R., Čapek, P., De Baets, S., Diáková, K., Ernakovich, J., Estop-Aragones, C., Graham, D.E., Hartley, I.P., Iversen, C.M., Kane, E., Knoblauch, C., Lupascu, M., Martikainen, P.J., Natali, S.M., Norby, R.J., O'Donnell, J.A., Chowdhury, T.R., Šantrůčková, H., Shaver, G., Sloan, V.L., Treat, C.C., Turetsky, M.R., Waldrop, M.P. and Wickland, K.P. 2016. Potential carbon emissions

dominated by carbon dioxide from thawed permafrost soils. *Nature Climate Change*. **6**(10), pp.950–953.

Schädel, C., Koven, C.D., Lawrence, D.M., Celis, G., Garnello, A.J., Hutchings, J., Mauritz, M., Natali, S.M., Pegoraro, E., Rodenhizer, H., Salmon, V.G., Taylor, M.A., Webb, E.E., Wieder, W.R. and Schuur, E.A. 2018. Divergent patterns of experimental and model-derived permafrost ecosystem carbon dynamics in response to Arctic warming. *Environmental Research Letters*. **13**(10), p.105002.

Schielzeth, H. 2010. Simple means to improve the interpretability of regression coefficients. *Methods in Ecology and Evolution*. **1**(2), pp.103–113.

Sejrup, H.P., Seppä, H., McKay, N.P., Kaufman, D.S., Geirsdóttir, Á., de Vernal, A., Renssen, H., Husum, K., Jennings, A. and Andrews, J.T. 2016. North Atlantic-Fennoscandian Holocene climate trends and mechanisms. *Quaternary Science Reviews*. **147**, pp.365–378.

Seppä, H. and Birks, H.J.B. 2001. July mean temperature and annual precipitation trends during the Holocene in the Fennoscandian tree-line area: pollen-based climate reconstructions. *The Holocene*. **11**(5), pp.527–539.

Seppälä, M. 1982. An experimental study of the formation of palsas. In: French, H.M. ed. *Proceedings of the Fourth Canadian Permafrost Conference, March 2-6 1981, Calgary*. Ottawa: National Research Council of Canada, pp.36–42.

Seppälä, M. 1986. The origin of palsas. *Geografiska Annaler: Series A, Physical Geography*. **68**(3), pp.141–147.

Seppälä, M. 1994. Snow depth controls palsa growth. *Permafrost and Periglacial Processes*. **5**(4), pp.283–288.

Seppälä, M. 2003. Surface abrasion of palsas by wind action in Finnish Lapland. *Geomorphology*. **52**(1), pp.141–148.

Seppälä, M. 2011. Synthesis of studies of palsa formation underlining the importance of local environmental and physical characteristics. *Quaternary Research*. **75**(2), pp.366–370.

Serreze, M.C. and Barry, R.G. 2011. Processes and impacts of Arctic amplification: A research synthesis. *Global and planetary change*. **77**(1–2), pp.85–96.

Signorell, A., Aho, K., Alfons, A., Anderegg, N., Aragon, T., Arachchige, C., Arppe, A., Baddeley, A., Barton, K. and Bolker, B. 2022. DescTools: Tools for descriptive statistics. R package version 0.99. 47.

Sim, T.G., Swindles, G.T., Morris, P.J., Gałka, M., Mullan, D. and Galloway, J.M. 2019. Pathways for ecological change in Canadian High Arctic wetlands under rapid twentieth century warming. *Geophysical Research Letters*. **46**(9), pp.4726–4737.

Sim, T.G., Swindles, G.T., Morris, P.J., Baird, A.J., Charman, D.J., Amesbury, M.J., Beilman, D., Channon, A. and Gallego-Sala, A.V. 2021a. Ecology of peatland testate amoebae in Svalbard and the development of transfer functions for reconstructing past water-table depth and pH. *Ecological Indicators*. **131**, p.108122.

Sim, T.G., Swindles, G.T., Morris, P.J., Baird, A.J., Cooper, C.L., Gallego-Sala, A.V., Charman, D.J., Roland, T.P., Borken, W., Mullan, D., Aquino-López, M.A. and Gałka, M. 2021b. Divergent responses of permafrost peatlands to recent climate change. *Environmental Research Letters*. **16**(3), p.034001.

Sjogersten, S., Ledger, M., Siewert, M., de la Barreda-Bautista, B., Sowter, A., Gee, D., Foody, G. and Boyd, D.S. 2023. Capabilities of optical and radar Earth observation data for up-scaling methane emissions linked to subsidence and permafrost degradation in sub-Arctic peatlands. *Biogeosciences Discussions*. pp.1–30.

Smith, L.C., Beilman, David.W., Kremenetski, K.V., Sheng, Y., MacDonald, G.M., Lammers, R.B., Shiklomanov, A.I. and Lapshina, E.D. 2012. Influence of permafrost on water storage in West Siberian peatlands revealed from a new database of soil properties. *Permafrost and Periglacial Processes*. **23**(1), pp.69–79.

Smith, M. and Riseborough, D. 2002. Climate and the limits of permafrost: a zonal analysis. *Permafrost and Periglacial Processes*. **13**(1), pp.1–15.

Smith, N.D., Burke, E.J., Schanke Aas, K., Althuizen, I.H.J., Boike, J., Christiansen, C.T., Etzelmüller, B., Friborg, T., Lee, H., Rumbold, H., Turton, R.H., Westermann, S. and Chadburn, S.E. 2022. Explicitly modelling microtopography in permafrost landscapes in a land surface model (JULES vn5.4_microtopography). *Geoscientific Model Development*. **15**(9), pp.3603–3639.

Surridge, B.W.J., Baird, A.J. and Heathwaite, A.L. 2005. Evaluating the quality of hydraulic conductivity estimates from piezometer slug tests in peat. *Hydrological Processes*. **19**(6), pp.1227–1244.

Swedish Meteorological and Hydrological Institute 2023. Download Meteorological Observations | SMHI. [Accessed 4 April 2023]. Available from: https://www.smhi.se.

Swindles, G.T., Morris, P.J., Mullan, D., Watson, E.J., Turner, T.E., Roland, T.P., Amesbury, M.J., Kokfelt, U., Schoning, K., Pratte, S., Gallego-Sala, A., Charman, D.J., Sanderson, N., Garneau, M., Carrivick, J.L., Woulds, C., Holden, J., Parry, L. and Galloway, J.M. 2015. The long-term fate of permafrost peatlands under rapid climate warming. *Scientific Reports*. **5**(1), p.17951.

Swindles, G.T., Morris, P.J., Mullan, D.J., Payne, R.J., Roland, T.P., Amesbury, M.J., Lamentowicz, M., Turner, T.E., Gallego-Sala, A., Sim, T., Barr, I.D., Blaauw, M., Blundell, A., Chambers, F.M., Charman, D.J., Feurdean, A., Galloway, J.M., Gałka, M., Green, S.M., Kajukało, K., Karofeld, E., Korhola, A., Lamentowicz, Ł., Langdon, P., Marcisz, K., Mauquoy, D., Mazei, Y.A., McKeown, M.M., Mitchell, E.A.D., Novenko, E., Plunkett, G., Roe, H.M., Schoning, K., Sillasoo, Ü., Tsyganov, A.N., van der Linden, M., Väliranta, M. and Warner, B. 2019. Widespread drying of European peatlands in recent centuries. *Nature Geoscience*. **12**(11), pp.922–9**28.**

Szumigalski, A.R. and Bayley, S.E. 1996. Net above-ground primary production along a bog-rich fen gradient in Central Alberta, Canada. *Wetlands*. **16**(4), pp.467–476.

Tebaldi, C., Debeire, K., Eyring, V., Fischer, E., Fyfe, J., Friedlingstein, P., Knutti, R., Lowe, J., O'Neill, B. and Sanderson, B. 2021. Climate model

projections from the scenario model intercomparison project (ScenarioMIP) of CMIP6. *Earth System Dynamics*. **12**(1), pp.253–293.

Teltewskoi, A., Beermann, F., Beil, I., Bobrov, A., De Klerk, P., Lorenz, S., Lüder, A., Michaelis, D. and Joosten, H. 2016. 4000 years of changing wetness in a permafrost polygon peatland (Kytalyk, NE Siberia): A comparative high-resolution multi-proxy study. *Permafrost and Periglacial Processes*. **27**(1), pp.76–95.

Terentieva, I.E., Glagolev, M.V., Lapshina, E.D., Sabrekov, A.F. and Maksyutov, S. 2016. Mapping of West Siberian taiga wetland complexes using Landsat imagery: implications for methane emissions. *Biogeosciences*. **13**(16), pp.4615–4626.

Thomas, S.K., Conta, J.F., Severson, E.D. and Galbraith, J.M. 2016. *Measuring Saturated Hydraulic Conductivity in Soil* [Online]. Virginia Cooperative Extension. CSES-141P.

Thurner, M., Beer, C., Santoro, M., Carvalhais, N., Wutzler, T., Schepaschenko, D., Shvidenko, A., Kompter, E., Ahrens, B. and Levick, S.R. 2014. Carbon stock and density of northern boreal and temperate forests. *Global Ecology and Biogeography*. **23**(3), pp.297–310.

Title, P.O. and Bemmels, J.B. 2018. ENVIREM: an expanded set of bioclimatic and topographic variables increases flexibility and improves performance of ecological niche modeling. *Ecography*. **41**(2), pp.291–307.

Tokarska, K.B., Stolpe, M.B., Sippel, S., Fischer, E.M., Smith, C.J., Lehner, F. and Knutti, R. 2020. Past warming trend constrains future warming in CMIP6 models. *Science Advances*. **6**(12), p.eaaz9549.

Treat, C.C., Jones, M.C., Camill, P., Gallego-Sala, A., Garneau, M., Harden, J.W., Hugelius, G., Klein, E.S., Kokfelt, U., Kuhry, P., Loisel, J., Mathijssen, P.J.H., O'Donnell, J.A., Oksanen, P.O., Ronkainen, T.M., Sannel, A.B.K., Talbot, J., Tarnocai, C. and Väliranta, M. 2016. Effects of permafrost aggradation on peat properties as determined from a pan-Arctic synthesis of plant macrofossils. *Journal of Geophysical Research: Biogeosciences*. **121**(1), pp.78–94.

Treat, C.C. and Jones, M.C. 2018. Near-surface permafrost aggradation in Northern Hemisphere peatlands shows regional and global trends during the past 6000 years. *The Holocene*. **28**(6), pp.998–1010.

Treat, C.C., Bloom, A.A. and Marushchak, M.E. 2018. Nongrowing season methane emissions–a significant component of annual emissions across northern ecosystems. *Global Change Biology*. **24**(8), pp.3331–3343.

Treat, C.C., Jones, M.C., Alder, J., Sannel, A.B.K., Camill, P. and Frolking, S. 2021a. Predicted Vulnerability of Carbon in Permafrost Peatlands With Future Climate Change and Permafrost Thaw in Western Canada. *Journal of Geophysical Research: Biogeosciences*. **126**(5), e2020JG005872.

Treat, C.C., Jones, M.C., Brosius, L., Grosse, G., Walter Anthony, K. and Frolking, S. 2021b. The role of wetland expansion and successional processes in methane emissions from northern wetlands during the Holocene. *Quaternary Science Reviews*. **257**, p.106864.

Treat, C.C., Jones, M.C., Alder, J. and Frolking, S. 2022. Hydrologic Controls on Peat Permafrost and Carbon Processes: New Insights From Past and Future Modeling. *Frontiers in Environmental Science*. **10**.

Tremblay, S., Bhiry, N. and Lavoie, M. 2014. Long-term dynamics of a palsa in the sporadic permafrost zone of northwestern Quebec (Canada) A. de Vernal, ed. *Canadian Journal of Earth Sciences*. **51**(5), pp.500–509.

Turetsky, M.R., Wieder, R.K. and Vitt, D.H. 2002. Boreal peatland C fluxes under varying permafrost regimes. *Soil Biology and Biochemistry*. **34**(7), pp.907–912.

Turetsky, M.R., Wieder, R.K., Vitt, D.H., Evans, R.J. and Scott, K.D. 2007. The disappearance of relict permafrost in boreal north America: Effects on peatland carbon storage and fluxes. *Global Change Biology*. **13**(9), pp.1922–1934.

Turetsky, M.R., Treat, C.C., Waldrop, M.P., Waddington, J.M., Harden, J.W. and McGuire, A.D. 2008. Short-term response of methane fluxes and methanogen activity to water table and soil warming manipulations in an Alaskan peatland. *Journal of Geophysical Research: Biogeosciences*. **113**(G3).

Turetsky, M.R., Kane, E.S., Harden, J.W., Ottmar, R.D., Manies, K.L., Hoy, E. and Kasischke, E.S. 2011. Recent acceleration of biomass burning and carbon losses in Alaskan forests and peatlands. *Nature Geoscience*. **4**(1), pp.27–31.

Turetsky, M.R., Benscoter, B., Page, S., Rein, G., van der Werf, G.R. and Watts, A. 2015. Global vulnerability of peatlands to fire and carbon loss. *Nature Geoscience*. **8**(1), pp.11–14.

Turetsky, M.R., Abbott, B.W., Jones, M.C., Anthony, K.W., Olefeldt, D., Schuur, E.A.G., Grosse, G., Kuhry, P., Hugelius, G., Koven, C., Lawrence, D.M., Gibson, C., Sannel, A.B.K. and McGuire, A.D. 2020. Carbon release through abrupt permafrost thaw. *Nature Geoscience*. **13**(2), pp.138–143.

Turunen, J., Tomppo, E., Tolonen, K. and Reinikainen, A. 2002. Estimating carbon accumulation rates of undrained mires in Finland–application to boreal and subarctic regions. *The Holocene*. **12**(1), pp.69–80.

Ullman, D.J., Carlson, A.E., Hostetler, S.W., Clark, P.U., Cuzzone, J., Milne, G.A., Winsor, K. and Caffee, M. 2016. Final Laurentide ice-sheet deglaciation and Holocene climate-sea level change. *Quaternary Science Reviews*. **152**, pp.49–59.

Valdes, P.J., Armstrong, E., Badger, M.P.S., Bradshaw, C.D., Bragg, F., Crucifix, M., Davies-Barnard, T., Day, J.J., Farnsworth, A., Gordon, C., Hopcroft, P.O., Kennedy, A.T., Lord, N.S., Lunt, D.J., Marzocchi, A., Parry, L.M., Pope, V., Roberts, W.H.G., Stone, E.J., Tourte, G.J.L. and Williams, J.H.T. 2017. The BRIDGE HadCM3 family of climate models: HadCM3@Bristol v1.0. *Geoscientific Model Development*. **10**(10), pp.3715–3743.

Väliranta, M., Kaakinen, A. and Kuhry, P. 2003. Holocene climate and landscape evolution East of the Pechora Delta, East-European Russian Arctic. *Quaternary Research*. **59**(3), pp.335–344.

Väliranta, M., Salojärvi, N., Vuorsalo, A., Juutinen, S., Korhola, A., Luoto, M. and Tuittila, E.-S. 2017. Holocene fen–bog transitions, current status in Finland and future perspectives. *The Holocene*. **27**(5), pp.752–764.

Väliranta, M., Marushchak, M.E., Tuovinen, J.-P., Lohila, A., Biasi, C., Voigt, C., Zhang, H., Piilo, S., Virtanen, T., Räsänen, A., Kaverin, D., Pastukhov, A., Sannel, A.B.K., Tuittila, E.-S., Korhola, A. and Martikainen, P.J. 2021. Warming climate forcing impact from a sub-arctic peatland as a result of late Holocene permafrost aggradation and initiation of bare peat surfaces. *Quaternary Science Reviews*. **264**, p.107022.

van Bellen, S., Garneau, M. and Booth, R.K. 2011. Holocene carbon accumulation rates from three ombrotrophic peatlands in boreal Quebec, Canada: Impact of climate-driven ecohydrological change. *The Holocene*. **21**(8), pp.1217–1231.

Van Bellen, S., Garneau, M., Ali, A.A., Lamarre, A., Robert, É.C., Magnan, G., Asnong, H. and Pratte, S. 2013. Poor fen succession over ombrotrophic peat related to late Holocene increased surface wetness in subarctic Quebec, Canada. *Journal of Quaternary Science*. **28**(8), pp.748–760.

van Breemen, N. 1995. How Sphagnum bogs down other plants. *Trends in Ecology & Evolution*. **10**(7), pp.270–275.

Vardy, S.R., Warner, B.G. and Aravena, R. 1997. Holocene Climate Effects on the Development of a Peatland on the Tuktoyaktuk Peninsula, Northwest Territories1. *Quaternary Research*. **47**(1), pp.90–104.

Vardy, S.R., Warner, B.G. and Aravena, R. 1998. Holocene Climate and the Development of a Subarctic Peatland near Inuvik, Northwest Territories, Canada. *Climatic Change*. **40**(2), pp.285–313.

Vardy, S.R., Warner, B.G. and Asada, T. 2005. Holocene environmental change in two polygonal peatlands, south-central Nunavut, Canada. *Boreas*. **34**(3), pp.324–334.

Varner, R.K., Crill, P.M., Frolking, S., McCalley, C.K., Burke, S.A., Chanton, J.P., Holmes, M.E., Isogenie Project Coordinators, Saleska, S. and Palace, M.W. 2022. Permafrost thaw driven changes in hydrology and vegetation cover increase trace gas emissions and climate forcing in Stordalen Mire from 1970 to 2014. *Philosophical Transactions of the Royal Society A: Mathematical, Physical and Engineering Sciences*. **380**(2215), p.20210022.

Verdonen, M., Störmer, A., Lotsari, E., Korpelainen, P., Burkhard, B., Colpaert, A. and Kumpula, T. 2023. Permafrost degradation at two monitored palsa mires in north-west Finland. *The Cryosphere*. **17**(5), pp.1803–1819.

Viau, A.E. and Gajewski, K. 2009. Reconstructing Millennial-Scale, Regional Paleoclimates of Boreal Canada during the Holocene. *Journal of Climate*. **22**(2), pp.316–330.

Vicherová, E., Hájek, M. and Hájek, T. 2015. Calcium intolerance of fen mosses: Physiological evidence, effects of nutrient availability and successional drivers. *Perspectives in Plant Ecology, Evolution and Systematics*. **17**(5), pp.347–359.

Vitt, D.H., Halsey, L.A. and Zoltai, S.C. 1994. The bog landforms of continental western Canada in relation to climate and permafrost patterns. *Arctic and Alpine Research*. **26**(1), pp.1–13.

Vitt, D., Halsey, L. and Zoltai, S. 2000. The changing landscape of Canada's western boreal forest. *Canadian Journal of Forest Research-revue Canadienne De Recherche Forestiere - CAN J FOREST RES*. **30**, pp.283–287.

Vitt, D.H. 2006. Functional Characteristics and Indicators of Boreal Peatlands *In*: R. K. Wieder and D. H. Vitt, eds. *Boreal Peatland Ecosystems* [Online]. Ecological Studies. Berlin, Heidelberg: Springer, pp.9–24. [Accessed 24 August 2022]. Available from: https://doi.org/10.1007/978-3-540-31913-9_2.

Voigt, C., Marushchak, M.E., Mastepanov, M., Lamprecht, R.E., Christensen, T.R., Dorodnikov, M., Jackowicz-Korczyński, M., Lindgren, A., Lohila, A., Nykänen, H., Oinonen, M., Oksanen, T., Palonen, V., Treat, C.C., Martikainen, P.J. and Biasi, C. 2019. Ecosystem carbon response of an Arctic peatland to simulated permafrost thaw. *Global Change Biology*. **25**(5), pp.1746–1764.

Walker, M., Head, M.J., Lowe, J., Berkelhammer, M., BjÖrck, S., Cheng, H., Cwynar, L.C., Fisher, D., Gkinis, V., Long, A., Newnham, R., Rasmussen, S.O. and Weiss, H. 2019. Subdividing the Holocene Series/Epoch: formalization of stages/ages and subseries/subepochs, and designation of GSSPs and auxiliary stratotypes. *Journal of Quaternary Science*. **34**(3), pp.173–186.

Wang, Y., Way, R.G., Beer, J., Forget, A., Tutton, R. and Purcell, M.C. 2023. Significant underestimation of peatland permafrost along the Labrador Sea coastline in northern Canada. *The Cryosphere*. **17**(1), pp.63–78.

Wania, R., Ross, I. and Prentice, I.C. 2009. Integrating peatlands and permafrost into a dynamic global vegetation model: 1. Evaluation and sensitivity of physical land surface processes. *Global Biogeochemical Cycles*. **23**(3).

Weckström, J., Seppä, H. and Korhola, A. 2010. Climatic influence on peatland formation and lateral expansion in sub-arctic Fennoscandia. *Boreas*. **39**(4), pp.761–769.

Werner, J.P., Divine, D.V., Charpentier Ljungqvist, F., Nilsen, T. and Francus, P. 2018. Spatio-temporal variability of Arctic summer temperatures over the past 2 millennia. *Climate of the Past*. **14**(4), pp.527–557.

Wetterich, S., Davidson, T.A., Bobrov, A., Opel, T., Windirsch, T., Johansen, K.L., González-Bergonzoni, I., Mosbech, A. and Jeppesen, E. 2019. Stable isotope signatures of Holocene syngenetic permafrost trace seabird presence in the Thule District (NW Greenland). *Biogeosciences*. **16**(21), pp.4261–4275.

Wetzel, H., Fleige, H. and Horn, R. 2003. Chemical and physical properties of palsas-degradation of palsas in the region of northern Norway *In*:, pp.21–25.

Wolfe, S.A., Stevens, C.W., Gaanderse, A.J. and Oldenborger, G.A. 2014. Lithalsa distribution, morphology and landscape associations in the Great Slave Lowland, Northwest Territories, Canada. *Geomorphology*. **204**, pp.302–313.

Wolter, J., Lantuit, H., Fritz, M., Macias-Fauria, M., Myers-Smith, I. and Herzschuh, U. 2016. Vegetation composition and shrub extent on the Yukon coast, Canada, are strongly linked to ice-wedge polygon degradation. *Polar Research*. **35**(1), p.27489.

Woo, M. and Young, K.L. 2006. High Arctic wetlands: Their occurrence, hydrological characteristics and sustainability. *Journal of Hydrology*. **320**(3), pp.432–450.

Xu, J., Morris, P.J., Liu, J. and Holden, J. 2018. PEATMAP: Refining estimates of global peatland distribution based on a meta-analysis. *Catena*. **160**, pp.134–140.

Yin, P. and Fan, X. 2001. Estimating R 2 Shrinkage in Multiple Regression: A Comparison of Different Analytical Methods. *The Journal of Experimental Education*. **69**(2), pp.203–224.

Yu, Z., Loisel, J., Brosseau, D.P., Beilman, D.W. and Hunt, S.J. 2010. Global peatland dynamics since the Last Glacial Maximum. *Geophysical Research Letters*. **37**(13).

Yu, Z., Joos, F., Bauska, T.K., Stocker, B.D., Fischer, H., Loisel, J., Brovkin, V., Hugelius, G., Nehrbass-Ahles, C., Kleinen, T. and Schmitt, J. 2021. No support for carbon storage of >1,000 GtC in northern peatlands. *Nature Geoscience*. **14**(7), pp.465–467.

Zelinka, M.D., Myers, T.A., McCoy, D.T., Po-Chedley, S., Caldwell, P.M., Ceppi, P., Klein, S.A. and Taylor, K.E. 2020. Causes of Higher Climate Sensitivity in CMIP6 Models. *Geophysical Research Letters*. **47**(1), e2019GL085782.

Zhang, H., Piilo, S.R., Amesbury, M.J., Charman, D.J., Gallego-Sala, A.V. and Väliranta, M.M. 2018. The role of climate change in regulating Arctic permafrost peatland hydrological and vegetation change over the last millennium. *Quaternary Science Reviews*. **182**, pp.121–130.

Zhang, H., Amesbury, M.J., Piilo, S.R., Garneau, M., Gallego-Sala, A. and Väliranta, M.M. 2020. Recent Changes in Peatland Testate Amoeba Functional Traits and Hydrology Within a Replicated Site Network in Northwestern Québec, Canada. *Frontiers in Ecology and Evolution*. **8**.

Zhang, H., Väliranta, M., Swindles, G.T., Aquino-López, M.A., Mullan, D., Tan, N., Amesbury, M., Babeshko, K.V., Bao, K., Bobrov, A., Chernyshov, V., Davies, M.A., Diaconu, A.-C., Feurdean, A., Finkelstein, S.A., Garneau, M., Guo, Z., Jones, M.C., Kay, M., Klein, E.S., Lamentowicz, M., Magnan, G., Marcisz, K., Mazei, N., Mazei, Y., Payne, R., Pelletier, N., Piilo, S.R., Pratte, S., Roland, T., Saldaev, D., Shotyk, W., Sim, T.G., Sloan, T.J., Słowiński, M.,

Talbot, J., Taylor, L., Tsyganov, A.N., Wetterich, S., Xing, W. and Zhao, Y. 2022. Recent climate change has driven divergent hydrological shifts in high-latitude peatlands. *Nature Communications*. **13**(1), p.4959.

Zhao, B. and Zhuang, Q. 2023. Peatlands and their carbon dynamics in northern high latitudes from 1990 to 2300: a process-based biogeochemistry model analysis. *Biogeosciences*. **20**(1), pp.251–270.

Zoltai, S. and Tarnocai, C. 1971. Properties of a wooded palsa in northern Manitoba. *Arctic and Alpine Research*. **3**(2), pp.115–129.

Zoltai, S. and Tarnocai, C. 1975. Perennially Frozen Peatlands in the Western Arctic and Subarctic of Canada. *Canadian Journal of Earth Sciences*. **12**(1), pp.28–43.

Zoltai, S. 1993. Cyclic Development of Permafrost in the Peatlands of Northwestern Alberta, Canada. *Arctic and Alpine Research*. **25**(3), p.240.

Zoltai, S. 1995. Permafrost Distribution in Peatlands of West-Central Canada During the Holocene Warm Period 6000 Years BP. *Géographie physique et Quaternaire*. **49**(1), pp.45–54.

Zoltai, S., Johnson, J. and Siltanen, R. 2000. *A wetland data base for the western boreal, subarctic, and arctic regions of Canada*. Northern Forestry Centre.

Zuidhoff, F.S. and Kolstrup, E. 2005. Palsa Development and Associated Vegetation in Northern Sweden. *Arctic, Antarctic, and Alpine Research*. **37**(1), pp.49–60.